# ARTS Theory

edited by

**Patrick Eriksson and Stefan Buehler**

December 5, 2017
ARTS Version 2.2.64

**The content and usage of ARTS are not only described by this document. An overview of ARTS documentation and help features is given in *ARTS User Guide*, Section 1.2. For continuous reports on changes of the source code and this user guide, subscribe to the ARTS developers mailing list at http://www.radiativetransfer.org/contact/.**

**We welcome gladly comments and reports on errors in the document. Send then an e-mail to:** `patrick.eriksson (at) chalmers.se` **or** `sbuehler (at) ltu.se`**.**

**If you use data generated by ARTS in a scientific publication, then please mention this and cite the most appropriate of the ARTS publications that are summarized on http://www.radiativetransfer.org/docs/.**

# Contributing authors


| Author/email | Main contribution(s) |
|---|---|
| Stefan Buehler[a]<br>sbuehler (at) ltu.se | Editor, Chapters 2 and 3. |
| Cory Davis[d]<br>cory.davis (at) metservice.com | Chapter 8. |
| Claudia Emde[c]<br>claudia.emde (at) dlr.de | Chapter 6. |
| Patrick Eriksson[b]<br>patrick.eriksson (at) chalmers.se | Editor, Chapters 1, 6 and 7. |
| Nikolay Koulev | Section 2.1. |
| Thomas Kuhn<br>olemke (at) core-dump.info | Chapters 2 and 3. |
| Oliver Lemke[a]<br>olemke (at) core-dump.info | Latex fixes. |
| Christian Melsheimer[c]<br>melsheimer (at) uni-bremen.de | Chapter 5. |

The present address is given for active contributors, while for others the address to the institute where the work was performed is given:
[a] Department of Computer Science, Electrical and Space Engineering, Division of Space Technology, Luleå University of Technology, Box 812, SE-98128 Kiruna, Sweden.
[b] Department of Earth and Space Sciences, Chalmers University of Technology, SE-41296 Gothenburg, Sweden.
[c] Institute of Environmental Physics, University of Bremen, P.O. Box 33044, D-28334 Bremen, Germany.
[d] Institute for Atmospheric and Environmental Science, University of Edinburgh, EH93JZ Edinburgh, Scotland, UK.

# Contents

# Chapter 1

# Theoretical formalism

In this section, a theoretical framework of the forward model is presented. The presentation follows *Rodgers* [1990], but some extensions are made, for example, the distinction between the atmospheric and sensor parts of the forward model is also discussed. After this chapter was written, C.D. Rodgers published a textbook [*Rodgers*, 2000] presenting the formalism in more detail than *Rodgers* [1990].

## 1.1 The forward model

The radiative intensity, $I$, at a point in the atmosphere, $r$, for frequency $\nu$ and traversing in the direction, $\psi$, depends on a variety of physical processes and continuous variables such as the temperature profile, $T$:

$$I = F(\nu, r, \psi, T, \ldots) \tag{1.1}$$

To detect the spectral radiation some kind of sensor, having a finite spatial and frequency resolution, is needed, and the observed spectrum becomes a vector, $\mathbf{y}$, instead of a continuous function. The atmospheric radiative transfer is simulated by a computer model using a limited number of parameters as input (that is, a discrete model), and the forward model, $\mathcal{F}$, used in practice can be expressed as

$$\mathbf{y} = \mathcal{F}(\mathbf{x}_\mathcal{F}, \mathbf{b}_\mathcal{F}) + \varepsilon(\mathbf{x}_\varepsilon, \mathbf{b}_\varepsilon) \tag{1.2}$$

where $\mathbf{x}_\mathcal{F}$, $\mathbf{b}_\mathcal{F}$, $\mathbf{x}_\varepsilon$ and $\mathbf{b}_\varepsilon$ together give a total description of both the atmospheric and sensor states, and $\varepsilon$ is the measurement errors. The parameters are divided in such way that $\mathbf{x}$, the state vector, contains the parameters to be retrieved, and the remainder is given by $\mathbf{b}$, the model parameter vector. The total state vector is

$$\mathbf{x} = \begin{bmatrix} \mathbf{x}_\mathcal{F} \\ \mathbf{x}_\varepsilon \end{bmatrix} \tag{1.3}$$

---

**History**

| | |
|---|---|
| 110610 | Outdated information was removed (Patrick Eriksson). |
| 000306 | Written by Patrick Eriksson, partly based on *Eriksson* [1999] and *Eriksson et al.* [2002]. |

and the total model parameter vector is

$$\mathbf{b} = \begin{bmatrix} \mathbf{b}_{\mathcal{F}} \\ \mathbf{b}_{\varepsilon} \end{bmatrix} \tag{1.4}$$

The actual forward model consists of either empirically determined relationships, or numerical counterparts of the physical relationships needed to describe the radiative transfer and sensor effects. The forward model described here is mainly of the latter type, but some parts are more based on empirical investigations, such as the parameterisations of continuum absorption.

Both for the theoretical formalism and the practical implementation, it is suitable to make a separation of the forward model into two main sections, a first part describing the atmospheric radiative transfer for pencil beam (infinite spatial resolution) monochromatic (infinite frequency resolution) signals,

$$\mathbf{i} = \mathcal{F}_r(\mathbf{x}_r, \mathbf{b}_r) \tag{1.5}$$

and a second part modelling sensor characteristics,

$$\mathbf{y} = \mathcal{F}_s(\mathbf{i}, \mathbf{x}_s, \mathbf{b}_s) + \varepsilon(\mathbf{x}_\varepsilon, \mathbf{b}_\varepsilon) \tag{1.6}$$

where $\mathbf{i}$ is the vector holding the spectral values for the considered set of frequencies and viewing angles ($\mathbf{i}^i = I(\nu^i, \psi^i, \ldots)$, where $i$ is the vector index), and $\mathbf{x}_{\mathcal{F}}$ and $\mathbf{b}_{\mathcal{F}}$ are separated correspondingly, that is, $\mathbf{x}_{\mathcal{F}}^T = [\mathbf{x}_r^T, \mathbf{x}_s^T]$ and $\mathbf{b}_{\mathcal{F}}^T = [\mathbf{b}_r^T, \mathbf{b}_s^T]$. The vectors $\mathbf{x}$ and $\mathbf{b}$ can now be expressed as

$$\mathbf{x} = \begin{bmatrix} \mathbf{x}_r \\ \mathbf{x}_s \\ \mathbf{x}_\varepsilon \end{bmatrix} \tag{1.7}$$

and

$$\mathbf{b} = \begin{bmatrix} \mathbf{b}_r \\ \mathbf{b}_s \\ \mathbf{b}_\varepsilon \end{bmatrix}, \tag{1.8}$$

respectively. The subscripts of $\mathbf{x}$ and $\mathbf{b}$ are below omitted as the distinction should be clear by the context.

## 1.2 The sensor transfer matrix

The modelling of the different sensor parts can be described by a number of analytical expressions that together makes the basis for the sensor model. These expressions are throughout linear operations and it possible, as suggested in *Eriksson et al.* [2002], to implement the sensor model as a straightforward matrix multiplication:

$$\mathbf{y} = \mathbf{H}\mathbf{i} + \varepsilon \tag{1.9}$$

where $\mathbf{H}$ is here denoted as the sensor transfer matrix. Expressions to determine $\mathbf{H}$ are given by *Eriksson et al.* [2006].

The matrix $\mathbf{H}$ can further incorporate effects of a data reduction and the total transfer matrix is then

$$\mathbf{H} = \mathbf{H}_d\mathbf{H}_s \tag{1.10}$$

as

$$\mathbf{y} = \mathbf{H}_d\mathbf{y}' = \mathbf{H}_d(\mathbf{H}_s\mathbf{i} + \varepsilon') = \mathbf{H}\mathbf{i} + \varepsilon \tag{1.11}$$

where $\mathbf{H}_d$ is the data reduction matrix, $\mathbf{H}_s$ the sensor matrix, and $\mathbf{y}'$ and $\varepsilon'$ are the measurement vector and the measurement errors, respectively, before data reduction.

## 1.3 Weighting functions

### 1.3.1 Basics

A weighting function is the partial derivative of the spectrum vector $\mathbf{y}$ with respect to some variable used by the forward model. As the input of the forward model is divided between $\mathbf{x}$ or $\mathbf{b}$, the weighting functions are divided correspondingly between two matrices, the state weighting function matrix

$$\mathbf{K}_\mathbf{x} = \frac{\partial \mathbf{y}}{\partial \mathbf{x}} \tag{1.12}$$

and the model parameter weighting function matrix

$$\mathbf{K}_\mathbf{b} = \frac{\partial \mathbf{y}}{\partial \mathbf{b}} \tag{1.13}$$

For the practical calculations of the weighting functions, it is important to note that the atmospheric and sensor parts can be separated. For example, if $\mathbf{x}$ only hold atmospheric and spectroscopic variables, $\mathbf{K}_\mathbf{x}$ can be expressed as

$$\mathbf{K}_\mathbf{x} = \frac{\partial \mathbf{y}}{\partial \mathbf{i}}\frac{\partial \mathbf{i}}{\partial \mathbf{x}} = \mathbf{H}\frac{\partial \mathbf{i}}{\partial \mathbf{x}} \tag{1.14}$$

This equation shows that the new parts needed to calculate atmospheric weighting functions, are functions giving $\partial\mathbf{i}/\partial\mathbf{x}$ where $\mathbf{x}$ can represent the vertical profile of a species, atmospheric temperatures, spectroscopic data etc.

### 1.3.2 Transformation between vector spaces

It could be of interest to transform a weighting function matrix from one vector space to another[1]. The new vector, $\mathbf{x}'$, is here assumed to be of length $n$ ($\mathbf{x}' \in \mathbf{R}^{n\times 1}$), while the original vector, $\mathbf{x}$ is of length $p$ ($\mathbf{x} \in \mathbf{R}^{p\times 1}$). The relationship between the two vector spaces is described by a transformation matrix $\mathbf{B}$:

$$\mathbf{x} = \mathbf{B}\mathbf{x}' \tag{1.15}$$

where $\mathbf{B}\in\mathbf{R}^{p\times n}$. For example, if $\mathbf{x}'$ is assumed to be piecewise linear, then the columns of $\mathbf{B}$ contain tenth functions, that is, a function that are 1 at the point of interest and decreases linearly down to zero at the neighbouring points. The matrix can also hold a reduced set of eigenvectors.

The weighting function matrix corresponding to $\mathbf{x}'$ is

$$\mathbf{K}_{\mathbf{x}'} = \frac{\partial \mathbf{y}}{\partial \mathbf{x}'} \tag{1.16}$$

[1] This subject is also discussed in *Rodgers* [2000], published after writing this.

This matrix is related to the weighting function matrix of $\mathbf{x}$ (Eq. 1.12) as

$$\mathbf{K}_{\mathbf{x}'} = \frac{\partial \mathbf{y}}{\partial \mathbf{x}} \frac{\partial \mathbf{x}}{\partial \mathbf{x}'} = \frac{\partial \mathbf{y}}{\partial \mathbf{x}} \mathbf{B} = \mathbf{K}_{\mathbf{x}} \mathbf{B} \tag{1.17}$$

Note that

$$\mathbf{K}_{\mathbf{x}'} \mathbf{x}' = \mathbf{K}_{\mathbf{x}} \mathbf{B} \mathbf{x}' = \mathbf{K}_{\mathbf{x}} \mathbf{x} \tag{1.18}$$

However, it should be noted that this relationship only holds for those $\mathbf{x}$ that can be represented perfectly by some $\mathbf{x}'$ (or vice versa), that is, $\mathbf{x} = \mathbf{B}\mathbf{x}'$, and not for all combinations of $\mathbf{x}$ and $\mathbf{x}'$.

If $\mathbf{x}'$ is the vector to be retrieved, we have that [*Rodgers*, 1990]

$$\hat{\mathbf{x}}' = \mathcal{I}(\mathbf{y}, \mathbf{c}) = \mathcal{T}(\mathbf{x}, \mathbf{b}, \mathbf{c}) \tag{1.19}$$

where $\mathcal{I}$ and $\mathcal{T}$ are the inverse and transfer model, respectively.

The contribution function matrix is accordingly

$$\mathbf{D}_{\mathbf{y}} = \frac{\partial \hat{\mathbf{x}}'}{\partial \mathbf{y}} \tag{1.20}$$

that is, $\mathbf{D}_{\mathbf{y}}$ corresponds to $\mathbf{K}_{\mathbf{x}'}$, not $\mathbf{K}_{\mathbf{x}}$.

We have now two possible averaging kernel matrices

$$\mathbf{A}_{\mathbf{x}} = \frac{\partial \hat{\mathbf{x}}'}{\partial \mathbf{x}} = \frac{\partial \hat{\mathbf{x}}'}{\partial \mathbf{y}} \frac{\partial \mathbf{y}}{\partial \mathbf{x}} = \mathbf{D}_{\mathbf{y}} \mathbf{K}_{\mathbf{x}} \tag{1.21}$$

$$\mathbf{A}_{\mathbf{x}'} = \frac{\partial \hat{\mathbf{x}}'}{\partial \mathbf{x}'} = \frac{\partial \hat{\mathbf{x}}'}{\partial \mathbf{y}} \frac{\partial \mathbf{y}}{\partial \mathbf{x}} \frac{\partial \mathbf{x}}{\partial \mathbf{x}'} = \mathbf{D}_{\mathbf{y}} \mathbf{K}_{\mathbf{x}'} = \mathbf{A}_{\mathbf{x}} \mathbf{B} \tag{1.22}$$

where $\mathbf{A}_{\mathbf{x}} \in \mathbf{R}^{p \times n}$ and $\mathbf{A}_{\mathbf{x}'} \in \mathbf{R}^{p \times p}$, that is, only $\mathbf{A}_{\mathbf{x}'}$ is square. If $p > n$, $\mathbf{A}_{\mathbf{x}}$ gives more detailed information about the shape of the averaging kernels than the standard matrix ($\mathbf{A}_{\mathbf{x}'}$). If the retrieval grid used is coarse, it could be the case that $\mathbf{A}_{\mathbf{x}'}$ will not resolve all the oscillations of the averaging kernels, as shown in *Eriksson* [1999, Figure 11].

# Chapter 2

# Gas absorption

This chapter contains theoretical background and scientific details for gas absorption calculations in ARTS. A more practical overview, with focus on how to set up calculations, is given in *ARTS User Guide*, Chapter 6.

Gas absorption generally consists of a superposition of spectral lines and continua. Depending on the gas species, the continua either have a real physical meaning, or they are more or less empirical corrections for deficits in the explicit line-by-line calculation. In the latter case the magnitude of the continuum term will depend strongly on the exact setup of the line-by-line calculation. Combining continua and line-by-line calculation therefore requires expertise.

This chapter is structured in three main parts: Line absorption, continuum absorption, and complete absorption models. It should be noted that the three topics are tightly related. In particular, complete absorption models will normally include a line part and a continuum part. Some absorption models, notably those by Rosenkranz and Liebe will show up under both continua and complete absorption models. The continuum section then treats specifically the continuum parameterization of these model, the complete absorption model section puts more focus on the line part and the model as a whole.

Each of the main parts first introduces the theoretical background to the topic, then presents aspects of the specific implementation in ARTS.

## 2.1 Line absorption

### 2.1.1 Theoretical background

We will introduce here the main concepts concerning line absorption. The aim is to give some overview and show some key equations, not to give a full treatment of the theory. To really understand line absorption, you should refer to one of the cited books, or some other book on spectroscopy.

**History**

| | |
|---|---|
| 2012-09-21 | Added pressure broadening and shift documentation, Stefan Buehler. |
| 2011-07-05 | Revised for ARTS2 by Stefan Buehler. |
| 2001-11-21 | Continuum absorption part written, Thomas Kuhn. |
| 2001-10-05 | Line absorption part written, Nikolay Koulev. |

### Basic expressions

An absorption line is described by the corresponding absorption coefficient as a function of frequency $\alpha(\nu)$, which can be written as [*Goody and Yung*, 1989]:

$$\alpha(\nu) = nS(T)F(\nu) \tag{2.1}$$

where $S(T)$ is called the line strength, $T$ is the temperature, $F(\nu)$ is called the line shape function, and $n$ is the number density of the absorber. The line shape function is normalized as:

$$\int F(\nu)d\nu = 1 \tag{2.2}$$

The values of $S(T)$ at reference temperature $T_0$ are contained in spectroscopic databases (more on this below). The conversion to different temperatures is done by

$$S(T) = S(T_0)\,\frac{Q(T_0)}{Q(T)}\,\frac{e^{-E_f/(kT)} - e^{-E_i/(kT)}}{e^{-E_f/(kT_0)} - e^{-E_i/(kT_0)}} \tag{2.3}$$

given the energies $E_f$ and $E_i$ of the two levels between which the transition occurs as well as the partition function $Q(T)$ [*Rothman et al.*, 1998]. The databases contain the lower state energy $E_l$ tabulated along with the $S$ and the transition frequency $\nu$, so that the upper state energy can be computed by $E_u$=$E_l$+h$\nu$. Partition functions for the different molecular species are commonly available along with the spectroscopic databases, given in the form of tabulated values for a set temperatures (e.g., for JPL catalogue) or through some computer code (e.g., the TIPS program coming with the HITRAN catalogue).

As absorption is additive, the total absorption coefficient is derived by adding up the absorption contributions of all spectral lines of all molecular species.

The following subsections discuss common descriptions of the line shape function, present partition functions and their calculation formalism more in depth, and introduce the Zeeman effect.

### Line shape functions

So far, there exists no complete analytical function that accurately describes the line shape in all atmospheric conditions and for all frequencies. But for most cases very accurate approximations are available. Which approximation is appropriate depends mostly on the atmospheric pressure, and on whether the frequencies of interest are close to the line center, or far out in the line wing.

There are three phenomena which contribute to the line shape. These are, in increasing order of importance, the finite lifetime of an excited state in an isolated molecule, the thermal movement of the gas molecules, and their collisions with each other. They result in corresponding effects to the line shape: natural broadening, Doppler, and pressure broadening. Of these, the first one is completely negligible compared to the other two for typical atmospheric conditions. Nevertheless, we will pay a special attention to the natural broadening because its implications are of a conceptual importance for the broadening processes.

The spectral line shape can be derived in the case of natural broadening from basic physical considerations and a well-known Fourier transform theorem from the time to the frequency domain [*Thorne et al.*, 1999]. If we consider classically the spontaneous decay of the excited state of a two-level system in the absence of external radiation, then the population $n$ of the upper level decreases according to

$$\frac{dn(t)}{dt} = -A\,n(t) \tag{2.4}$$

where $A$ is Einstein A coefficient. This equation can also be interpreted as the rate of the spontaneously emitted photons because of decay. The integral form of this relation is

$$n(t) = n(0)\,e^{-At} = n(0)e^{-t/\tau} \tag{2.5}$$

where $\tau$ is the mean lifetime of the excited state. Thus, the number of spontaneously emitted photons and in this way the flux of the emitted radiation then will be proportional to $n$. Therefore we can write for the flux $L$ that

$$L(t) = L(0)\,e^{-t/\tau} = L(0)\,e^{-\gamma t} \tag{2.6}$$

By the afore mentioned theorem, multiplying in the time domain by $e^{-\gamma t}$ is equivalent to convolving in the frequency domain with a function $1/[\nu^2 - (\gamma/4\pi)^2]$. Accordingly, the line profile of a spectral line at frequency $\nu_0$ as a normalized line shape function will be, as defined in *Thorne et al.* [1999],

$$F(\nu) = \frac{1}{\pi}\frac{\gamma/4\pi}{(\nu-\nu_0)^2 + (\gamma/4\pi)^2} \tag{2.7}$$

This gives a bell-shaped profile and the function itself is called Lorentzian. The dependence on the position of the line is apparent through $\nu_0$, that is why some authors prefer to denote the function by $F(\nu, \nu_0)$. The result is important because of two major reasons. Firstly, without the natural broadening the line would be the delta function $\delta(\nu - \nu_o)$, as pointed out in *Bernath* [1995]. So the spontaneous decay of the excited state is responsible for the finite width and the certain shape of the line shape function. Secondly, the Lorentzian type of function comes significantly into play when explaining some of the other broadening effects or the complete picture of the broadened line [*Thorne et al.*, 1999].

The second effect, Doppler broadening, is important for the upper stratosphere and mesosphere for microwave frequencies. The line shape follows the velocity distribution of the particles. Under the conditions of thermodynamic equilibrium, we have a probability distribution for the relative velocity $u$ between the gas molecule and the observer of Maxwell type

$$p(u) = \sqrt{\frac{m}{2\pi kT}}\; exp\left[-\frac{mu^2}{2kT}\right] \tag{2.8}$$

where $m$ is the mass of the molecule. Using then the formula for the Doppler shift for the non-relativistic region $\nu$- $\nu_0$ = $\nu_0 u$ / $c$ , one can easily derive the line shape function [*Bernath*, 1995],

$$F_D(\nu) = \frac{1}{\gamma_D\sqrt{\pi}}\; exp\left[-\left(\frac{\nu-\nu_0}{\gamma_D}\right)^2\right] \tag{2.9}$$

where the quantity $\gamma_D$ is called Doppler line width and equals

$$\gamma_D = \frac{\nu}{c}\sqrt{\frac{2kT}{m}} \tag{2.10}$$

In contrast to the line shape function for the natural broadening, the Doppler broadening leads to a Gaussian line shape function $F(\nu)$. The Doppler line width $\gamma_D$ is so defined that it is equal to the half width at half of the maximum (HWWM) of the line shape function. A similar notation is used for all other width parameters $\gamma_{xy}$ below.

The third broadening mechanism is pressure broadening. It is the most complicated broadening mechanism, and still subject to theoretical and experimental research. So far, there is no way to derive the exact shape of a pressure-broadened line from first principles, at least not for the far wing region. The various approximations, which are therefore used, are immanently limited to the certain line regions they deal with. The most popular among these approximations is the *impact approximation* which postulates that the duration of the collisions of the gas particles is very small compared to the average time between the collisions. Due to the Fourier-pair relationship between time and frequency, the line shape that follows from the impact approximation can only be expected to be accurate near the line center, not in the far wings of the line.

Lorentz was the first to achieve a result exploiting the impact approximation, the Lorentz line shape function:

$$F_L(\nu) = \frac{\gamma_L}{\pi} \frac{1}{(\nu - \nu_0)^2 + \gamma_L^2} \tag{2.11}$$

where $\gamma_L$ is the Lorentz line width [*Thorne et al.*, 1999]. As one can see, the result Eq. 2.11 is pretty similar to Eq. 2.7 but the specific line parameters $\gamma$ and $\gamma_L$ make them differ significantly in the corresponding frequency regions of interest. For atmospheric pressures $\gamma_L$ is much greater and because of that, of experimental significance in contrast to $\gamma$.
Elaborating the model of Lorentz, van Vleck and Weisskopf made a correction to it [*Van Vleck and Weisskopf*, 1945], particularly for the microwave region:

$$F_{VVW}(\nu) = \left(\frac{\nu}{\nu_0}\right)^2 \frac{\gamma_L}{\pi} \left[\frac{1}{(\nu - \nu_0)^2 + \gamma_L^2} + \frac{1}{(\nu + \nu_0)^2 + \gamma_L^2}\right] \tag{2.12}$$

which can be reduced to a Lorentzian for $(\nu - \nu_0) << \nu_0$ and $0 << \nu_0$. Except for the additional factor $(\nu/\nu_0)^2$ , $F_{VVW}$ can be regarded as the sum of two $F_L$ lines, one with its center frequency at $\nu_0$, the other at $-\nu_o$.

The van Vleck and Huber lineshape [*Van Vleck and Huber*, 1977] is similar to Eq. 2.12, except for the factor $(\nu/\nu_0)^2$ which is replaced by $(\nu * \tanh(h * \nu/(2kT)))/(\nu_0 * \tanh(h * \nu_0/(2kT)))$, with $k$ the Boltzmann constant, $h$ the Planck constant, and $T$ the atmospheric temperature (the denominator is actually a consequence of the line strength definition in the spectroscopic catalogs). The lineshape Eq. 2.12 with this factor can be used for the entire frequency range, since the microwave approximation: $\tanh(x) = x$, that leads to the factor $(\nu/\nu_0)^2$, is not made.

The combined picture of a simultaneously Doppler and pressure broadened line is the next step of the approximations development. The line shape function has to approximated in this case by the Voigt line shape function

$$F_{Voigt}(\nu, \nu_0) = \int F_L(\nu, \nu')\, F_D(\nu', \nu_0)\, d\nu' \tag{2.13}$$

though there's no strict justification for its use - the two processes are assumed to act independently, which in reality is not the fact. Regardless of this flaw, it is the only way up to now to model the combination of the broadening processes. The integral in Eq. 2.13 can not be computed analytically, so certain approximation algorithms must be used.

Another possibility would be the combination of the last two equations Eq. 2.12 and Eq. 2.13. The respective result then will be

$$F_S = \left(\frac{\nu}{\nu_0}\right)^2 \left[F_{Voigt}(\nu, \nu_0) + F_{Voigt}(\nu, -\nu_0)\right] \tag{2.14}$$

The advantage of such a model is that it behaves like a van Vleck-Weisskopf line shape function in the high pressure limit and like a Voigt one in the low pressure limit. There is one important caveat to the equation Eq. 2.14: it has to be made sure that the algorithm that is used to compute the Voigt function really produces a Lorentz line in the high pressure limit. Another point of significance is the demand that the model yields meaningful results far from the line center, since the line center from the “mirror” line at -$\nu_0$ is situated approximately $2\nu_0$ away from the frequency $\nu_0$ of computation. We explicitly verified that the algorithms of *Drayson* [1976], *Oliveiro and Longbothum* [1977], and *Kuntz and Höpfner* [1999] satisfy both requirements, while this was found to be not true for some other algorithms commonly used for Voigt-shape computation. In particular, it is not true for the Hui-Armstrong-Wray Formula, as defined in *Hui et al.* [1978] and in Equation 2.60 of *Rosenkranz* [1993]. Provided the condition above is fulfilled, the $F_S$ line shape gives a smooth transition from high tropospheric pressures to low stratospheric ones, and should be valid near the line centers throughout the microwave region. With a Van Vleck / Huber forefactor instead of the Van Vleck / Weisskopf forefactor, it should be valid throughout the thermal infrared spectral range, but there the mirror line at negative frequency is negligible anyway, because it is so far away.

**Partition functions**

Partition functions are needed to compute the temperature dependence of the line intensities (Equation 2.3 on page 6). They are related to the molecular energy states and their statistical distribution during the radiation process.

In any case of spectroscopic interest the free molecules of a gas are not optically thick at all frequencies, so the radiation energy is not represented by blackbody radiation. The most common assumption made, which is sufficient in the case of tropospheric and low stratospheric research, is the *local thermodynamic equilibrium* or *LTE*. According to it, it’s possible to find a common temperature, which may vary from place to place, that fits the Boltzmann energy population distribution and the Maxwell velocities distribution. This practically means, that under $LTE$ the collisional processes must be of greater importance than radiative ones. In other words, an excited state must have a higher probability of de-excitation by collision than by spontaneous radiation. This is the important factor which makes natural broadening differ quantitatively so much from the pressure (collisional) one, though both are described qualitatively almost identically by Lorentzian line shape functions.

According to the Maxwell-Boltzmann distribution law, in $LTE$ the total number of gas particles $N_n$ in a state $E_n$ is given by

$$N_n = N_0 \frac{g_n}{g_0} e^{-E_n/kT} \tag{2.15}$$

where $N_0$ is particle number in the ground state, and $g_n$, $g_o$ are the statistical weights (degeneracies) of the $n-$state and the ground state [*Gordy and Cook*, 1970]. Thus the total particle number $N$ is given by

$$N = \frac{N_0}{g_0} \sum_{n=0}^{\infty} g_n \, e^{-E_n/kT} = \frac{N_0}{g_0} \, Q(T) \qquad (2.16)$$

The quantity $Q(T)$ is the *partition function* of the gas, which generally speaking describes the energy states distribution of the gas particles.

The partition function for a perfect gas molecule can be represented by the product of the *translational* and the *internal* partition functions, as defined in *Herzberg* [1945],

$$Q = Q_{tr} \, Q_{int} \qquad (2.17)$$

bearing in mind that the respective energies, translational and internal, are independent of each other. The first quantity $Q_{tr}$ accounts for the distribution of the translational energy of the gas particles - it takes into account that the translational velocities of the particles fulfill the Maxwell distribution. However, for Equation 2.3, the quantity we are interested in is the *internal* partition function (or the *total internal partition function*) because the transitions between the discrete internal energy states are responsible for the absorption or emittance of radiation. Accordingly $Q_{int}$ describes the distribution of energy among the internal energy states of the gas particles.

The internal partition function for free gaseous molecules is a function of the electronic, the vibrational, the rotational, and the nuclear spin states. An approximation is used in *Gordy and Cook* [1970] in order to display the individual contributions explicitly

$$Q_{int} = Q_e \, Q_v \, Q_r \, Q_n \qquad (2.18)$$

and thus the interaction between these various states is neglected. For practically all polyatomic molecules the excited electronic states are entirely negligible to those of the ground states, i.e. $Q_e = 1$ . Only for the very few polyatomic molecules with a multiplet ground state ($NO_2$ , $ClO_2$ , and free radicals) the electronic contribution has to be considered.
If we neglect the anharmonicities, the vibrational partition function, with vibrational energy levels measured with respect to the ground state for the *harmonic oscillator*, is according to *Herzberg* [1945]

$$Q_v = \left( \sum_{\nu_1} e^{-\nu_1 h\omega_1/kT} \right) \left( \sum_{\nu_2} e^{-\nu_2 h\omega_2/kT} \right) ... \qquad (2.19)$$

where $\nu_1$, $\nu_2$,..., the vibrational quantum numbers, can each have the values 0,1,2,... and $\omega_1$, $\omega_2$,..are the frequencies of the fundamental modes of vibration. The summation is taken over all values of $\nu_1$, $\nu_2$,..., and each fundamental mode is counted separately. This result is valid for non-degenerate vibrations. If we use the simple expression for geometric progression

$$\sum_{\nu_i} e^{-\nu_i h\omega_i/kT} = \frac{1}{1 - e^{h\omega_i/kT}} \qquad (2.20)$$

and the degeneracies $d_1$, $d_2$,... of the fundamental modes, we get finally for the vibrational partition function

$$Q_v = \left(1 - e^{h\omega_1/kT}\right)^{-d_1} \left(1 - e^{h\omega_2/kT}\right)^{-d_2} ... \qquad (2.21)$$

The rotational partition function looks differently for the different symmetry types of molecules. For diatomic and linear polyatomic molecules with no center of symmetry the corresponding expression is, as defined in *Gordy and Cook* [1970]

$$\begin{aligned} Q_r &= \sum_{J=0}^{\infty}(2J+1)e^{-hBJ(J+1)/kT} \\ &= \frac{kT}{hB}+\frac{1}{3}+\frac{1}{15}\frac{hB}{kT}+\frac{4}{315}\left(\frac{hB}{kT}\right)^2+... \\ &\cong \frac{kT}{hB} \end{aligned} \tag{2.22}$$

For *rigid symmetric-*, *asymmetric-*, and *spherical* top molecules there are also other factors to be taken into consideration, such as the spatial structure of the molecules, nuclear spin, inversion and internal rotation. The general expression in the case of a *rigid symmetric-* top molecule according to *Herzberg* [1945] is

$$Q_r = \frac{1}{\sigma}\sum_{J=0}^{\infty}\sum_{K=-J}^{J}(2J+1)\, e^{-h[BJ(J+1)+(A-B)K^2]/kT} \tag{2.23}$$

where $\sigma$ is a measure of the degree of symmetry. The usual symmetric top has $C_3$ or $C_{3\nu}$ symmetry, therefore $\sigma$ = 3. To a good approximation, the summation above can expressed as in *Gordy and Cook* [1970]

$$Q_r = \frac{1}{\sigma}\left[\left(\frac{\pi}{B^2A}\right)\left(\frac{kT}{h}\right)^3\right]^{1/2} = \frac{5.34\times10^6}{\sigma}\left(\frac{T^3}{B^2A}\right)^{1/2} \tag{2.24}$$

For an *asymmetric* top the formula would then be

$$Q_r = \frac{5.34\times10^6}{\sigma}\left(\frac{T^3}{ABC}\right)^{1/2} \tag{2.25}$$

and for a *spherical* top, using the current notation of *Gordy and Cook* [1970] in the respective expression in *Herzberg* [1945],

$$Q_r = \frac{5.34\times10^6}{\sigma}\left(\frac{T^3}{A^3}\right)^{1/2} \tag{2.26}$$

#### The Zeeman Effect for $O_2$

The Zeeman effect implementation in ARTS is described by *Larsson et al.* [2014].

### 2.1.2 Line-specific data and line catalogue data in ARTS

ARTS has an internal representation of spectral line data that maps naturally to a native catalogue format, which we will discuss below. This internal catalogue data exists and can be handled in two variants, the so-called ARTSCAT-3 and ARTSCAT-4 – versions 3 and 4 of the ARTS catalogue format. The spectroscopic databases commonly used in Earth atmospheric research contain the spectroscopic parameters representative for Earth conditions. This regards particular the foreign broadened width, often called the air broadened width as it considerers the contribution from nitrogen and oxygen that make up for the vast majority of gases in the Earth atmosphere, and the pressure shift. ARTSCAT-3 contains these "classical" spectroscopic parameters. ARTSCAT-4 on the other hand has been developed with view on planetary science. That is, it holds these parameters separately for the different molecular species. Theoretically this has to list all cross-combinations of species. However, most species show only very low abundances and can safely be neglected. For now, the main atmospheric constituents of Earth, Mars, Venus, and Jupiter, namely N2, O2, H2O, CO2, H2, and He are considered in the database. It should be noted, that both line data formats can behandled simultaneously within one calculation (writing to file of mixed format data, however, is not possible).

Besides its own internal format, ARTS can also read several other catalogue formats, in particular HITRAN and JPL format. If these other catalogues are used, line data are converted to the internal ARTSCAT-3 representation during reading. In other words, all unit conversions are done by the reading routines.

The ARTS internal spectral line data files (both ARTSCAT-3 and -4) contain an XML header and footer, and between them one entry for each spectral line. Each entry starts with with an '@' character. It then contains the different line parameters, separated by one or more blank characters. Scientific notation is allowed, e.g. 501.12345e9.

In contrast to other catalogues that are optimized for processing with programs written in the FORTRAN language, ARTS does not use fixed column widths. The advantage of this is that the precision of the parameters is not limited by the format.

The first column of each entry contains the species and isotopologue, following the naming scheme described below. Note that the intensity is per molecule, i.e., it does not contain the isotopologue ratio. This is similar to JPL, but different to HITRAN. The definition of the further entries differ between the two ARTSCAT representations.

**The ARTSCAT-3 line format is:**

```
Col  Variable                      Label    Unit
------------------------------------------------
 0   '@'                          ENTRY        -
 1   molecule & isotopologue tag  NAME         -
 2   center frequency                F        Hz
 3   pressure shift of F           PSF     Hz/Pa
 4   line intensity per molecule    I0    m^2/Hz
 5   reference temp. for I0       T_I0         K
 6   lower state energy           ELOW         J
 7   air broadened width           AGAM    Hz/Pa
 8   self broadened width          SGAM    Hz/Pa
 9   AGAM temp. exponent           NAIR        -
10   SGAM temp. exponent          NSELF        -
11   ref. temp. for AGAM, SGAM    T_GAM        K
12   number of aux. parameters    N_AUX        -
13   auxiliary parameter           AUX1        -
14   ...
15   error for F                     DF       Hz
16   error for I0                   DI0        %
17   error for AGAM               DAGAM        %
18   error for SGAM               DSGAM        %
19   error for NAIR               DNAIR        %
20   error for NSELF             DNSELF        %
21   error for PSF                 DPSF        %
```

The parameters 0-12 must be present, the others can be missing, since they are not needed for the calculation. For the error fields (15-21), a $-1$ means that no value exists.

Some species may need special parameters that are not needed by other species (for example overlap coefficients for $O_2$). In the case of oxygen two parameters are sufficient to describe the overlap, but other species, e.g., methane, may need more coefficients. The default for `N_AUX` is zero. In that case, no further `AUX` fields are present.

**The ARTSCAT-4 line format is:**

```
Col  Variable                          Label     Unit
--------------------------------------------------
 0   `@'                               ENTRY        -
 1   molecule & isotopologue tag        NAME        -
 2   center frequency                      F       Hz
 3   line intensity                       I0  Hz*m^2
 4   reference temperature              T_I0        K
 5   lower state energy                 ELOW        J
 6   Einstein A-coefficient                A      1/s
 7   Upper state stat. weight        G_upper        -
 8   Lower state stat. weight        G_lower        -
 9   broadening parameter self          SGAM    Hz/Pa
10   broadening parameter N2        GAMMA_N2    Hz/Pa
11   broadening parameter O2        GAMMA_O2    Hz/Pa
12   broadening parameter H2O      GAMMA_H2O    Hz/Pa
13   broadening parameter CO2      GAMMA_CO2    Hz/Pa
14   broadening parameter H2        GAMMA_H2    Hz/Pa
15   broadening parameter He        GAMMA_He    Hz/Pa
16   GAM temp. exponent self           NSELF        -
17   GAM temp. exponent N2              N_N2        -
18   GAM temp. exponent O2              N_O2        -
19   GAM temp. exponent H2O            N_H2O        -
20   GAM temp. exponent CO2            N_CO2        -
21   GAM temp. exponent H2              N_H2        -
22   GAM temp. exponent He              N_He        -
23   F pressure shift N2            DELTA_N2    Hz/Pa
24   F pressure shift O2            DELTA_O2    Hz/Pa
25   F pressure shift H2O          DELTA_H2O    Hz/Pa
26   F pressure shift CO2          DELTA_CO2    Hz/Pa
27   F pressure shift H2            DELTA_H2    Hz/Pa
28   F pressure shift He            DELTA_He    Hz/Pa
29   Vib. & rotational assignments       VRA        -
```

Parameters 0-28 must be present. Parameter 29 contains coded quantum numbers. The coding conventions are species specific. The definitions are given in file `ARTSCAT-4_Col29_Conventions.txt`, which is available along with the first incarnation of an ARTSCAT-4 type spectroscopic catalog from the `arts-xml-data` package.

| | ARTSCAT-3 | ARTSCAT-4 |
|---|---|---|
| Atmospheric variables | pressure $p$<br>temperature $T$<br>VMR of current species $x_{\text{self}}$ | pressure $p$<br>temperature $T$<br>VMR of current species $x_{\text{self}}$<br>broadening species VMRs $x_i$ (where $i$ is the index of the gas species) |
| Spectral line parameters | T_GAM, AGAM, SGAM, NAIR, NSELF, PSF (see Section 2.1.2 for definitions) | T_I0, SGAM, GAMMA_N2, GAMMA_O2, GAMMA_H2O, GAMMA_CO2, GAMMA_H2, GAMMA_He, NSELF, N_N2, N_O2, N_H2O, N_CO2, N_H2, N_He, DELTA_N2, DELTA_O2, DELTA_H2O, DELTA_CO2, DELTA_H2, DELTA_He (see Section 2.1.2 for definitions) |

Table 2.1: Pressure broadening and pressure shift input variables for different ARTSCAT versions.

### 2.1.3 Pressure broadening and shift calculation

The pressure broadened line width $\gamma_L$ (see Equations 2.11 and 2.12) is calculated from spectral line parameters and atmospheric state variables. At the same time, a pressure shift $\Delta\nu$ is also calculated. The calculations are different for ARTSCAT-3 and ARTSCAT-4 lines. Table 2.1 lists the input variables for the two different cases.

#### ARTSCAT-3

With ARTSCAT-3, the pressure broadened line width is calculate as

$$\begin{aligned}\gamma_L &= x_{\text{self}}\, p\, \text{SGAM} \left(\frac{\text{T\_GAM}}{T}\right)^{\text{NSELF}} \\ &\quad + (1 - x_{\text{self}})\, p\, \text{AGAM} \left(\frac{\text{T\_GAM}}{T}\right)^{\text{NAIR}} , \end{aligned} \tag{2.27}$$

and the pressure shift is calculated as

$$\Delta\nu = p\, \text{PSF} \left(\frac{\text{T\_GAM}}{T}\right)^{(0.25+1.5*\text{NAIR})} , \tag{2.28}$$

where all variables are defined as in Table 2.1.

#### ARTSCAT-4

With ARTSCAT-4, the pressure broadened line width is calculate as

$$\gamma_L = x_{\text{self}}\, p\, \text{SGAM} \left(\frac{\text{T\_I0}}{T}\right)^{\text{NSELF}}$$

$$+ (1 - x_{\text{self}})\, p \, \frac{\sum_i \left[ x_i \text{ GAMMA}_i \left( \frac{\text{T\_I0}}{T} \right)^{\text{N}_i} \right]}{\sum_i x_i} \,, \tag{2.29}$$

where index $i$ runs over the six different broadening species $N_2$, $O_2$, $H_2O$, $CO_2$, $H_2$, and He, and all other variables are defined as in Table 2.1. Note that there is no separate reference temperature for the broadening and shift parameters in ARTSCAT-4. Instead we use T_I0 the same reference temperature as for the line intensity.

Similarly, the pressure shift is calculated as

$$\Delta\nu = p \, \frac{\sum_i \left[ x_i \text{ DELTA}_i \left( \frac{\text{T\_I0}}{T} \right)^{(0.25+1.5*\text{N}_i)} \right]}{\sum_i x_i} \,. \tag{2.30}$$

The normalisation by $\sum_i x_i$ in both formulas accounts for the fact that the sum of the foreign broadening species usually will not exactly add up to 1. With this normalisation, the ARTSCAT-4 broadening and shift reproduce the ARTSCAT-3 results if all foreign parameters are filled with the ARTSCAT-3 value. To make sure that the broadening species account for a reasonable part of the atmosphere, we throw a runtime error if their VMR sum deviates from 1 by more than 10%.

Two other caveats should be mentioned here. Caveat 1: The species list for the absorption calculation may contain multiple tags groups for the same molecular species, for example corresponding to different isotopes or even individual spectral lines. For the broadening and shift calculation we always use the VMR belonging to the first tag group. For example, if the species list is [“H2O-161”,“H2O-181”,“O3-666”,“O3-668”], then the VMRs of “H2O-161” and “O3-666” will be the ones that are used for the broadening and shift calculations.

Caveat 2: If the species to which the line belongs is equal to one of the broadening species, then the VMR of the species itself will be used for broadening, even if it is not first in the list. With the same absorption species as above, if the line that we are working on belongs to “O3-668”, then the VMRs of “H2O-161” and “O3-668” will be used for the calculation, and the VMR of “O3-666” will be ignored.

Both these caveats mean that the broadening calculation may give unexpected results in the presence of drastically different VMRs that belong to the same molecular species, because in that case it makes a difference which of the VMR is selected for broadening.

### 2.1.4 Species-specific data in ARTS

A line absorption species in ARTS is a particular isotopologue of a particular molecule. Quantities such as the molecular mass and the isotopologue ratio are specific and constant for each species. Here is a list of all species-specific information that is needed:

- Molecule name
- Isotopologue name
- Isotopologue ratio
- Molecular mass
- Corresponding tag in different catalogues (MYTRAN, HITRAN, JPL)

- Partition function data

These data are currently stored in two source code files, `species_data.cc` and `partition_function_data.cc`. That is, these values are basically hard-coded. However, at present at least isotopologue ratios can be replaced via controlfile settings, which is useful, e.g., for calculations for other planets.

*Buehler et al.* [2005] contains an explicit list of species that were implemented at the time of writing of that article. We do not include such a list here, because it is hard to maintain. Instead, we directly refer the user to check for the implemented species directly in file `species_data.cc`. There, also the different sources of data are documented.

#### Partition function data

ARTS uses third order polynomials to approximate partition functions, so four polynomial coefficients have to be stored for each isotopologue species. These data are stored in file `partition_function_data.cc`. The file also contains documentation, including the source of the data for the different species.

The consistency of partition function data from different sources, and the impact of partition function errors on sub-millimeter wave limb sounder retrievals, was studied in detail in *Verdes et al.* [2005]. The partition function data collection in ARTS is based on that study.

In general, the data in general are derived from the following sources:

**TIPS:** Default.

**JPL:** Only species (including individual isotopologues) not covered by TIPS.

**Agnes Perrin:** Personal communication, only for species BrO.

The TIPS program is developed and maintained by B. Gamache. In conjunction with HITRAN it is the suggested way to derive the partition functions and is part of the HITRAN distributions. More recent versions might be available via B. Gmache's website (`http://faculty.uml.edu/robert_gamache/`, 'Software and Data' section). TIPS covers all molecular species and isotopolgues found in the respective version of the HITRAN database. Often it includes some more species than HITRAN, and extensions for other species (e.g., species of astrophysical interest) can be derived from the Gamache website.

Earlier versions of TIPS (until at least 1997) provided 3rd order polynomial coefficients, which were then used in ARTS. Newer versions (from at latest 2003) provide partition functions for a specific molecule and isotopologue at a specific temperature, and tabulated values can be obtained through successive runs of the program. Polynomial coefficients then need to be derived by a fit to the TIPS output. Here, partition functions were calculated on a 1K-step grid, and the polynomial coefficients derived by a least-square fit between 150 – 300 K (unless otherwise noted in `partition_function_data.cc`).

The coefficients for the few species which are not covered in TIPS are calculated from JPL values. The JPL catalogue has a different way to calculate the partition function. It provides the partition function at a set of specific temperatures: 300, 225, 150, 75, 37.5, 18.75, 9.375 K. An interpolation scheme is given for values inbetween: the partition functions are assumed to be proportional to $T^{1.5}$ for non-linear molecules (degrees of freedom: 3) and proportional to $T$ for linear molecules (degrees of freedom 2). From these data polynomial coefficients are derived in the same way as from TIPS output: first, partition functions are tabulated on a 1K-step grid, then a least-square fit over T = 150 – 300 K is performed.

The partition function data for BrO were provided by Agnes Perrin, Orsay, France.

The temperature range used for deriving the polynomial fit was judged to be representative of the range of temperatures occuring in the Earth atmosphere. For calculations in planetary atmospheres it might be advantageous being able to use other data, e.g. such derived for temperatures prevailing there. We are exploring options to allow for that (e.g., read data from include files as done for isotopologue ratios, or replacement of parameterized partition functions by directly calculated ones through embedding TIPS and the JPL scheme in ARTS).

## 2.2 Continuum absorption

As pointed out above, some molecules show beside the resonant line absorption also non-resonant continuum absorption. The main qualitative difference is the smooth dependence on frequency of the non-resonant absorption part in contrast to the resonant absorption part who shows strong local maxima and minima.

The implemented continuum absorption modules are connected with water vapor ($H_2O$), oxygen ($O_2$), nitrogen ($N_2$), and carbon dioxide ($CO_2$). Since these molecules have various permanent electric or magnetic multipoles, the physical explanations for the continuum absorption is different for each of these molecules.

Water Vapor has a strong electric dipole moment and posses therefore a wealth of rotational transitions in the microwave up to the submillimeter range. One explanation for the $H_2O$-continuum absorption is the inadequate formulation of the far wings of a spectral line, since the usually employed *Van Vleck and Weisskopf* [1945] line shape is according to its derivation only valid in the near wing zone. Other explanations are (see *Rosenkranz* [1993] for details) far wing contribution from far-infrared water vapor lines, collision induced absorption (CIA), and water polymer absorption. At present one can not definitively decide which of these possibilities is the correct one, probably all of them play a more or less important role, depending on the frequency range.

Oxygen is special, because it has no permanent electric dipole moment, but a permanent magnetic dipole moment. The aligned spins of the two valence electrons gives a $^3\Sigma$ ground state of molecular oxygen. Due to the selection rules for magnetic dipole transitions, transitions with resonance frequency equal to zero are allowed. Such transitions have a characteristic Debye line shape function.

The homonuclear nitrogen molecule has in lowest order an electric quadrupole moment of modest magnitude. For the frequency range below 1 THz the collision induced rotation absorption band [*Goody and Yung*, 1989] is of most importance. The band center is around 3 THz and at 1 THz the band strength is approximately 1/6 of the maximum value (see Figure 5.2 of *Goody and Yung* [1989]). The electric field of the quadrupole moment of one molecule induces a dipole moment in the second molecule. This allows rotational transitions according to the electric quadrupole selection rules, $|\Delta J| = 0,2$ (see *Rosenkranz* [1993] for details).

In a similar way, carbon dioxide also exhibits a collision induced absorption band (maximum around 1.5 THz, Figure 5.10 of *Goody and Yung* [1989]). Characteristic for collision induced absorption is the dependency on the square of the molecular density.

### 2.2.1 Water vapor continuum models

As shown by *Liebe and Layton* [1987], *Rosenkranz* [1998], and *Ma and Tipping* [1990], the water vapor continuum absorption can be well described by

$$\alpha_{\mathrm{c}} = \nu^2 \cdot \Theta^3 \cdot (C^{\mathrm{o}}_{\mathrm{H_2O}} \cdot P^2_{\mathrm{H2O}} \cdot \Theta^{\mathrm{ns}} + C^{\mathrm{o}}_{\mathrm{d}} \cdot P_{\mathrm{H2O}} \cdot P_{\mathrm{d}} \cdot \Theta^{\mathrm{nf}}) \tag{2.31}$$

where the microwave approximation ($h\nu \ll k_B T$ ) of the radiation field term is already applied. The adjustment of Eq. 2.31 to the data is performed through the parameter set $C^{\mathrm{o}}_{\mathrm{H_2O}}$, $\mathrm{n_s}$, $C^{\mathrm{o}}_{\mathrm{d}}$, and $\mathrm{n_f}$. Table 2.2 gives some commonly used continuum parameter sets.

| model | $C^{\mathrm{o}}_{\mathrm{H_2O}}$ $\left[\frac{\mathrm{dB/km}}{\mathrm{hPa^2\ GHz^2}}\right]$ | $\mathrm{n_s}$ [1] | $C^{\mathrm{o}}_{\mathrm{d}}$ $\left[\frac{\mathrm{dB/km}}{\mathrm{hPa^2\ GHz^2}}\right]$ | $\mathrm{n_d}$ [1] | ref. |
|---|---|---|---|---|---|
| MPM87 | $6.50 \cdot 10^{-8}$ | 7.5 | $0.206 \cdot 10^{-8}$ | 0.0 | *Liebe and Layton* [1987] |
| MPM89 | $6.50 \cdot 10^{-8}$ | 7.3 | $0.206 \cdot 10^{-8}$ | 0.0 | *Liebe* [1989] |
| CP98 | $8.04 \cdot 10^{-8}$ | 7.5 | $0.254 \cdot 10^{-8}$ | 0.0 | *Cruz Pol et al.* [1998] |
| PWR98 | $7.80 \cdot 10^{-8}$ | 4.5 | $0.236 \cdot 10^{-8}$ | 0.0 | *Rosenkranz* [1998] |
| MPM93* | $7.73 \cdot 10^{-8}$ | 4.55 | $0.253 \cdot 10^{-8}$ | 1.55 | *Liebe et al.* [1993] |

Table 2.2: Values of commonly used continuum parameter sets. The last line (MPM93*) represents an approximation of the pseudo-line continuum of MPM93 in the form of Eq. 2.31.

#### The MPM93 continuum parameterization

In the MPM93 model [*Liebe et al.*, 1993], the water vapor continuum is treated as a pseudo-line located in the far infrared around 2 THz. The pseudo-line continuum has therefore not four but seven parameters, the pseudo-line center frequency ($\nu^*$) and the six pseudo-line parameters ($\mathrm{b}^*_1,\cdots,\mathrm{b}^*_6$):

$$\alpha^{\mathrm{MPM93}}_{\mathrm{c}} = 0.1820 \cdot \frac{\mathrm{b}^*_1}{\nu^*} \cdot P_{\mathrm{H2O}} \cdot \Theta^{3.5} \cdot \exp\left(\mathrm{b}^*_2 \cdot (1-\Theta)\right) \cdot \nu^2 \cdot F_c(\nu,\nu_{\mathrm{k}}) \tag{2.32}$$

$$F_c(\nu,\nu_{\mathrm{k}}) = \left[\frac{\gamma_{\mathrm{c}}}{(\nu^*+\nu)^2+\gamma^2_{\mathrm{c}}} + \frac{\gamma_{\mathrm{c}}}{(\nu^*-\nu)^2+\gamma^2_{\mathrm{c}}}\right] \tag{2.33}$$

$$\gamma_{\mathrm{c}} = \mathrm{b}^*_3 \cdot \left(\mathrm{b}^*_4 \cdot \mathrm{P_{H2O}} \cdot \Theta^{\mathrm{b}^*_6} + \mathrm{P_d} \cdot \Theta^{\mathrm{b}^*_5}\right) \tag{2.34}$$

Table 2.3 lists the values of this continuum parameter set. It is remarkable that all these parameters are much larger compared to the physical water vapor line parameters of the same model. The only exception is $\mathrm{b}^*_2$, the parameter which governs the exponential temperature behavior of the line strength. The magnitude of the pseudo-line width is shown for four

| $\nu^*$ [GHz] | $\mathrm{b}^*_1$ $[\frac{\mathrm{kHz}}{\mathrm{hPa}}]$ | $\mathrm{b}^*_2$ [1] | $\mathrm{b}^*_3$ $[\frac{\mathrm{MHz}}{\mathrm{hPa}}]$ | $\mathrm{b}^*_4$ [1] | $\mathrm{b}^*_5$ [1] | $\mathrm{b}^*_6$ [1] |
|---|---|---|---|---|---|---|
| 1780.000 | 2230.000 | 0.952 | 17.620 | 30.50 | 2.00 | 5.00 |

Table 2.3: List of the MPM93 pseudo-line water vapor continuum parameters.

| | contribution | | total |
|---|---|---|---|
| | $H_2O$–$H_2O$ | $H_2O$–air | |
| $\gamma_c(200\,K)$ | 40.8 GHz | 80.4 GHz | 121.2 GHz |
| $\gamma_c(300\,K)$ | 5.4 GHz | 23.0 GHz | 28.4 GHz |

Table 2.4: Magnitude of the line width of the pseudo-line of the continuum term in MPM93. Assumed is a total pressure of 1000 hPa and a water vapor partial pressure of 10 hPa.

different cases in Table 2.4.

This change of continuum parameterization makes it difficult to compare MPM93 with the models which use Eq. (2.31). However, with respect to microwave frequencies, the line shape function, $F_c(\nu)$, can be approximated since the magnitude of the pseudo-line width is much smaller compared to the distance between microwave frequencies and $\nu^*$, as shown for four different cases in Table 2.4:

$$F_c(\nu, \nu_k) \approx 2 \cdot \frac{\gamma_c}{\nu_c^2} \tag{2.35}$$

Inserting Eq. (2.35) into Eq. (2.32) gives a quadratic frequency dependence of the MPM93 continuum, similar to the continuum parameterization expressed in Eq. (2.31). By additionally approximating the temperature dependence to the simple form

$$\begin{aligned} n_s \cdot \ln(\Theta) &= \ln\left(\Theta^{3.5} \cdot e^{b_2^* \cdot (1-\Theta)}\right) \\ n_s &= 3.5 + b_2^* \cdot \frac{1-\Theta}{\ln(\Theta)} \\ n_s &\approx 3.5 - b_2^* = 2.55 \qquad \text{with} \;\; \ln(\Theta) \approx (\Theta - 1) \end{aligned} \tag{2.36}$$

one can rearrange the pseudo-line continuum to fit Eq. (2.31) (denoted by MPM93*). The so deduced continuum parameter set is given in Table 2.2.
The MPM93* continuum parameters $C^o_{H_2O}$ and $C^o_d$ are 20 % and 15 % larger, respectively, than in the case of MPM87/MPM89. Large discrepancies exist for the temperature exponents $n_s$ and $n_d$ between MPM93* and earlier model versions. The exponent $n_s$ is in MPM93* only 60 % of the corresponding value in MPM89 and the temperature dependence of the $H_2O$-air term is significant larger than for earlier MPM versions. This reduction of $n_s$ is mainly due to additional measurements considered in MPM93 [*Becker and Autler*, 1946; *Godon et al.*, 1992], while the continuum parameters in MPM87/MPM89 are determined by a single laboratory measurement at 138 GHz.

### 2.2.2 Oxygen continuum absorption

As pointed out by *Van Vleck* [1987], the standard theory for non-resonant absorption is that of Debye (see also *Townes and Schawlow* [1955]). The Debye line shape is obtained from the VVW line shape function by the limiting case $\nu_k \rightarrow 0$. Both, *Liebe et al.* [1993] and *Rosenkranz* [1993] adopted the Debye theory for their models. The only difference is the formulation of the line broadening, where the influence of water vapor is treated slightly different:

$$\alpha_c = C \cdot P_d \cdot \Theta^2 \cdot \frac{\nu^2 \cdot \gamma}{\nu^2 + \gamma^2} \tag{2.37}$$

$$\gamma = w \cdot (P_\mathrm{d} \cdot \Theta^{0.8} + 1.1 \cdot P_\mathrm{H2O} \cdot \Theta) \quad : \text{Rosenkranz} \tag{2.38}$$
$$\gamma = w \cdot P_\mathrm{tot} \cdot \Theta^{0.8} \quad : \text{MPM93} \tag{2.39}$$

where $P_\mathrm{d}$ denotes the dry air partial pressure ($P_\mathrm{d} = P_\mathrm{tot} - P_\mathrm{H2O}$). The value for the strength is $C = 2.56 \cdot 10^{-20}$ 1/(m Pa Hz) in the case of the Rosenkranz model and $C = 2.57 \cdot 10^{-20}$ 1/(m Pa Hz) in the case of the MPM93 model. The MPM93 value for $C$ is therefore about 0.4 % larger than in the Rosenkranz model. Since the volume mixing ratio of oxygen in dry air is constant in the lower Earth atmosphere (0.20946 [*Goody*, 1995]), both models incorporate the oxygen $VMR$ ($VMR_{O_2}$) in the constant $C$. In the arts model the separation between the oxygen $VMR$ and the constant $C$ is explicitely done. In this case follows:

$$C = 0.20946 \cdot \widehat{C} \tag{2.40}$$
$$\widehat{C} = 1.22 \cdot 10^{-19} \text{ [1/(m Hz Pa)]} \quad : \text{Rosenkranz} \tag{2.41}$$
$$\widehat{C} = 1.23 \cdot 10^{-19} \text{ [1/(m Hz Pa)]} \quad : \text{MPM93} \tag{2.42}$$

The width parameter $w$ is in both models the same, $w = 5.6 \cdot 10^3$ Hz/Pa. If we define the width $\gamma$ in a more general way like

$$\gamma = w \cdot (A \cdot P_\mathrm{d} \cdot \Theta^{n_d} + B \cdot P_\mathrm{H2O} \cdot \Theta^{n_w}) \tag{2.43}$$

we can fit both models, the Rosenkranz and the MPM93 model, into the same parameterization with ($A = 1$, $B = 1.1$, $n_d = 0.8$, $n_w = 1.0$) for the Rosenkranz model and ($A = 1.0$, $B = 1.0$, $n_d = 0.8$, $n_w = 0.8$) for MPM93.

The oxygen continuum absorption term is proportional to the collision frequency of a single oxygen molecule with other air molecules and thus proportional to the dry air pressure[1].

### 2.2.3 Nitrogen continuum absorption

Since molecular nitrogen has in its unperturbed state no electric or magnetic dipole moment (but an electric quadrupole moment), it shows no rotational spectral signature in the microwave region. Regardless of this, nitrogen absorbs radiation in this frequency range due to collision induced absorption (CIA). Far–infrared roto-translational band structures from free–free interactions give rise to far wing absorption below 1 THz.

Different parameterizations of this absorption term for the frequency range below 1 THz are available *Rosenkranz* [1993]; *Liebe et al.* [1993]; *Borysow and Frommhold* [1986]. Common to all these models is the quadratic dependency on $N_2$ partial pressure which is a direct consequence of the underlying CIA processes involved. The simplest model is given by *Rosenkranz* [1993], which uses the same parameterization as for the water vapor continuum, described in Equation 2.31:

$$\alpha_\mathrm{c} = C \cdot \nu^{n_\nu} \cdot \Theta^{n_T} \cdot P_\mathrm{N2}^{n_p} \tag{2.44}$$

with $C = 4.56 \cdot 10^{-13}$ dB/(km hPa$^2$ GHz$^2$), $n_\nu = 2$, $n_T = 3.55$, and $n_p = 2$, respectively. The laboratory data set for the determination of $C$ is manly from *Dagg et al.* [1975, 1978] around 70 and 140 GHz, respectively.

[1] The absorption due to weakly bound complexes of $O_2$–$X$ with $X = H_2O,\ N_2$ is treated separately and therefore not included in this Debye formula.

The MPM models has compared with Equation 2.44 an additional frequency dependent term which leads to the following expression

$$\alpha_c = \widehat{C} \cdot (1.0 - 1.2 \cdot 10^{-5} \cdot \nu^{1.5}) \cdot \nu^2 \cdot \Theta^{3.5} \cdot P_d^2 \quad : \text{MPM89} \tag{2.45}$$

$$\alpha_c = \widehat{C} \cdot \frac{\nu^2}{(1.0 + a \cdot \nu^{n_\nu})} \cdot \Theta^{3.5} \cdot P_d^2 \quad : \text{MPM93} \tag{2.46}$$

$$a =$$

where the parameter is $\widehat{C} = 2.55 \cdot 10^{-13}$ dB/(km hPa$^2$ GHz$^2$), $a$ =1.9·10$^{-5}$ GHz$^{-n_\nu}$, and $n_\nu$ = 1.5. based on data from *Stankevich* [1974] and *Stone et al.* [1984]. With respect to the 22 GHz water vapor line, the additional frequency terms in brackets in Equations 2.45 and 2.46 are nearly unity and therefore not essential. Therefore all three parameterizations have the same frequency and temperature relationship, but the absolute magnitude is in the case of Rosenkranz 80 % higher compared with the MPM models.

The model of Borysow and Frommhold[2] is somewhat different since their focus is mainly on the radiative transfer in the Titan's atmosphere with the infrared interferometer spectrometer, IRIS, on board the Voyager Spacecraft. This detailed model is primarily designed to parameterize each of the roto-translational spectral lines around 200 cm$^{-1}$ ($\approx$ 6 THz) accurately. The analyzed data set incorporate the data source used by the Rosenkranz but is largely extended with measurements in the far–infrared.

### 2.2.4 Carbon dioxide continuum absorption

*Rosenkranz* [1993] gives a similar parameterization for the $CO_2$-continuum absorption term as for the nitrogen continuum, with

$$\alpha_c = \cdot \nu^2 \cdot \left[ C_s \cdot P_{CO2}^2 \cdot \Theta^{n_s} + C_f \cdot P_{CO2} \cdot P_{N2} \cdot \Theta^{n_f} \right] \tag{2.47}$$

where the parameter values $C_s = 3.23 \cdot 10^{-11}$ dB/(km hPa$^2$ GHz$^2$), $C_f = 1.18 \cdot 10^{-11}$ dB/(km hPa$^2$ GHz$^2$), $n_s = 5.08$, and $n_f = 4.7$, respectively, are determined from laboratory measurements of *Ho et al.* [1966]; *Dagg et al.* [1975]. Since the foreign term includes only nitrogen as perturber, one can get an estimate for dry air by replacing $P_{N2}$ by the dry air partial pressure in Equation 2.47. Because nitrogen is usually a more efficient perturber than oxygen, this estimation can be regarded as an upper limit. Concerning the Earth's atmosphere, the foreign broadening term is more interesting since the carbon dioxide partial pressure is only approximately 0.04 % of the nitrogen partial pressure up to 90 km.

## 2.3 Complete absorption models

The MPM absorption model of Liebe and coworkers consists of modules for water vapor and oxygen absorption. The Rosenkranz (PWR98) absorption model include also $H_2O$ and $O_2$ while the Cruz-Pol et al. (CP98) absorption models include absorption due to water vapor. Additionally the CP98 model has a strongly reduced parameter set for the $H_2O$-line absorption since it is especially intended for the range around the 22 GHz water line. The MPM and R98 are valid from the microwave up to the submillimeter frequency range (1-1000 GHz).

Implemented in ARTS are the following modules of the above mentioned models:

[2] the source code of this model can be downloaded from the home page of A. Borysow: http://www.astro.ku.dk/~aborysow/

| species | model |
|---|---|
| $H_2O$ | MPM87, MPM89, MPM93, PWR98, CP98 |
| $O_2$ | MPM93, PWR98 |

### 2.3.1 Complete water vapor models

In ARTS several complete water vapor absorption models are implemented and can easily be used. Implemented models are the versions MPM87 [*Liebe and Layton*, 1987], MPM89 [*Liebe*, 1989], and MPM93 [*Liebe et al.*, 1993] of the Liebe Millimeter-wave Propagation Model and additionally the models of Cruz-Pol et al. (CP98) [*Cruz Pol et al.*, 1998] and P. W. Rosenkranz (PWR98) [*Rosenkranz*, 1998]. MPM and PWR98 are especially desigend for fast absorption calculations in the frequency range of 1-1000 GHz while the CP98 model is a reduced model for a narrow frequency band around the 22 GHz $H_2O$-line (especially used by ground-based radiometers).

The total water vapor absorption ($\alpha_{\rm tot}$) is in all the stated models described by a line absorption ($\alpha_\ell$) term and a continuum absorption ($\alpha_{\rm c}$) term:

$$\alpha_{\rm tot} = \alpha_\ell + \alpha_{\rm c} \tag{2.48}$$

The main differences between the different models is the line shape used for $\alpha_\ell$ and the formulation of $\alpha_{\rm c}$.

It has to be emphasized that, $\alpha_\ell$ and $\alpha_{\rm c}$ of different models are not necessarily compatible and should therefore not be interchanged between different models.

#### MPM87 water vapor absorption model

This version, which is described in *Liebe and Layton* [1987] and follows the general line of the MPM model to divide the total water vapor absorption, $\alpha_{\rm tot}^{\rm MPM87}$, into a spectral line term, $\alpha_\ell^{\rm MPM87}$, and a continuum term not attributed to spectral lines, $\alpha_{\rm c}^{\rm MPM87}$:

$$\alpha_{\rm tot}^{\rm MPM87} = \alpha_\ell^{\rm MPM87} + \alpha_{\rm c}^{\rm MPM87} \qquad \text{dB/km} \tag{2.49}$$

**Water vapor line absorption:** The MPM87 [*Liebe and Layton*, 1987] water vapor line catalog consists of 30 lines from 22 GHz up to 988 GHz. The center frequencies and parameter values are listed in Table 2.5. To describe the line absorption, a set of three parameters ($\rm b_{1,k}$ and $\rm b_{3,k}$) per line are used: two for the line strength and one for the line width. The total line absorption coefficient (in units of dB/km) is the sum over all individual line absorption coefficients[3]:

$$\alpha_\ell^{\rm MPM87} = 0.1820 \cdot \nu_{\rm k} \cdot P_{\rm H2O} \cdot \sum_k S_{\rm k}(T) \cdot F(\nu, \nu_{\rm k}) \qquad \text{dB/km} \tag{2.50}$$

where $S_{\rm k}(T)$ is the line intensity described by the parameterization

$$S_{\rm k}(T) = \rm b_{1,k} \cdot P_{H2O} \cdot \Theta^{3.5} \cdot \exp\left(b_{2,k} \cdot [1 - \Theta]\right) \qquad \text{kHz} \tag{2.51}$$

with $\nu_{\rm k}$ as the line center frequency, $P_{\rm H2O}$ the water vapor partial pressure and $\Theta = 300\,{\rm K}/T$.

[3] The factor $0.1820 \cdot 10^6$ is equal to $(4\,\pi/c) \cdot 10\log(e)$ (the term $(4\,\pi/c)$ comes from the definition of the absorption coefficient in terms of the dielectric constant and the term $10\,\log(e)$ is due to the definition of the Decibel.) The velocity of light is defined as $c = 2.9979 \cdot 10^{-4}$ km GHz. The factor $10^6$ is incorporated into the line strength and does therefore not appear in the pre-factor.

The line shape function, $F(\nu, \nu_\text{k})$, in Eq. (2.50) is the standard Van Vleck-Weisskopf (VVW) function, given by:

$$F(\nu, \nu_\text{k}) = \left(\frac{\nu}{\nu_\text{k}}\right) \cdot \left[\frac{\gamma_\text{k}}{(\nu - \nu_\text{k})^2 + \gamma_\text{k}^2} + \frac{\gamma_\text{k}}{(\nu + \nu_\text{k})^2 + \gamma_\text{k}^2}\right] \tag{2.52}$$

(2.53)

The pressure broadened line width, $\gamma_\text{k}$, is calculated with the single parameter $\text{b}_{3,\text{k}}$ in the following way:

$$\gamma_\text{k} = \text{b}_{3,\text{k}} \cdot (4.80 \cdot \text{P}_{\text{H2O}} \cdot \Theta^{1.1} + \text{P}_\text{d} \cdot \Theta^{0.6}) \qquad \text{GHz} \tag{2.54}$$

where $P_\text{d}$ is the partial pressure of dry air ($P_\text{d} = P_\text{tot} - P_{\text{H2O}}$). The parameterizations of $S_\text{k}(T)$ and $\gamma_\text{k}$ are already in use for the early version of MPM81 [*Liebe*, 1981].

| $k$ | $\nu_k$ [GHz] | $\text{b}_{1,\text{k}}$ $[\frac{\text{kHz}}{\text{kPa}}]$ | $\text{b}_{2,\text{k}}$ [1] | $\text{b}_{3,\text{k}}$ $[\frac{\text{GHz}}{\text{kPa}}]$ |
|---|---|---|---|---|
| 1 | 22.235080 | 0.1090 | 2.143 | $27.84 \cdot 10^{-3}$ |
| 2 | 67.813960 | 0.0011 | 8.730 | $27.60 \cdot 10^{-3}$ |
| 3 | 119.995940 | 0.0007 | 8.347 | $27.00 \cdot 10^{-3}$ |
| 4 | 183.310117 | 2.3000 | 0.653 | $31.64 \cdot 10^{-3}$ |
| 5 | 321.225644 | 0.0464 | 6.156 | $21.40 \cdot 10^{-3}$ |
| 6 | 325.152919 | 1.5400 | 1.515 | $29.70 \cdot 10^{-3}$ |
| 7 | 336.187000 | 0.0010 | 9.802 | $26.50 \cdot 10^{-3}$ |
| 8 | 380.197372 | 11.9000 | 1.018 | $30.36 \cdot 10^{-3}$ |
| 9 | 390.134508 | 0.0044 | 7.318 | $19.00 \cdot 10^{-3}$ |
| 10 | 437.346667 | 0.0637 | 5.015 | $13.70 \cdot 10^{-3}$ |
| 11 | 439.150812 | 0.9210 | 3.561 | $16.40 \cdot 10^{-3}$ |
| 12 | 443.018295 | 0.1940 | 5.015 | $14.40 \cdot 10^{-3}$ |
| 13 | 448.001075 | 10.6000 | 1.370 | $23.80 \cdot 10^{-3}$ |
| 14 | 470.888947 | 0.3300 | 3.561 | $18.20 \cdot 10^{-3}$ |
| 15 | 474.689127 | 1.2800 | 2.342 | $19.80 \cdot 10^{-3}$ |
| 16 | 488.491133 | 0.2530 | 2.814 | $24.90 \cdot 10^{-3}$ |
| 17 | 503.568532 | 0.0374 | 6.693 | $11.50 \cdot 10^{-3}$ |
| 18 | 504.482692 | 0.0125 | 6.693 | $11.90 \cdot 10^{-3}$ |
| 19 | 556.936002 | 510.0000 | 0.114 | $30.00 \cdot 10^{-3}$ |
| 20 | 620.700807 | 5.0900 | 2.150 | $22.30 \cdot 10^{-3}$ |
| 21 | 658.006500 | 0.2740 | 7.767 | $30.00 \cdot 10^{-3}$ |
| 22 | 752.033227 | 250.0000 | 0.336 | $28.60 \cdot 10^{-3}$ |
| 23 | 841.073593 | 0.0130 | 8.113 | $14.10 \cdot 10^{-3}$ |
| 24 | 859.865000 | 0.1330 | 7.989 | $28.60 \cdot 10^{-3}$ |
| 25 | 899.407000 | 0.0550 | 7.845 | $28.60 \cdot 10^{-3}$ |
| 26 | 902.555000 | 0.0380 | 8.360 | $26.40 \cdot 10^{-3}$ |
| 27 | 906.205524 | 0.1830 | 5.039 | $23.40 \cdot 10^{-3}$ |
| 28 | 916.171582 | 8.5600 | 1.369 | $25.30 \cdot 10^{-3}$ |
| 29 | 970.315022 | 9.1600 | 1.842 | $24.00 \cdot 10^{-3}$ |
| 30 | 987.926764 | 138.0000 | 0.178 | $28.60 \cdot 10^{-3}$ |

Table 2.5: List of $H_2O$ spectral lines and their spectroscopic parameters ($H_2O$-air mixture) for the MPM87 model [*Liebe and Layton*, 1987].

**Water vapor continuum absorption:** The water vapor continuum absorption coefficient in MPM87, $\alpha_c^{\mathrm{MPM87}}$, is determined from laboratory measurements at 137.8 GHz by Liebe and Layton covering the following parameter range:

| | |
|---|---|
| temperature | 282-316 K |
| relative humidity | 0-95 % |
| dry air pressure | 0 - 160 kPa |

The mathematical expression of $\alpha_c^{\mathrm{MPM87}}$ is derived from the far wing approximation of the line absorption and is expressed as follows

$$\alpha_c^{\mathrm{MPM87}} = \nu^2 \cdot P_{\mathrm{H2O}} \cdot (C^{\mathrm{o}}_{\mathrm{H_2O}} \cdot P_{\mathrm{H2O}} \cdot \Theta^{\mathrm{ns}} + C^{\mathrm{o}}_{\mathrm{d}} \cdot P_{\mathrm{d}} \cdot \Theta^{\mathrm{n}}\mathrm{f}), \tag{2.55}$$

with the continuum parameter set $C^{\mathrm{o}}_{\mathrm{H_2O}}$, $C^{\mathrm{o}}_{\mathrm{d}}$, $\mathrm{n_s}$, and $\mathrm{n_f}$. The determined values of the continuum parameters are:

$C^{\mathrm{o}}_{\mathrm{H_2O}} = 6.496 \cdot 10^{-6}$ (dB/km) / (hPa·GHz)$^2$

$\mathrm{n_s} = 10.5$

$C^{\mathrm{o}}_{\mathrm{d}} = 0.206 \cdot 10^{-6}$ (dB/km) / (hPa·GHz)$^2$

$\mathrm{n_d} = 3.0$

### MPM89 water vapor absorption model

MPM89 is described in *Liebe* [1989] and follows the general line of the MPM model to devide the total water vapor absorption, $\alpha_{\mathrm{tot}}^{\mathrm{MPM89}}$, into a spectral line term, $\alpha_\ell^{\mathrm{MPM89}}$, and a continuum term not attributed to spectral lines, $\alpha_c^{\mathrm{MPM89}}$:

$$\alpha_{\mathrm{tot}}^{\mathrm{MPM89}} = \alpha_\ell^{\mathrm{MPM89}} + \alpha_c^{\mathrm{MPM89}} \qquad \mathrm{dB/km} \tag{2.56}$$

All the absorption coefficients are calculated in units of dB/km.

**Water vapor line absorption:** The MPM89 water vapor line catalog consists of the same 30 lines like MPM87 from 22 GHz up to 988 GHz. The center frequencies and parameter values are listed in Table 2.6. To describe the line absorption, a set of six parameters ($\mathrm{b_{1,k}}$ and $\mathrm{b_{6,k}}$) per line are used: two for the line strength and four for the line width. The total line absorption coefficient (in units of dB/km) is the sum over all individual line absorption coefficients[4]:

$$\alpha_\ell^{\mathrm{MPM89}} = 0.1820 \cdot \nu_{\mathrm{k}} \cdot P_{\mathrm{H2O}} \cdot \sum_k S_{\mathrm{k}}(T) \cdot F(\nu, \nu_{\mathrm{k}}) \qquad \mathrm{dB/km} \tag{2.57}$$

where $S_{\mathrm{k}}(T)$ is the line intensity described by the parameterization

$$S_{\mathrm{k}}(T) = \mathrm{b_{1,k}} \cdot \mathrm{P_{H2O}} \cdot \Theta^{3.5} \cdot \exp\left(\mathrm{b_{2,k}} \cdot [1-\Theta]\right) \qquad \mathrm{kHz} \tag{2.58}$$

whit $\nu_{\mathrm{k}}$ as the line center frequency, $P_{\mathrm{H2O}}$ the water vapor partial pressure and $\Theta = 300\,\mathrm{K}/T$.

[4] see footnote for MPM97 line absorption

The line shape function, $F(\nu, \nu_k)$, in Eq. (2.57) is the standard Van Vleck-Weisskopf (VVW) function, given by

$$F(\nu, \nu_k) = \left(\frac{\nu}{\nu_k}\right) \cdot \left[\frac{\gamma_k}{(\nu - \nu_k)^2 + \gamma_k^2} + \frac{\gamma_k}{(\nu + \nu_k)^2 + \gamma_k^2}\right] \tag{2.59}$$

where the pressure broadened line width, $\gamma_k$, is calculated as

$$\gamma_k = \mathrm{b}_{3,k} \cdot (\mathrm{b}_{5,k} \cdot \mathrm{P}_{H2O} \cdot \Theta^{\mathrm{b}_{6,k}} + \mathrm{P_d} \cdot \Theta^{\mathrm{b}_{4,k}}) \cdot 10^{-3} \qquad \mathrm{GHz} \tag{2.60}$$

with $P_d = P_{tot} - P_{H2O}$ as the dry air partial pressure. The only difference between MPM87 and MPM89 with respect to the line absorption is the parameterization of the pressure broadened line width, $\gamma_k$, which is calculated with the four parameters $\mathrm{b}_{3,k}$ to $\mathrm{b}_{6,k}$ in the case of MPM89 whereas in MPM87 a single parameter ($\mathrm{b}_{3,k}$) is used (see Eq. (2.54)).

| $k$ | $\nu_k$ [GHz] | $\mathrm{b}_{1,k}$ $[\frac{kHz}{kPa}]$ | $\mathrm{b}_{2,k}$ [1] | $\mathrm{b}_{3,k}$ $[\frac{MHz}{kPa}]$ | $\mathrm{b}_{4,k}$ [1] | $\mathrm{b}_{5,k}$ [1] | $\mathrm{b}_{6,k}$ [1] |
|---|---|---|---|---|---|---|---|
| 1 | 22.235080 | 0.1090 | 2.143 | 28.11 | 0.69 | 4.80 | 1.00 |
| 2 | 67.813960 | 0.0011 | 8.735 | 28.58 | 0.69 | 4.93 | 0.82 |
| 3 | 119.995940 | 0.0007 | 8.356 | 29.48 | 0.70 | 4.78 | 0.79 |
| 4 | 183.310074 | 2.3000 | 0.668 | 28.13 | 0.64 | 5.30 | 0.85 |
| 5 | 321.225644 | 0.0464 | 6.181 | 23.03 | 0.67 | 4.69 | 0.54 |
| 6 | 325.152919 | 1.5400 | 1.540 | 27.83 | 0.68 | 4.85 | 0.74 |
| 7 | 336.187000 | 0.0010 | 9.829 | 26.93 | 0.69 | 4.74 | 0.61 |
| 8 | 380.197372 | 11.9000 | 1.048 | 28.73 | 0.69 | 5.38 | 0.84 |
| 9 | 390.134508 | 0.0044 | 7.350 | 21.52 | 0.63 | 4.81 | 0.55 |
| 10 | 437.346667 | 0.0637 | 5.050 | 18.45 | 0.60 | 4.23 | 0.48 |
| 11 | 439.150812 | 0.9210 | 3.596 | 21.00 | 0.63 | 4.29 | 0.52 |
| 12 | 443.018295 | 0.1940 | 5.050 | 18.60 | 0.60 | 4.23 | 0.50 |
| 13 | 448.001075 | 10.6000 | 1.405 | 26.32 | 0.66 | 4.84 | 0.67 |
| 14 | 470.888947 | 0.3300 | 3.599 | 21.52 | 0.66 | 4.57 | 0.65 |
| 15 | 474.689127 | 1.2800 | 2.381 | 23.55 | 0.65 | 4.65 | 0.64 |
| 16 | 488.491133 | 0.2530 | 2.853 | 26.02 | 0.69 | 5.04 | 0.72 |
| 17 | 503.568532 | 0.0374 | 6.733 | 16.12 | 0.61 | 3.98 | 0.43 |
| 18 | 504.482692 | 0.0125 | 6.733 | 16.12 | 0.61 | 4.01 | 0.45 |
| 19 | 556.936002 | 510.0000 | 0.159 | 32.10 | 0.69 | 4.11 | 1.00 |
| 20 | 620.700807 | 5.0900 | 2.200 | 24.38 | 0.71 | 4.68 | 0.68 |
| 21 | 658.006500 | 0.2740 | 7.820 | 32.10 | 0.69 | 4.14 | 1.00 |
| 22 | 752.033227 | 250.0000 | 0.396 | 30.60 | 0.68 | 4.09 | 0.84 |
| 23 | 841.073593 | 0.0130 | 8.180 | 15.90 | 0.33 | 5.76 | 0.45 |
| 24 | 859.865000 | 0.1330 | 7.989 | 30.60 | 0.68 | 4.09 | 0.84 |
| 25 | 899.407000 | 0.0550 | 7.917 | 29.85 | 0.68 | 4.53 | 0.90 |
| 26 | 902.555000 | 0.0380 | 8.432 | 28.65 | 0.70 | 5.10 | 0.95 |
| 27 | 906.205524 | 0.1830 | 5.111 | 24.08 | 0.70 | 4.70 | 0.53 |
| 28 | 916.171582 | 8.5600 | 1.442 | 26.70 | 0.70 | 4.78 | 0.78 |
| 29 | 970.315022 | 9.1600 | 1.920 | 25.50 | 0.64 | 4.94 | 0.67 |
| 30 | 987.926764 | 138.0000 | 0.258 | 29.85 | 0.68 | 4.55 | 0.90 |

Table 2.6: List of $H_2O$ spectral lines and their spectroscopic parameters ($H_2O$-air mixture) for the MPM89 model [*Liebe*, 1989].

**Water vapor continuum absorption:** The MPM89 continuum absorption coefficients in, $\alpha_c^{\mathrm{MPM89}}$, are identical as those in MPM87 (see Sec. 2.3.1 for details):

$$\alpha_c^{\mathrm{MPM89}} = \nu^2 \cdot P_{\mathrm{H2O}} \cdot (C^{\mathrm{o}}_{\mathrm{H_2O}} \cdot P_{\mathrm{H2O}} \cdot \Theta^{\mathrm{ns}} + C^{\mathrm{o}}_{\mathrm{d}} \cdot P_{\mathrm{d}} \cdot \Theta^{\mathrm{n}_\mathrm{f}}), \tag{2.61}$$

with

$C^{\mathrm{o}}_{\mathrm{H_2O}} = 6.496 \cdot 10^{-6}$ (dB/km) / (hPa·GHz)$^2$

$\mathrm{n_s} = 10.5$

$C^{\mathrm{o}}_{\mathrm{d}} = 0.206 \cdot 10^{-6}$ (dB/km) / (hPa·GHz)$^2$

$\mathrm{n_d} = 3.0$

### MPM93 water vapor absorption model

This version, which is described in *Liebe et al.* [1993] and follows the general line of the MPM model to devide the total water vapor absorption, $\alpha_{\mathrm{tot}}^{\mathrm{MPM93}}$, into a spectral line term, $\alpha_\ell^{\mathrm{MPM93}}$, and a continuum term not attributed to spectral lines, $\alpha_c^{\mathrm{MPM93}}$:

$$\alpha_{\mathrm{tot}}^{\mathrm{MPM93}} = \alpha_\ell^{\mathrm{MPM93}} + \alpha_c^{\mathrm{MPM93}} \qquad \mathrm{dB/km} \tag{2.62}$$

The continuum absorption is parameterized like a resonant spectral line of $H_2O$, a so-called pseudo-line. This is a fundamental change in the parameterization of the water vapor continuum in respect to all older versions of MPM, which makes it quite complicate to compare the different versions, especially to distinguish a self- and foreign broadening term in the continuum.

**Water vapor line absorption:** The water vapor line spectrum of MPM93 [*Liebe et al.*, 1993] consists of 34 lines below 1 THz (four more than in MPM89 and MPM87). To describe the MPM93 water vapor line absorption, a set of six parameters ($\mathrm{b_{1,k}}$ and $\mathrm{b_{3,k}}$) per line are used: two for the line strength and four for the line width. The total line absorption coefficient (in units of dB/km) is the sum over all individual line absorption coefficients[5]:

$$\alpha_\ell^{\mathrm{MPM93}} = 0.1820 \cdot \nu_{\mathrm{k}} \cdot P_{\mathrm{H2O}} \cdot \sum_k S_{\mathrm{k}}(T) \cdot F(\nu, \nu_{\mathrm{k}}) \qquad \mathrm{dB/km} \tag{2.63}$$

where $S_{\mathrm{k}}(T)$ is the line intensity described by the parameterization

$$S_{\mathrm{k}}(T) = \mathrm{b_{1,k}} \cdot \mathrm{P_{H2O}} \cdot \Theta^{3.5} \cdot \exp\left(\mathrm{b_{2,k}} \cdot [1-\Theta]\right) \qquad \mathrm{kHz} \tag{2.64}$$

with $\nu_{\mathrm{k}}$ as the line center frequency, $P_{\mathrm{H2O}}$ the water vapor partial pressure and $\Theta = 300\,\mathrm{K}/T$.
The line shape function, $F(\nu, \nu_{\mathrm{k}})$, in Eq. (2.50) is the standard Van Vleck-Weisskopf (VVW) function, given by:

$$F(\nu, \nu_{\mathrm{k}}) = \left(\frac{\nu}{\nu_{\mathrm{k}}}\right) \cdot \left[\frac{\gamma_{\mathrm{k}}}{(\nu-\nu_{\mathrm{k}})^2 + \gamma_{\mathrm{k}}^2} + \frac{\gamma_{\mathrm{k}}}{(\nu+\nu_{\mathrm{k}})^2 + \gamma_{\mathrm{k}}^2}\right] \tag{2.65}$$

(2.66)

[5]see footnote for MPM97 line absorption

The pressure broadened line width, $\gamma_k$, is calculated with the single parameter $b_{3,k}$ in the following way:

$$\gamma_k = b_{3,k} \cdot (4.80 \cdot P_{H2O} \cdot \Theta^{1.1} + P_d \cdot \Theta^{0.6}) \qquad \text{GHz} \tag{2.67}$$

where $P_d$ is the partial pressure of dry air ($P_d = P_{tot} - P_{H2O}$).

The parameterizations of $S_k(T)$ was already in use for the early version of MPM81 [*Liebe*, 1981]. The expression for $\gamma_k$ is the same as in MPM89. The main difference between MPM93 and MPM89 concerning the water vapor line absorption is the updated line catalog.

| $k$ | $\nu_k$ [GHz] | $b_{1,k}$ [$\frac{kHz}{hPa}$] | $b_{2,k}$ [1] | $b_{3,k}$ [$\frac{MHz}{hPa}$] | $b_{4,k}$ [1] | $b_{5,k}$ [1] | $b_{6,k}$ [1] |
|---|---|---|---|---|---|---|---|
| 1 | 22.235080 | 0.01130 | 2.143 | 2.811 | 4.80 | 0.69 | 1.00 |
| 2 | 67.803960 | 0.00012 | 8.735 | 2.858 | 4.93 | 0.69 | 0.82 |
| 3 | 119.995940 | 0.00008 | 8.356 | 2.948 | 4.78 | 0.70 | 0.79 |
| 4 | 183.310091 | 0.24200 | 0.668 | 3.050 | 5.30 | 0.64 | 0.85 |
| 5 | 321.225644 | 0.00483 | 6.181 | 2.303 | 4.69 | 0.67 | 0.54 |
| 6 | 325.152919 | 0.14990 | 1.540 | 2.783 | 4.85 | 0.68 | 0.74 |
| 7 | 336.222601 | 0.00011 | 9.829 | 2.693 | 4.74 | 0.69 | 0.61 |
| 8 | 380.197372 | 1.15200 | 1.048 | 2.873 | 5.38 | 0.54 | 0.89 |
| 9 | 390.134508 | 0.00046 | 7.350 | 2.152 | 4.81 | 0.63 | 0.55 |
| 10 | 437.346667 | 0.00650 | 5.050 | 1.845 | 4.23 | 0.60 | 0.48 |
| 11 | 439.150812 | 0.09218 | 3.596 | 2.100 | 4.29 | 0.63 | 0.52 |
| 12 | 443.018295 | 0.01976 | 5.050 | 1.860 | 4.23 | 0.60 | 0.50 |
| 13 | 448.001075 | 1.03200 | 1.405 | 2.632 | 4.84 | 0.66 | 0.67 |
| 14 | 470.888947 | 0.03297 | 3.599 | 2.152 | 4.57 | 0.66 | 0.65 |
| 15 | 474.689127 | 0.12620 | 2.381 | 2.355 | 4.65 | 0.65 | 0.64 |
| 16 | 488.491133 | 0.02520 | 2.853 | 2.602 | 5.04 | 0.69 | 0.72 |
| 17 | 503.568532 | 0.00390 | 6.733 | 1.612 | 3.98 | 0.61 | 0.43 |
| 18 | 504.482692 | 0.00130 | 6.733 | 1.612 | 4.01 | 0.61 | 0.45 |
| $19^+$ | 547.676440 | 0.97010 | 0.114 | 2.600 | 4.50 | 0.70 | 1.00 |
| $20^+$ | 552.020960 | 1.47700 | 0.114 | 2.600 | 4.50 | 0.70 | 1.00 |
| 21 | 556.936002 | 48.74000 | 0.159 | 3.210 | 4.11 | 0.69 | 1.00 |
| 22 | 620.700807 | 0.50120 | 2.200 | 2.438 | 4.68 | 0.71 | 0.68 |
| $23^+$ | 645.866155 | 0.00713 | 8.580 | 1.800 | 4.00 | 0.60 | 0.50 |
| 24 | 658.005280 | 0.03022 | 7.820 | 3.210 | 4.14 | 0.69 | 1.00 |
| 25 | 752.033227 | 23.96000 | 0.396 | 3.060 | 4.09 | 0.68 | 0.84 |
| 26 | 841.053973 | 0.00140 | 8.180 | 1.590 | 5.76 | 0.33 | 0.45 |
| 27 | 859.962313 | 0.01472 | 7.989 | 3.060 | 4.09 | 0.68 | 0.84 |
| 28 | 899.306675 | 0.00605 | 7.917 | 2.985 | 4.53 | 0.68 | 0.90 |
| 29 | 902.616173 | 0.00426 | 8.432 | 2.865 | 5.10 | 0.70 | 0.95 |
| 30 | 906.207325 | 0.01876 | 5.111 | 2.408 | 4.70 | 0.70 | 0.53 |
| 31 | 916.171582 | 0.83400 | 1.442 | 2.670 | 4.78 | 0.70 | 0.78 |
| $32^+$ | 923.118427 | 0.00869 | 10.220 | 2.900 | 5.00 | 0.70 | 0.80 |
| 33 | 970.315022 | 0.89720 | 1.920 | 2.550 | 4.94 | 0.64 | 0.67 |
| 34 | 987.926764 | 13.21000 | 0.258 | 2.985 | 4.55 | 0.68 | 0.90 |
| | $\nu^*$ | $b_1^*$ | $b_2^*$ | $b_3^*$ | $b_4^*$ | $b_5^*$ | $b_6^*$ |

Table 2.7: (continued on next page)

| $\nu_k$ | $b_{1,k}$ | $b_{2,k}$ | $b_{3,k}$ | $b_{4,k}$ | $b_{5,k}$ | $b_{6,k}$ |
|---|---|---|---|---|---|---|
| [GHz] | $[\frac{kHz}{hPa}]$ | [1] | $[\frac{MHz}{hPa}]$ | [1] | [1] | [1] |
| 1780.000000 | 2230.00000 | 0.952 | 17.620 | 30.50 | 2.00 | 5.00 |

Table 2.7: List of used $H_2O$ spectral lines and their spectroscopic coefficients of $H_2O$ in air for the MPM93 model [*Liebe et al.*, 1993]. The last separated line is the unphysical pseudo-line used in MPM93. The lines which are marked with a "+" were not in the MPM87/MPM89 line catalog.

**The MPM93 continuum parameterization:** In the MPM93 version the water vapor continuum is parameterized as an ordinary spectral line (Eqs. (2.64, 2.65)). The parameters of this continuum "pseudo-line" ($\nu^*$, $b_1^*$, $b_2^*$, $b_3^*$, $b_4^*$, $b_5^*$, $b_6^*$) are given in Table 2.7. More details about this continuum parameterization and its microwave approximation can be found in Section 2.2.1 of this guide.

### CP98 water vapor absorption model

**Line absorption** component [*Cruz Pol et al.*, 1998] for the water vapor line absorption is based on MPM87 with the main difference that the line catalog consists of only a single line at $\nu_o = 22$ GHz. The contributions from the other lines is put into the water vapor continuum module. The line absorption is therefore very quickly calculated (in units of Np/km) according to the formula

$$\alpha_\ell^{\mathrm{CP98}} = 0.0419 \cdot S_0(T) \cdot F(\nu, \nu_\mathrm{k}) \qquad (2.68)$$

with

$$\begin{aligned} S_0(T) &= 0.0109 \cdot C_L \cdot P_{\mathrm{H2O}} \cdot \nu_0 \cdot \Theta^{3.5} \cdot \exp\left(2.143 \cdot [1 - \Theta]\right) \\ \gamma &= 0.002784 \cdot C_W \cdot (P_\mathrm{d} \cdot \Theta^{0.6} + 4.8 \cdot P_{\mathrm{H2O}} \cdot \Theta^{1.1}) \end{aligned} \qquad (2.69)$$

where $P_{\mathrm{H2O}}$ and $P_\mathrm{d}$ are the partial pressure of water vapor and dry air in units of hPa, respectively and the Van Vleck-Weisskopf line shape, $F(\nu, \nu_\mathrm{k})$. The numbers correspond to the line parameters form MPM87 for this special line and the factors $C_L$ and $C_W$ are adjustable scaling factors to match the model with the measurements. Setting the scaling factors to $C_L$=1.00 and $C_W$=1.00 leads to the same results as for MPM87. According to the parameter estimation of Cruz–Pol et al. best agreement between data and model is obtained with $C_L = 1.0639 \pm 0.016$ and $C_W = 1.0658 \pm 0.0096$. The correlation between these two scaling factors was found to be negligible, as can be seen from Table 2.8.

The main reason why the Cruz-Pol model (CP98) considers only one line lies in the fact that CP98 is especially designed for the data analysis in the 20-31.4 GHz region. The determination of the scaling factors was performed with ground based radiometer data in the frequency range of from different locations[6] in the USA.

**Water vapor continuum absorption:** The CP98 model uses the same water vapor continuum parameterization as MPM87, just scaled with an empirical factor, $CC$, determined from the above mentioned data:

$$\alpha_\mathrm{c}^{\mathrm{CP98}} = C_C \cdot \alpha_\mathrm{c}^{\mathrm{MPM87}} \qquad (2.70)$$

[6] The data were recorded at San Diego, California (11. December 1991) and West Palm Beach, Florida (8.-21. March 1992)

| | $C_L$ | $C_W$ | $C_C$ | $C_X$ |
|---|---|---|---|---|
| value | 1.0639 | 1.0658 | 1.2369 | 1.0739 |
| std. dev. | 0.016 | 0.0096 | 0.155 | 0.252 |
| correlation | | | | |
| $C_L$ | 1 | -0.085 | 0.045 | -0.048 |
| $C_W$ | -0.085 | 1 | -0.513 | 0.485 |
| $C_C$ | 0.045 | -0.513 | 1 | -0.989 |
| $C_X$ | -0.048 | 0.485 | -0.989 | 1 |

Table 2.8: Scaling parameter values with standard deviation and correlation coefficients according to [*Cruz Pol et al.*, 1998]. The scaling parameters are $C_L$:22 GHz line strength, $C_W$:22 GHz line width, $C_C$:$H_2O$-continuum, and $C_X$:$O_2$-absorption. $C_X$ scales the entire oxygen absorption, the continuum as well as the line absorption. The Cruz-Pol et al. model uses the *Rosenkranz* [1993] oxygen absorption model.

The scaling factor $C_C$, as given in Table 2.8, gives a 23.69 % increased continuum absorption compared with MPM87 (see Table 2.2 for a comparison of the parameter values). But one has to keep in mind that $C_C$ has a high correlation with the scaling factor of the oxygen absorption, $C_X$, since these two components could not be completely distinguished in the data. Therefore the value of 23.69 % has a standard deviation of 15.5 % and is not so reliable than $C_L$ and $C_W$.

### PWR98 water vapor absorption model

The water vapor continuum formulation of *Rosenkranz* [1998] is a re-investigation of the existing models MPM87/MPM89, MPM93, and CKD_2.1 especially for the frequency region below 1-1000 GHz. in the context of the available laboratory and atmospheric data [*Bauer et al.*, 1989, 1993, 1995; *Becker and Autler*, 1946; *English et al.*, 1994; *Godon et al.*, 1992; *Liebe*, 1984; *Liebe and Layton*, 1987; *Westwater et al.*, 1980].

Rosenkranz adopted the structure of MPM89 for his improved model (R98). However, some important differences exist compared with MPM89:

- the water vapor line catalogs are different
- the R98 uses the Van Vleck–Weisskopf line shape function with cutoff and MPM89 without cutoff

**Water vapor line absorption:** The local line absorption is defined as

$$\begin{aligned}\alpha_\ell^{\mathrm{R98}} &= N_{H_2O} \cdot \sum_k S_{\mathrm{k}}(T) \cdot F_c(\nu, \nu_{\mathrm{k}}) \\ &= N_{H_2O} \cdot \sum_k S_{\mathrm{k}}(T) \cdot \left(\frac{\nu}{\nu_{\mathrm{k}}}\right)^2 \cdot [f_c(\nu, +\nu_{\mathrm{k}}) + f_c(\nu, -\nu_{\mathrm{k}})] \;\; \mathrm{Np/km} \qquad (2.71)\end{aligned}$$

where $N_{H_2O}$ is the number density of water molecules, $\nu$ the frequency and $S$ the line intensity, calculated from the HITRAN92 data base *Rothman et al.* [1992]. Considered for this re-investigation are 15 lines with a frequency lower than 1 THz as listed in Table 2.9.

The line shape function $F_c(\nu, \nu_{\mathrm{k}})$ has a cutoff frequency, $\nu_{\mathrm{cutoff}}$, and a baseline subtraction similar to the CKD model [*Clough et al.*, 1989]. The introduction of a cutoff frequency has two advantages: (1) the cutoff avoids applying the line shape to distant frequencies where the line form is theoretically not well understood and (2) the cutoff also establishes a limit to the summation in Eq. (2.71) where lines far away from the cutoff limit do not contribute to the sum. The Rosenkranz formulation uses the same value for the cutoff frequency as the CKD model:

$$\nu_{\mathrm{cutoff}} = 750\ \mathrm{GHz} \tag{2.72}$$

The explicit mathematical form of the line shape function is defined in such a way that in the limit $\nu_{\mathrm{cutoff}} \rightarrow \infty$ the combination of Eq. (2.71) with the line shape function would be equivalent to a Van Vleck–Weisskopf [*Van Vleck and Weisskopf*, 1945] line shape:

$$f_c(\nu, \pm\nu_{\mathrm{k}}) = \begin{cases} \frac{\gamma_{\mathrm{k}}}{\pi} \left\{ \frac{1}{(\nu \mp \nu_{\mathrm{k}})^2 + \gamma_{\mathrm{k}}^2} - \frac{1}{\nu_{\mathrm{cutoff}}^2 + \gamma_{\mathrm{k}}^2} \right\} & : \ |\nu \pm \nu_{\mathrm{k}}| < \nu_{\mathrm{cutoff}} \\ 0 & : \ |\nu \pm \nu_{\mathrm{k}}| \geq \nu_{\mathrm{cutoff}} \end{cases} \tag{2.73}$$

$\nu_{\mathrm{k}}$ is the line center frequency and $\gamma_{\mathrm{k}}$ the line half width, which is calculated according to

$$\gamma_{\mathrm{k}} = w_{\mathrm{s,k}} \cdot P_{\mathrm{H2O}} \cdot \Theta^{\mathrm{ns}} + w_{\mathrm{f,k}} \cdot P_{\mathrm{d}} \cdot \Theta^{\mathrm{nf}} \qquad \mathrm{GHz} \tag{2.74}$$

with $P_{\mathrm{H2O}}$ and $P_{\mathrm{d}}$ as the partial pressure of water vapor and of dry air, respectively. The line depending parameters $w_{\mathrm{s,k}}$, $\mathrm{n_s}$, $w_{\mathrm{f,k}}$, and $\mathrm{n_f}$ are listed in Table 2.9 and the dimensionless parameter $\Theta$ is defined as $\Theta = 300\ \mathrm{K}/T$.

Because of the structural similarity to MPM89, the line broadening parameters differ only in minor respects from the values used therein (only the parameters $x_{\mathrm{s},1}$, $w_{\mathrm{f},2}$ and $\mathrm{w_{s,2}}$ are significantly different).

| index k | $\nu_{\mathrm{k}}$ [GHz] | $w_{\mathrm{f,k}}$ [GHz/kPa] | $\mathrm{n_f}$ [1] | $w_{\mathrm{s,k}}$ [GHz/kPa] | $\mathrm{n_s}$ [1] |
|---|---|---|---|---|---|
| 1 | 22.2351 | 0.00281 | 0.69 | 0.01349 | 0.61 |
| 2 | 183.3101 | 0.00281 | 0.64 | 0.01491 | 0.85 |
| 3 | 321.2256 | 0.00230 | 0.67 | 0.01080 | 0.54 |
| 4 | 325.1529 | 0.00278 | 0.68 | 0.01350 | 0.74 |
| 5 | 380.1974 | 0.00287 | 0.54 | 0.01541 | 0.89 |
| 6 | 439.1508 | 0.00210 | 0.63 | 0.00900 | 0.52 |
| 7 | 443.0183 | 0.00186 | 0.60 | 0.00788 | 0.50 |
| 8 | 448.0011 | 0.00263 | 0.66 | 0.01275 | 0.67 |
| 9 | 470.8890 | 0.00215 | 0.66 | 0.00983 | 0.65 |
| 10 | 474.6891 | 0.00236 | 0.65 | 0.01095 | 0.64 |
| 11 | 488.4911 | 0.00260 | 0.69 | 0.01313 | 0.72 |
| 12 | 556.9360 | 0.00321 | 0.69 | 0.01320 | 1.00 |
| 13 | 620.7008 | 0.00244 | 0.71 | 0.01140 | 0.68 |
| 14 | 752.0332 | 0.00306 | 0.68 | 0.01253 | 0.84 |
| 15 | 916.1712 | 0.00267 | 0.70 | 0.01275 | 0.78 |

Table 2.9: Line parameters of the Rosenkranz absorption model (PWR98) (values taken from *Rosenkranz* [1998]).

**Water vapor continuum absorption:** The continuum absorption in R98 has the same functional dependence on frequency, pressure, and temperature like in MPM87/MPM89 (see Sec. 2.3.1 for details):

$$\alpha_c^{R98} = \nu^2 \cdot P_{H2O} \cdot (C^o_{H_2O} \cdot P_{H2O} \cdot \Theta^{ns} + C^o_d \cdot P_d \cdot \Theta^{nf}) \tag{2.75}$$

with

$C^o_{H_2O} = 7.80 \cdot 10^{-8}$ (dB/km) / (hPa·GHz)$^2$

$n_s = 7.5$

$C^o_d = 0.236 \cdot 10^{-8}$ (dB/km) / (hPa·GHz)$^2$

$n_d = 3.0$

The main difference to the MPM versions are the values of these parameters, since Rosenkranz used additional data to fit his set of parameters. A second point is the cutoff in the line shape of the line absorption calculation. Since this cutoff decreases the line absorption in the window regions, the continuum absorption tends to compensate this decrease to get the same total absorption as withouot cutoff. This effects mainly the parameters $C^o_{H_2O}$ and $C^o_d$ but has also an influence in the temperature dependence and therefore on $n_s$ and $n_d$.

### 2.3.2 Complete oxygen models

Since the Maxwell equations are symmetric in the electric and magnetic fields, electric as well as magnetic dipole transitions are both possible although magnetic dipoles are in general some orders of magnitudes weaker and therefore not relevant in atmospheric radiative transfer models. An exception to this is the complex around 60 GHz of the paramagnetic oxygen magnetic dipole transitions. This bulk of lines arise due to the fact that for rotational quantum numbers $K > 1$ the allowed transitions $\Delta J = \pm 1$ have an energy gap of approximately 60 GHz.
The most frequently used absorption model for this absorption effect is that of Liebe, Rosenkranz, and Hufford [*Liebe et al.*, 1992] (also reported in *Rosenkranz* [1993] with a slightly different parameterization).

For oxygen – like for water vapor – the total absorption ($\alpha_{tot}$) is modelled as the line absorption ($\alpha_\ell$) plus a continuum absorption ($\alpha_c$):

$$\alpha_{tot} = \alpha_\ell + \alpha_c \tag{2.76}$$

It has to be emphasized that, $\alpha_\ell$ and $\alpha_c$ of different models are not necessarily compatible and should therefore not be interchanged.

#### PWR93 oxygen absorption model

**Resonant oxygen absorption** The oxygen absorption model of Rosenkranz is described in *Rosenkranz* [1993]. It is based on the investigations made by Liebe, Rosenkranz, and Hufford [*Liebe et al.*, 1992]. The FORTRAN77 computer program of Rosenkranz for the $O_2$ absorption calculation can be downloaded via anonymous ftp from mesa.mit.edu/phil/lbl_rt.

The oxygen line catalog has 40 lines from which 33 lines build the complex around 60 GHz. The parameterization of the line absorption, $\alpha_\ell^{\mathrm{R98}}$, is:

$$\alpha_\ell^{\mathrm{R98}} = \frac{n_{\mathrm{O_2}}}{\pi} \cdot \sum_{k=1}^{40} S_k(T) \cdot F(\nu, \nu_k) \tag{2.77}$$

line intensity:

$$S_k(T) = S_k(300\,\mathrm{K}) \ / \ \exp(b_k \cdot \Theta) \tag{2.78}$$

line shape function:

$$F(\nu, \nu_k) = \left(\frac{\nu}{\nu_\mathrm{k}}\right)^2 \cdot \left[\frac{\Gamma_k + (\nu - \nu_\mathrm{k}) \cdot Y_k}{(\nu - \nu_k)^2 + \Gamma_k^2} + \frac{\Gamma_k - (\nu + \nu_\mathrm{k}) \cdot Y_k}{(\nu + \nu_k)^2 + \Gamma_k^2}\right]$$

line width:

$$\Gamma_k = w_k \cdot \left(P_\mathrm{d} \cdot \Theta^{0.8} + 1.1 \cdot P_{\mathrm{H2O}} \cdot \Theta\right) \tag{2.79}$$

line coupling:

$$Y_k = P_{\mathrm{air}} \cdot \Theta^{0.8} \cdot [y_k + (\Theta - 1) \cdot v_k]$$

number density of $O_2$:

$$n_{\mathrm{O_2}} = (0.20946 \cdot P_{\mathrm{air}})/(k_B \cdot T)$$

where $S_k(300\,\mathrm{K})$ denotes the reference line intensity at T=300 K ant the exponential term approximates the exact partition function. All model parameters (see Refs. *Rosenkranz* [1993] and *Liebe et al.* [1992] for the laboratory measurements and the fitting parameters) are tabulated in Table 2.10.

| index $k$ | $\nu_\mathrm{k}$ [GHz] | $S_k(300\,\mathrm{K})$ [cm$^2$ Hz] | $b_k$ [1] | $w_k$ [$\frac{\mathrm{MHz}}{\mathrm{hPa}}$] | $y_k$ [$\frac{10^{-3}}{\mathrm{hPa}}$] | $v_k$ [$\frac{10^{-3}}{\mathrm{hPa}}$] |
|---|---|---|---|---|---|---|
| 1 | 118.7503 | $.2936\cdot 10^{-14}$ | .009 | 1.63 | -0.0233 | 0.0079 |
| 2 | 56.2648 | $.8079\cdot 10^{-15}$ | .015 | 1.646 | 0.2408 | -0.0978 |
| 3 | 62.4863 | $.2480\cdot 10^{-14}$ | .083 | 1.468 | -0.3486 | 0.0844 |
| 4 | 58.4466 | $.2228\cdot 10^{-14}$ | .084 | 1.449 | 0.5227 | -0.1273 |
| 5 | 60.3061 | $.3351\cdot 10^{-14}$ | .212 | 1.382 | -0.5430 | 0.0699 |
| 6 | 59.5910 | $.3292\cdot 10^{-14}$ | .212 | 1.360 | 0.5877 | -0.0776 |
| 7 | 59.1642 | $.3721\cdot 10^{-14}$ | .391 | 1.319 | -0.3970 | 0.2309 |
| 8 | 60.4348 | $.3891\cdot 10^{-14}$ | .391 | 1.297 | 0.3237 | -0.2825 |
| 9 | 58.3239 | $.3640\cdot 10^{-14}$ | .626 | 1.266 | -0.1348 | 0.0436 |
| 10 | 61.1506 | $.4005\cdot 10^{-14}$ | .626 | 1.248 | 0.0311 | -0.0584 |
| 11 | 57.6125 | $.3227\cdot 10^{-14}$ | .915 | 1.221 | 0.0725 | 0.6056 |
| 12 | 61.8002 | $.3715\cdot 10^{-14}$ | .915 | 1.207 | -0.1663 | -0.6619 |
| 13 | 56.9682 | $.2627\cdot 10^{-14}$ | 1.260 | 1.181 | 0.2832 | 0.6451 |
| 14 | 62.4112 | $.3156\cdot 10^{-14}$ | 1.260 | 1.171 | -0.3629 | -0.6759 |
| 15 | 56.3634 | $.1982\cdot 10^{-14}$ | 1.660 | 1.144 | 0.3970 | 0.6547 |
| 16 | 62.9980 | $.2477\cdot 10^{-14}$ | 1.665 | 1.139 | -0.4599 | -0.6675 |
| 17 | 55.7838 | $.1391\cdot 10^{-14}$ | 2.119 | 1.110 | 0.4695 | 0.6135 |
| 18 | 63.5685 | $.1808\cdot 10^{-14}$ | 2.115 | 1.108 | -0.5199 | -0.6139 |
| 19 | 55.2214 | $.9124\cdot 10^{-15}$ | 2.624 | 1.079 | 0.5187 | 0.2952 |
| 20 | 64.1278 | $.1230\cdot 10^{-14}$ | 2.625 | 1.078 | -0.5597 | -0.2895 |
| 21 | 54.6712 | $.5603\cdot 10^{-15}$ | 3.194 | 1.05 | 0.5903 | 0.2654 |

Table 2.10: (continued on next page)

| index | $\nu_k$ | $S_k(300\,\mathrm{K})$ | $b_k$ | $w_k$ | $y_k$ | $v_k$ |
|---|---|---|---|---|---|---|
| 22 | 64.6789 | $.7842 \cdot 10^{-15}$ | 3.194 | 1.05 | -0.6246 | -0.2590 |
| 23 | 54.1300 | $.3228 \cdot 10^{-15}$ | 3.814 | 1.02 | 0.6656 | 0.3750 |
| 24 | 65.2241 | $.4689 \cdot 10^{-15}$ | 3.814 | 1.02 | -0.6942 | -0.3680 |
| 25 | 53.5957 | $.1748 \cdot 10^{-15}$ | 4.484 | 1.00 | 0.7086 | 0.5085 |
| 26 | 65.7648 | $.2632 \cdot 10^{-15}$ | 4.484 | 1.00 | -0.7325 | -0.5002 |
| 27 | 53.0669 | $.8898 \cdot 10^{-16}$ | 5.224 | .97 | 0.7348 | 0.6206 |
| 28 | 66.3021 | $.1389 \cdot 10^{-15}$ | 5.224 | .97 | -0.7546 | -0.6091 |
| 29 | 52.5424 | $.4264 \cdot 10^{-16}$ | 6.004 | .94 | 0.7702 | 0.6526 |
| 30 | 66.8368 | $.6899 \cdot 10^{-16}$ | 6.004 | .94 | -0.7864 | -0.6393 |
| 31 | 52.0214 | $.1924 \cdot 10^{-16}$ | 6.844 | .92 | 0.8083 | 0.6640 |
| 32 | 67.3696 | $.3229 \cdot 10^{-16}$ | 6.844 | .92 | -0.8210 | -0.6475 |
| 33 | 51.5034 | $.8191 \cdot 10^{-17}$ | 7.744 | .89 | 0.8439 | 0.6729 |
| 34 | 67.9009 | $.1423 \cdot 10^{-16}$ | 7.744 | .89 | -0.8529 | -0.6545 |
| 35 | 368.4984 | $.6460 \cdot 10^{-15}$ | .048 | 1.92 | 0.0000 | 0.0000 |
| 36 | 424.7631 | $.7047 \cdot 10^{-14}$ | .044 | 1.92 | 0.0000 | 0.0000 |
| 37 | 487.2494 | $.3011 \cdot 10^{-14}$ | .049 | 1.92 | 0.0000 | 0.0000 |
| 38 | 715.3932 | $.1826 \cdot 10^{-14}$ | .145 | 1.81 | 0.0000 | 0.0000 |
| 39 | 773.8397 | $.1152 \cdot 10^{-13}$ | .141 | 1.81 | 0.0000 | 0.0000 |
| 40 | 834.1453 | $.3971 \cdot 10^{-14}$ | .145 | 1.81 | 0.0000 | 0.0000 |

Table 2.10: List of $O_2$ spectral lines of the Rosenkranz absorption model [*Rosenkranz*, 1993].

**Oxygen continuum absorption:** As pointed out by Van Vleck [*Van Vleck*, 1987], the standard theory for non-resonant absorption is that of Debye (see also Ref. *Townes and Schawlow* [1955]). The Debye line shape is obtained from the VVW line shape function by the limiting case $\nu_\mathrm{k} \to 0$. Rosenkranz *Rosenkranz* [1993] adopt the Debye theory for his models:

$$\alpha_\mathrm{c} = C \cdot P_\mathrm{d} \cdot \Theta^2 \cdot \frac{\nu^2 \cdot \gamma}{\nu^2 + \gamma^2} \tag{2.80}$$

$$\gamma = w \cdot (P_\mathrm{d} \cdot \Theta^{0.8} + 1.1 \cdot P_\mathrm{H2O} \cdot \Theta) \tag{2.81}$$

The values for the parameters are $C = 1.11 \cdot 10^{-5}$ dB/km/(hPa GHz) and $w = 5.6 \cdot 10^{-4}$ GHz/hPa, respectively. This absorption term is proportional to the collision frequency of a single oxygen molecule and thus proportional to the dry air pressure[7].

### MPM93 oxygen absorption model

**Oxygen line absorption:** The oxygen line catalog has 44 lines from which 37 lines build the complex around 60 GHz [*Liebe et al.*, 1993]. The parameterization of the line absorption, $\alpha_\ell^\mathrm{MPM}$, is (in units of dB/km):

$$\alpha_\ell^\mathrm{MPM} = 0.1820 \cdot \nu^2 \cdot \sum_{k=1}^{44} S_k(T) \cdot F(\nu, \nu_k) \quad \mathrm{dB/km} \tag{2.82}$$

[7]The absorption due to weakly bound complexes of $O_2$–$X$ with $X = H_2O,\ N_2$ is treated separately and therefore not included in this Debye formula.

with

$$
\begin{aligned}
& \text{line intensity:} \\
S_k(T) &= \frac{a_{1,k}}{\nu_\mathrm{k}} \cdot P_\mathrm{d} \cdot \Theta^3 \cdot \exp\left[a_{2,k} \cdot (1-\Theta)\right] && (2.83) \\
& \text{line shape function:} \\
F(\nu, \nu_k) &= \left[ \frac{\gamma_k + (\nu - \nu_\mathrm{k}) \cdot \delta_k}{(\nu - \nu_k)^2 + \gamma_k^2} + \frac{\gamma_k - (\nu + \nu_\mathrm{k}) \cdot \delta_k}{(\nu + \nu_k)^2 + \gamma_k^2} \right] \\
& \text{line width:} \\
\gamma_k &= a_{3,k} \cdot 10^{-3} \cdot (P_\mathrm{d} \cdot \Theta^{a_{4,k}} + 1.10 \cdot P_\mathrm{H2O} \cdot \Theta) && (2.84) \\
& \text{line coupling:} \\
\delta_k &= P_\mathrm{air} \cdot \Theta^{0.8} \cdot [a_{5,k} + \Theta \cdot a_{6,k}]
\end{aligned}
$$

where $a_{1-5,k}$ are the fitted parameters due to laboratory measurements [*Liebe et al.*, 1992]. All model parameters are tabulated in Table 2.11. One has to note that in the MPM93 code is a threshold value for $\alpha_\ell^\mathrm{MPM}$ implemented:

$$
\alpha_\ell^\mathrm{MPM} = \begin{cases} \alpha_\ell^\mathrm{MPM} & : \quad \alpha_\ell^\mathrm{MPM} > 0 \\ 0 & : \quad \alpha_\ell^\mathrm{MPM} < 0 \end{cases} \tag{2.85}
$$

Therefore the oxygen absorption in the wings of the strong $O_2$-lines is remarkably higher than in the R93 model.

| index $k$ | $\nu_\mathrm{k}$ [GHz] | $a_{1,k}$ $[\frac{\mathrm{kHz}}{\mathrm{hPa}}]$ | $a_{2,k}$ [1] | $a_{3,k}$ $[\frac{\mathrm{MHz}}{\mathrm{hPa}}]$ | $a_{4,k}$ [1] | $a_{5,k}$ $[\frac{10^3}{\mathrm{hPa}}]$ | $a_{6,k}$ $[\frac{10^3}{\mathrm{hPa}}]$ |
|---|---|---|---|---|---|---|---|
| 1 | 50.474238 | 0.094 | 9.694 | 0.890 | 0.0 | 0.240 | 0.790 |
| 2 | 50.987749 | 0.246 | 8.694 | 0.910 | 0.0 | 0.220 | 0.780 |
| 3 | 51.503350 | 0.608 | 7.744 | 0.940 | 0.0 | 0.197 | 0.774 |
| 4 | 52.021410 | 1.414 | 6.844 | 0.970 | 0.0 | 0.166 | 0.764 |
| 5 | 52.542394 | 3.102 | 6.004 | 0.990 | 0.0 | 0.136 | 0.751 |
| 6 | 53.066907 | 6.410 | 5.224 | 1.020 | 0.0 | 0.131 | 0.714 |
| 7 | 53.595749 | 12.470 | 4.484 | 1.050 | 0.0 | 0.230 | 0.584 |
| 8 | 54.130000 | 22.800 | 3.814 | 1.070 | 0.0 | 0.335 | 0.431 |
| 9 | 54.671159 | 39.180 | 3.194 | 1.100 | 0.0 | 0.374 | 0.305 |
| 10 | 55.221367 | 63.160 | 2.624 | 1.130 | 0.0 | 0.258 | 0.339 |
| 11 | 55.783802 | 95.350 | 2.119 | 1.170 | 0.0 | -0.166 | 0.705 |
| 12 | 56.264775 | 54.890 | 0.015 | 1.730 | 0.0 | 0.390 | -0.113 |
| 13 | 56.363389 | 134.400 | 1.660 | 1.200 | 0.0 | -0.297 | 0.753 |
| 14 | 56.968206 | 176.300 | 1.260 | 1.240 | 0.0 | -0.416 | 0.742 |
| 15 | 57.612484 | 214.100 | 0.915 | 1.280 | 0.0 | -0.613 | 0.697 |
| 16 | 58.323877 | 238.600 | 0.626 | 1.330 | 0.0 | -0.205 | 0.051 |
| 17 | 58.446590 | 145.700 | 0.084 | 1.520 | 0.0 | 0.748 | -0.146 |
| 18 | 59.164207 | 240.400 | 0.391 | 1.390 | 0.0 | -0.722 | 0.266 |
| 19 | 59.590983 | 211.200 | 0.212 | 1.430 | 0.0 | 0.765 | -0.090 |
| 20 | 60.306061 | 212.400 | 0.212 | 1.450 | 0.0 | -0.705 | 0.081 |
| 21 | 60.434776 | 246.100 | 0.391 | 1.360 | 0.0 | 0.697 | -0.324 |
| 22 | 61.150560 | 250.400 | 0.626 | 1.310 | 0.0 | 0.104 | -0.067 |
| 23 | 61.800154 | 229.800 | 0.915 | 1.270 | 0.0 | 0.570 | -0.761 |

Table 2.11: (continued on next page)

| index | $\nu_k$ | $a_{1,k}$ | $a_{2,k}$ | $a_{3,k}$ | $a_{4,k}$ | $a_{5,k}$ | $a_{6,k}$ |
|---|---|---|---|---|---|---|---|
| 24 | 62.411215 | 193.300 | 1.260 | 1.230 | 0.0 | 0.360 | -0.777 |
| 25 | 62.486260 | 151.700 | 0.083 | 1.540 | 0.0 | -0.498 | 0.097 |
| 26 | 62.997977 | 150.300 | 1.665 | 1.200 | 0.0 | 0.239 | -0.768 |
| 27 | 63.568518 | 108.700 | 2.115 | 1.170 | 0.0 | 0.108 | -0.706 |
| 28 | 64.127767 | 73.350 | 2.620 | 1.130 | 0.0 | -0.311 | -0.332 |
| 29 | 64.678903 | 46.350 | 3.195 | 1.100 | 0.0 | -0.421 | -0.298 |
| 30 | 65.224071 | 27.480 | 3.815 | 1.070 | 0.0 | -0.375 | -0.423 |
| 31 | 65.764772 | 15.300 | 4.485 | 1.050 | 0.0 | -0.267 | -0.575 |
| 32 | 66.302091 | 8.009 | 5.225 | 1.020 | 0.0 | -0.168 | -0.700 |
| 33 | 66.836830 | 3.946 | 6.005 | 0.990 | 0.0 | -0.169 | -0.735 |
| 34 | 67.369598 | 1.832 | 6.845 | 0.970 | 0.0 | -0.200 | -0.744 |
| 35 | 67.900867 | 0.801 | 7.745 | 0.940 | 0.0 | -0.228 | -0.753 |
| 36 | 68.431005 | 0.330 | 8.695 | 0.920 | 0.0 | -0.240 | -0.760 |
| 37 | 68.960311 | 0.128 | 9.695 | 0.900 | 0.0 | -0.250 | -0.765 |
| 38 | 118.750343 | 94.500 | 0.009 | 1.630 | 0.0 | -0.036 | 0.009 |
| 39 | 368.498350 | 6.790 | 0.049 | 1.920 | 0.6 | 0.000 | 0.000 |
| 40 | 424.763124 | 63.800 | 0.044 | 1.930 | 0.6 | 0.000 | 0.000 |
| 41 | 487.249370 | 23.500 | 0.049 | 1.920 | 0.6 | 0.000 | 0.000 |
| 42 | 715.393150 | 9.960 | 0.145 | 1.810 | 0.6 | 0.000 | 0.000 |
| 43 | 773.839675 | 67.100 | 0.130 | 1.820 | 0.6 | 0.000 | 0.000 |
| 44 | 834.145330 | 18.000 | 0.147 | 1.810 | 0.6 | 0.000 | 0.000 |

Table 2.11: List of $O_2$ spectral lines of the MPM93 absorption model [*Liebe et al.*, 1993].

**Oxygen continuum absorption:** As pointed out by Van Vleck [*Van Vleck*, 1987], the standard theory for non-resonant absorption is that of Debye (see also Ref. *Townes and Schawlow* [1955]). The Debye line shape is obtained from the VVW line shape function by the limiting case $\nu_{\text{k}} \to 0$. *Liebe et al.* [1993] adopt the Debye theory for his model:

$$\begin{aligned} \alpha_{\text{c}} &= C \cdot P_{\text{d}} \cdot \Theta^2 \cdot \frac{\nu^2 \cdot \gamma}{\nu^2 + \gamma^2} \\ \gamma &= w \cdot P_{\text{tot}} \cdot \Theta^{0.8} \end{aligned} \tag{2.86}$$

The values for the parameters are $C = 1.11 \cdot 10^{-5}$ dB/km/(hPa GHz) and $w = 5.6 \cdot 10^{-4}$ GHz/hPa, respectively. This absorption term is proportional to the collision frequency of a single oxygen molecule and thus proportional to the dry air pressure[8].

[8] The absorption due to weakly bound complexes of $O_2$–$X$ with $X = H_2O,\ N_2$ is treated separately and therefore not included in this Debye formula.

# Chapter 3

# Cloud absorption

## 3.1 Liquid water and ice particle absorption

So far only absorption due to air was described. However hydrometeors[1] can have a noticeable effect on the radiative transfer through the atmosphere. To treat hydrometeors you should normally set up a calculation with scattering, which needs input optical properties such as the phase matrix. Several chapters, both in *ARTS User Guide* and here in *ARTS Theory*, deal with such scattering simulations.

This very short chapter is not related to the scattering parts in ARTS. Instead, it describes some functions that handle only the absorption of hydrometeors, not the scattering. They may be useful in some special cases. Practically, they work exactly as the continuum and complete gas absorption models, just the 'VMR' is interpreted as a condensate amount.

The MPM93 model provides beside the absorption model of air also an absorption model for suspended liquid water droplets and ice particles [*Liebe et al.*, 1989, 1991; *Hufford*, 1991; *Liebe et al.*, 1993]. The model is applicable for the Rayleigh regime, for which the relation $r < 0.05 \cdot \lambda$ holds where $r$ is the particle radius and $\lambda$ is the wavelength[2], e. g. for a frequency of around 22 GHz this means $r < 500\,\mu$m. Considering *Salby* [1996], this criterium is – except for cirrus – nearly for every aerosol and cloud class satisfied. But one has to bear in mind that these values have a wide range of variability, for example, *Salby* [1996] states that the mean particle radius for stratus, cumulus, and nimbus clouds can be in the range of 10-1000 $\mu$m and that the particle radius distribution is highly unsymmetric.

With respect to the imaginary part of the complex refractivity, a unified parameterization of liquid and ice particle absorption is formulated in MPM93:

$$
\begin{aligned}
\alpha &= 0.1820 \cdot \nu \cdot N'' \qquad\qquad \text{dB/km} \\
N'' &= \frac{3}{2} \cdot \frac{w}{m} \cdot \mathrm{Im}[(\epsilon_r - 1)/(\epsilon_r + 2)] \\
N'' &= \frac{3}{2} \cdot \frac{w}{m} \cdot \left[ \frac{3 \cdot \epsilon_r''}{(\epsilon_r' + 2)^2 \; + \; (\epsilon_r'')^2} \right]
\end{aligned} \tag{3.1}
$$

where $w$ is the liquid water ($0.0 < LWC < 5.0$ g/m$^3$) or ice mass (0.0 $IWC$ 1.0 g/m$^3$) content and $m$ is the water or ice bulk density ($\rho_{\mathrm{l,i}}$=1.0 g/cm$^3$ and 0.916 g/cm$^3$, respectively). The difference between liquid water and ice absorption is put in the expressions for the

[1] We denote liquid water and ice particles, either suspended or precipitating, in the air as hydrometeors.

[2] See *Brussaard and Watson* [1995], page 81, for details.

complex permittivities (i. e. the relative dielectric constant), $\epsilon_r = \epsilon_r^{'} + i \cdot \epsilon_r^{''}$, which depend on frequency and temperature.

• Complex permittivity for suspended liquid water droplets:

$$\begin{aligned}
\epsilon_r^{'} &= \epsilon_o - \nu^2 \cdot \left[\frac{\epsilon_o - \epsilon_1}{\nu^2 + \gamma_1^2} + \frac{\epsilon_1 - \epsilon_2}{\nu^2 + \gamma_2^2}\right] \\
\epsilon_r^{''} &= \nu \cdot \left[\gamma_1 \cdot \frac{\epsilon_o - \epsilon_1}{\nu^2 + \gamma_1^2} + \gamma_2 \cdot \frac{\epsilon_1 - \epsilon_2}{\nu^2 + \gamma_2^2}\right] \\
\epsilon_o &= 77.66 + 103.3 \cdot (\Theta - 1) \qquad (3.2) \\
\epsilon_1 &= 0.0671 \cdot \epsilon_o \\
\epsilon_2 &= 3.52 \\
\gamma_1 &= 20.20 - 146 \cdot (\Theta - 1) + 316 \cdot (\Theta - 1)^2 \,\mathrm{GHz} \qquad (3.3) \\
\gamma_2 &= 39.8 \cdot \gamma_1 \,\mathrm{GHz} \\
\Theta &= 300\,\mathrm{K} \,/\, T
\end{aligned}$$

• Complex permittivity for ice crystals:

$$\begin{aligned}
\epsilon_r^{'} &= 3.15 \\
\epsilon_r^{''} &= \frac{a}{\nu} + b \cdot \nu \\
a &= (\Theta - 0.1871) \cdot \exp\left(17.0 - 22.1 \cdot \Theta\right) \qquad (3.4) \\
b &= \left[\left(\frac{0.233}{1 - 0.993/\Theta}\right)^2 + \frac{6.33}{\Theta} - 1.31\right] \cdot 10^{-5} \qquad (3.5) \\
\Theta &= 300\,\mathrm{K} \,/\, T
\end{aligned}$$

The absorption is directly proportional to the liquid or ice water content $LWC/IWC$ and inversely proportional to the density of a single liquid ice particle $\rho_{\mathrm{l,i}}$. Like the mean particle radius, the liquid and ice water content have a high variability. Table 3.1 reflects this variability by summarizing different literature values for several cloud types. Additional uncertainty of this absorption term comes from two sides: (1) the difference to the Rayleigh approximation of the order of 1-6% as reported in *Li et al.* [1997] and (2) from the fit of the complex permittivity. Since $\epsilon(\nu, T)$ was fitted to measurements which were mostly performed above 0°C, the extrapolated values for $T$ <0°C for super-cooled clouds are not well established. For example in *Liebe et al.* [1991] itself two different parameterizations for the so called primary relaxation frequency ($\gamma_1$ in Equation 3.2) are given, one polynomial in $\Theta$ as presented in Equation 3.2) and an exponential function derived from theory. Although the polynomial describes the selected data better than the exponential function, this might not be true for temperatures well below 0°C. The difference in $\gamma_1$ according to these two approaches can be more than 2 GHz for very low temperatures [*Lipton et al.*, 1999]. The resulting consequences from this discrepancy for the absorption calculation at three microwave frequencies are shown in Figure 3.1. A more detailed discussion about this source of uncertainty is given in Section 3.2.

## 3.2 Variability and uncertainty in cloud absorption

In the case of clouds three sources of uncertainties can be considered at first sight: (1) validity of the Rayleigh approximation (2) the parameterization of the relative dielectric

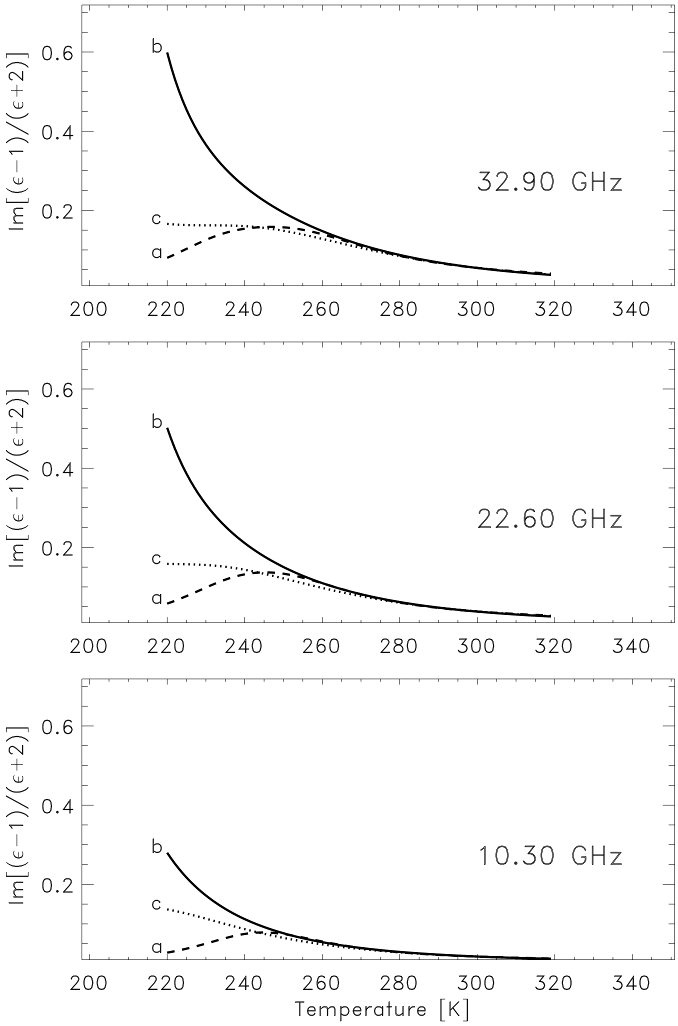


Figure 3.1: Comparison of the imaginary part of the expression $(\epsilon_r - 1)/(\epsilon_r + 2)$ for liquid water at the three frequencies of 32.9, 22.6, and 10,3 GHz. Plotted are the two common models of *Liebe et al.* [1991] (a) and *Ray* [1972] (b). The Ray parameterization is calculated with the F77 program of W. Wiscombe, NASA, GSFC, take from ftp://climate.gsfc.nasa.gov/pub/wiscombe/Refrac_Index/WATER/. Additionally the *Liebe et al.* [1991] parameterization (c) with the alternative expression for the first relaxation frequency, $\gamma_1 = 20.1 \cdot \exp[7.88 \cdot (1 - \Theta)]$, is plotted.

| cloud | class | liquid water content ($LWC$) (g/m$^3$) | reference |
|---|---|---|---|
| stratus | St | 0.15 | *Salby* [1996] |
| | | 0.09-0.9 | *Seinfeld and Pandis* [1998] |
| | | 0.28-0.3 | *Hess et al.* [1998] |
| | | 0.29 | *Kneizys et al.* [1996] |
| nimbostratus | Ns | 0.4 | *Salby* [1996] |
| | | 0.65 | *Kneizys et al.* [1996] |
| | | 0.05-0.3 | *Berton* [2000] |
| altostratus | As | <0.01-0.2 | *Seinfeld and Pandis* [1998] |
| | | 0.41 | *Kneizys et al.* [1996] |
| | | 0.1-1 | *Berton* [2000] |
| stratocumulus | Sc | 0.3 | *Salby* [1996] |
| | | <0.1-0.7 | *Seinfeld and Pandis* [1998] |
| | | 0.15 | *Kneizys et al.* [1996] |
| | | <0.5 | *Pawlowska et al.* [2000] |
| | | 0.05-1 | *Berton* [2000] |
| cumulus | Cu | 0.5 | *Salby* [1996] |
| | | 0.26-0.44 | *Hess et al.* [1998] |
| | | 1.00 | *Kneizys et al.* [1996] |
| cumulonimbus | Cb | 2.5 | *Salby* [1996] |
| | | 0.1-2 | *Berton* [2000] |
| cumulus congestus | Cg | 0.1-3.2 | *Berton* [2000] |
| FIRE-ACE | - | <0.7 | *Shupe et al.* [2000] |

| cloud | class | ice water content ($IWC$) (g/m$^3$) | reference |
|---|---|---|---|
| cirrus | Ci | 0.025 | *Salby* [1996] |
| | | 0.00193-0.0260 | *Hess et al.* [1998] |
| | | $3.128 \cdot 10^{-4}$-0.06405 | *Kneizys et al.* [1996] |
| | | 0.15-0.3 | *Larsen et al.* [1998] |
| | | <0.1 | *Berton* [2000] |
| cirrostratus | Cs | 0.2 | *Salby* [1996] |
| | | 0.05-2 | *Berton* [2000] |

Table 3.1: Stated values for the liquid and ice water content of several cloud classes from different sources.

constants ($\epsilon_r$) of water and ice in the microwave region, and (3) the statistical and climatological variability of the cloud liquid water and ice content.

As it was stated above (Section 3.1) the Rayleigh approximation is valid for particle sizes $< 500\,\mu$m. Figure 3.2 shows a particle size distribution for water clouds and ice clouds (cirrus) from the OPAC model [*Hess et al.*, 1998]. According to this model only cirrus clouds will have particles of size larger than $500\,\mu$m. Nevertheless one has to keep in mind that the variability of the particle size can be very high so that at certain conditions some cloud types (most probable is the cumulonimbus) a non-negligible large particle concentration can occur.

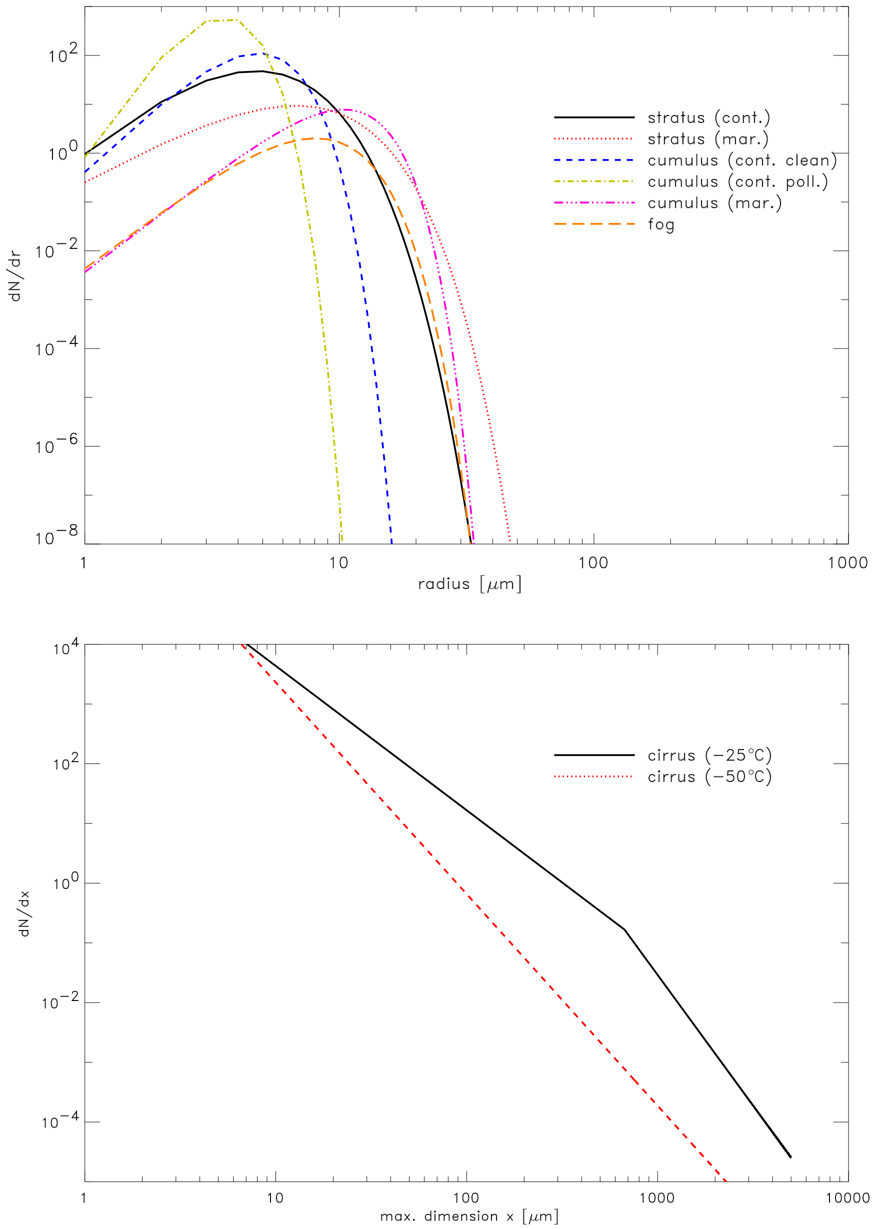


Figure 3.2: Cloud particle size distributions according to Equations 3a and 3c and the microphysical properties are from the Tables 1a and 1b of the OPAC model [*Hess et al.*, 1998]. For the liquid water clouds (upper plot) a modified gamma distribution is assumed whereas for the ice clouds (lower plot) exponential functions are taken.

The uncertainty in the relative dielectric constant of water (see e. g. *Lipton et al.* [1999]) is largest below the freezing temperature, since only a few measurements at -4°C contributed to the parameterization of $\epsilon_r$ in *Liebe et al.* [1991], which in turn is used in the cloud liquid water absorption model of MPM93. Figure 3.1 shows a comparison of *Liebe et al.* [1991] and *Ray* [1972][3] parameterizations for the temperature dependence of the expression $\mathrm{Im}[(\epsilon_r - 1)/(\epsilon_r + 2)]$, which is in the Rayleigh approximation one of the relevant terms in the absorption calculation (see Equation 3.1). Additionally the same calculations with the alternative expression of the first relaxation frequency, $\gamma_1$, as stated in Equation 2b of *Liebe et al.* [1991] is shown. The three versions give comparable results for temperatures warmer than 260 K but show significant differences for temperatures below 240 K. However, an uncertainty estimation of $\mathrm{Im}[(\epsilon_r - 1)/(\epsilon_r + 2)]$ is due to the lack of measurements not easy, but it will certainly increase with decreasing temperature.

The largest variability of the involved quantities of cloud absorption is the liquid and ice water content ($LWC$ and $IWC$) of the clouds (see Table 3.1). Even within a single cloud the $LWC$ ($IWC$) changes with altitude and the distance from the cloud center as can be seen for example in Figure 10 of *Ludlam and Mason* [1957] and in the model study of *Costa et al.* [2000].

[3]The calculations for this parameterizastion are performed with the computer code of W. Wiscombe, NASA, GSFC (ftp://climate.gsfc.nasa.gov/pub/wiscombe/Refrac_Index/WATER/) For the microwave frequency range this program uses the *Ray* [1972] temperature parameterization.

# Chapter 4

# Refractive index

Refractive index describes several effects of matter on propagation of electromagnetic waves. Refractive index is basically a complex quantity. However, in this chapter it is restricted to its real part, neglecting the imaginary part, which describes absorption. Effects the real part of the refractive index describes particularly include changes of the propagation speed of electromagnetic waves, which leads to a delay of the signal, as well as a change of the propagation direction, a bending of the propagation path. The latter is commonly called refraction.

Several components in the atmosphere contribute to refraction, hence to the refractive index: the gas mixture("air"), solid and liquid constituents (clouds, precipitation, aerosols), and electrons. Refractivity ($N$) describes the deviation of the refractive index of a medium $n$from the vacuum refractive index ($n_{\mathrm{vacuum}} = 1$): $N = n-1$. Contributions of the different components to refractivity are additive. One distinguishes between monochromatic and group refractive index, which differ in case of dispersion leading to diverging propagation paths at different frequencies. **FIXME: That needs to be more specific.**

## 4.1 Gases

According to *Newell and Baird* [1965], the refractivity $N$, i.e., the deviation of the refractive index $n$ from 1.0 ($N = n - 1$), of a gas can be assumed to be proportional to its density. *Newell and Baird* [1965] give no validity range for this assumption, but at least *Stratton* [1968] assumes that it is valid even for the relatively high densities in the Venusian atmosphere. We have not investigated whether this assumption may break down at some point in the Jupiter atmosphere.

If we accept the assumption of refractivity scaling with gas density, then the problem of parameterizing the refractivity can be separated into two sub-problems: (a) determining the refractivity index for reference conditions (reference pressure $p$ and temperature $T$), and (b) deciding which gas law to use to scale it to other conditions. The total refractivity is then simply the sum of all partial refractivities, in other words

$$N = N_{\mathrm{ref},1}\frac{n_1}{n_{\mathrm{ref},1}} + N_{\mathrm{ref},2}\frac{n_2}{n_{\mathrm{ref},2}} + \cdots \tag{4.1}$$

---

**History**

130802 Started based on AUG chapter and ESA-planetary TN1 (Jana Mendrok).

where $N$ is the total refractivity, $N_{\text{ref},1}$ is the partial refractivity for gas $i$ at reference conditions, $n_i$ is the partial density, and $n_{\text{ref,i}}$ is the reference density.

Different solutions have been proposed, where approaches specific for Earth atmosphere commonly are empirical parameterisations. Below we describe the background and formulas applied for the different methods implemented in ARTS.

### 4.1.1 Microwave general method (`refr_index_airMWgeneral`)

Apart from presenting a basic approach, *Newell and Baird* [1965] also provide a thorough study of both refractivity of different gases for reference conditions and which gas law to use to scale those to other conditions. They present laboratory refractivity measurements for dry $CO_2$-free air, argon, carbon dioxide, helium, hydrogen, nitrogen, and oxygen covering the most relevant gases (probably apart from water vapor) in planetary atmospheres. The actual refractivity values of *Newell and Baird* [1965] are stated in the paper abstract and are not repeated here. The conditions for the reported refractivity values are $T$ = 0°C and $p$ = 760 Torr. The measurements are for a frequency of 47.7 GHz. Out of the reference refractivities povided by *Newell and Baird* [1965], we apply those of $N_2$, $O_2$, $CO_2$, $H_2$, and He in this algorithm.

*Newell and Baird* [1965] also adress the question which gas law to use to scale the measurements to other $p$/$T$ conditions, chosing different approaches depending on the specific gas in question. While the more complicated gas laws they suggest can be expected to be more accurate in the relatively narrow range of $p$/$T$ conditions considered by *Newell and Baird* [1965], it is not easy to assess how well they will hold outside the range for which they were originally derived. We therefore simply use the ideal gas law, as given in Equation 7 of *Newell and Baird* [1965] for all gases. This results in the simple parameterization

$$N = \frac{273.15\,\text{K}}{760\,\text{Torr}} \left[ N_{\text{ref},1} \frac{p_1}{T} + N_{\text{ref},2} \frac{p_2}{T} + \cdots \right] \tag{4.2}$$

where $N(T, p)$ is the total refractivity, the first factor reflectes the reference conditions for the *Newell and Baird* [1965] data, $N_{\text{ref},1}$ are the partial refractivities as reported in the abstract of their article, $p_i$ are the partial pressures, and $T$ is temperature.

In addition to reference refractivities of the five species given by *Newell and Baird* [1965], we have derived an equivalent value for $H_2O$ from the $H_2O$ contribution in the parametrization by *Thayer* [1974] for a reference temperature of $T_0$=273.15 K. Using the ideal gas law reduces temperature dependence to inverse proportionality, whereas the *Thayer* [1974] parameterization also carries an inverse quadratic dependence. This causes notable deviations from $H_2O$ refractivity as given by *Thayer* [1974] when temperature is not close to the reference temperature applied. However, the deviations are significantly smaller than when refraction by $H_2O$ is not explicitly accounted for.

Hence, the above formulas can currently be used with up to six contributing gas species ($N_2$, $O_2$, $CO_2$, $H_2$, and He as well as $H_2O$). To account for contributions from further gases (i.e., when volume mixing ratios of these six do not add up to 1), the calculated refractivity from those five gases is normalised to a volume mixing ratio of 1. By adding reference refractive index data from further species – as done for water vapor –, the method can easily be extended and made more complete.

### 4.1.2 Microwave refractive index for Earth (`refr_index_airThayer`)

The microwave refractive index due to gases in the Earths atmosphere is calculated considering so-called compressibility factors (to cover non-ideal gas behaviour). The refractivity of "dry air" and water vapour is summed. All other gases are assumed to have a negligible contribution. [*Thayer*, 1974] **FIXME: be more specific and provide actual formula?**

### 4.1.3 Infrared refractive index for Earth (`refr_index_airIR`)

The infrared refractive index due to gases in the Earth's atmosphere is derived, but only refractivity of "dry air" is considered. The formula used is contributed by Michael Hoepfner, Forschungszentrum Karlsruhe. **FIXME: be more specific and document the actual formula?**

## 4.2 Free electrons

Free electrons, as exist in the ionosphere, will affect propagating radio waves in several ways. Free electrons will have an impact of the propagation speed of radio waves, hence a signal can be delayed and refracted.

An electromagnetic wave passing through a plasma (such as the ionosphere) will drive electrons to oscillate and re-radiating the wave frequency. This is the basic reason of the contribution of electrons to the refractive index. An important variable is the plasma frequency, $\nu_p$:

$$\omega_p = \sqrt{\frac{Ne^2}{\epsilon_0 m}}, \tag{4.3}$$

where $\omega_p = 2\pi\nu_p$, $N$ is the electron density, $e$ is the charge of an electron, $\epsilon_0$ is the permittivity of free space, and $m$ is the mass of an electron. For example, for the Earth's ionosphere $\nu_p \approx 9\,\mathrm{MHz}$. Waves having a frequency below $\nu_p$ are reflected by a plasma.

Neglecting influences of any magnetic field, the refractive index of a plasma is [e.g. *Rybicki and Lightman*, 1979]

$$n = \sqrt{1 - \frac{\omega_p^2}{\omega^2}} = \sqrt{1 - \frac{Ne^2}{\epsilon_0 m \omega^2}}, \tag{4.4}$$

where $\omega$ is the angular frequency ($\omega = 2\pi\nu$). This refractive index is less than unity (phase velocity is greater than the speed of light), but is approaching unity with increasing frequency. The group velocity is [*Rybicki and Lightman*, 1979]

$$v_g = c\sqrt{1 - \frac{Ne^2}{\epsilon_0 m \omega^2}} \tag{4.5}$$

which is clearly less than the speed of light. The energy (or information) of a signal propagating through the ionosphere travels with the group velocity, and the group speed refractive index ($n_g = \frac{c}{v_g}$) is

$$n_g = \left(1 - \frac{Ne^2}{\epsilon_0 m \omega^2}\right)^{-1/2}. \tag{4.6}$$

Equations 4.4 and 4.6 are implemented in refr_index_airFreeElectrons. The method demands that the radiative transfer frequency is at least twice the plasma frequency.

# Chapter 5

# Polarisation and Stokes parameters

The present version of ARTS implements the radiative transfer equation in tensor form, i.e., for the 4 components of the Stokes vector, not just for its first component, the intensity or radiance. This means that the model can include polarisation dependence in absorption or scattering processes. It is therefore necessary to give some details on the polarisation of radiation, the definition of the Stokes parameters, and the definition of antenna polarisation.

## 5.1 Polarisation directions

Electromagnetic waves in homogeneous, isotropic media are transverse waves, i.e., their oscillating electric and magnetic fields are in a plane perpendicular to the propagation direction. The choice of two basis vectors – we shall call them polarisation directions here – that span that transverse plane is arbitrary; often they are called "horizontal" and "vertical" and correspond to some horizontal and vertical direction of the particular setting. Nevertheless, what is meant by horizontal/vertical, or parallel/perpendicular, is purely a matter of definition.

Here, we stick to the system called laboratory frame or fixed frame, used by *Mishchenko et al.* [2002]: We use a coordinate system where the $z$-axis points toward local zenith. We denote the propagation direction of radiation by a unit vector $\mathbf{n} = \mathbf{k}/k$, where $k$ is the wave number. $\mathbf{n}$ is given by two angles, the zenith angle $\theta$ , i.e., the angle between $\mathbf{n}$ and the $z$-axis, and the azimuth angle $\phi$, i.e., the angle between the projection of $\mathbf{n}$ into the $xy$-plane and the $x$-axis:

$$\mathbf{n} = \begin{pmatrix} \cos\phi \sin\theta \\ \sin\phi \sin\theta \\ \cos\theta \end{pmatrix} \tag{5.1}$$

Then we define the polarisation directions by the partial derivatives of $\mathbf{n}$ with respect to $\theta$ and $\phi$. We shall call them $\theta$-direction (also: vertical) and $\phi$-direction (also: horizontal), respectively, see Figure 5.1. Their unit basis vectors are

---

**History**

040524 Section on scattering matrices added by Patrick Eriksson.

040426 Created and written by Christian Melsheimer.

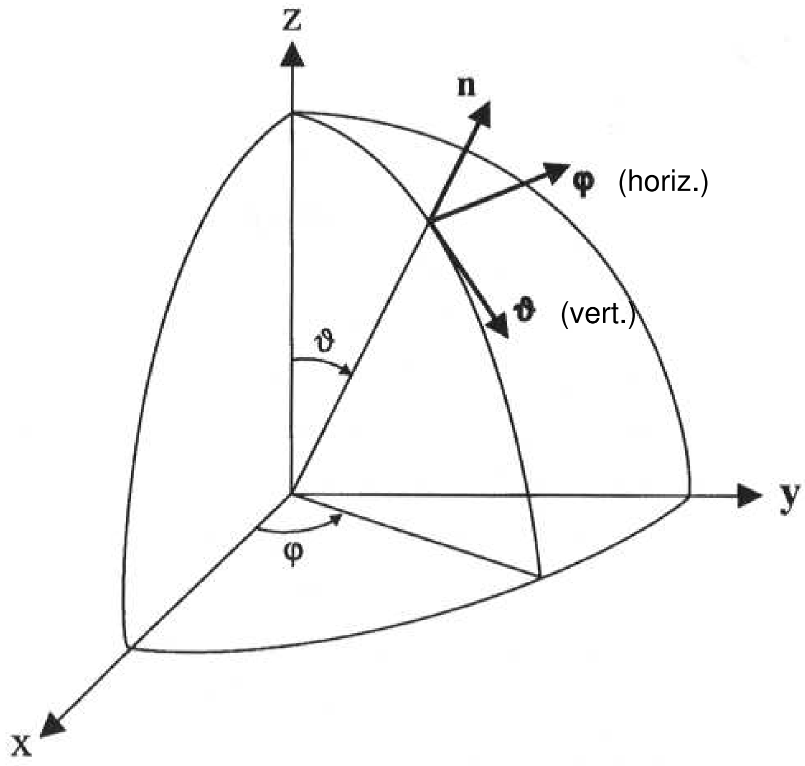


**Figure 1** Laboratory coordinate system.

Figure 5.1: The definition of the polarisation directions, adapted from *Mishchenko et al.* [2002]

$$\mathbf{e}_\theta = \mathbf{e}_v = \frac{\partial \mathbf{n}}{\partial \theta} \Big/ \left\| \frac{\partial \mathbf{n}}{\partial \theta} \right\| = \begin{pmatrix} \cos\phi\cos\theta \\ \sin\phi\cos\theta \\ -\sin\theta \end{pmatrix} \tag{5.2}$$

$$\mathbf{e}_\phi = \mathbf{e}_h = \frac{\partial \mathbf{n}}{\partial \phi} \Big/ \left\| \frac{\partial \mathbf{n}}{\partial \phi} \right\| = \begin{pmatrix} -\sin\phi \\ \cos\phi \\ 0 \end{pmatrix} \tag{5.3}$$

The vectors $\mathbf{n}$, $\mathbf{e}_\theta$ (=$\mathbf{e}_v$), $\mathbf{e}_\phi$ (=$\mathbf{e}_h$) are mutually orthogonal and define (in the mentioned order) a right-handed system, i.e., $(\mathbf{n} \times \mathbf{e}_\theta) \cdot \mathbf{e}_\phi = 1$ and the same for all cyclic permutations.

## 5.2 Plane monochromatic waves

Plane monochromatic electromagnetic waves are commonly written in the form

$$\mathbf{E}(\mathbf{x}, t) = \begin{bmatrix} E_v \\ E_h \end{bmatrix} e^{i(\mathbf{kx} - \omega t)} = (E_v \mathbf{e}_v + E_h \mathbf{e}_h)\, e^{i(\mathbf{kx} - \omega t)} \tag{5.4}$$

where $\mathbf{E}$ is the electric field vector, the subscripts $v$ and $h$ denote the components with vertical and horizontal polarisation, respectively. $E_v$ and $E_h$, the amplitudes, are complex numbers, $\mathbf{k}$ and $\omega$ are the wavenumber vector and the angular frequency, respectively, of the plane wave, and the unit vectors $\mathbf{e}_v = (1, 0)^T$, $\mathbf{e}_h = (0, 1)^T$. It is always implicitly understood that the actual, physical, electric field is the real part of the above expression. Rewriting the complex amplitudes $E_v$ and $E_h$ using real, non-negative amplitudes $a_v$ and $a_h$, and phases $\delta_v$ and $\delta_h$,

$$E_v = a_v e^{i\delta_v},\, E_h = a_h e^{i\delta_h} \tag{5.5}$$

the actual electric field vector $\tilde{\mathbf{E}}$ is

$$\tilde{\mathbf{E}}(\mathbf{x}, t) = \mathrm{Re}[\mathbf{E}(\mathbf{x}, t)] = \begin{bmatrix} a_v \cdot \cos(\mathbf{kx} - \omega t + \delta_v) \\ a_h \cdot \cos(\mathbf{kx} - \omega t + \delta_h) \end{bmatrix} \tag{5.6}$$

In general, instruments do not measure the electric or magnetic field vectors of an electromagnetic wave, but rather the time-averaged intensity, i.e., the energy flux, $F$. This is the time-averaged Poynting vector (which, in turn, is proportional to the square of the electric field), thus:

$$\begin{aligned} F &= \sqrt{\frac{\epsilon}{\mu}}\overline{(\tilde{\mathbf{E}}(\mathbf{x}, t))^2} \\ &= \sqrt{\frac{\epsilon}{\mu}} \left( a_v^2 \overline{\cos^2(\mathbf{kx} - \omega t + \delta_v)} + a_h^2 \overline{\cos^2(\mathbf{kx} - \omega t + \delta_h)} \right) \end{aligned} \tag{5.7}$$

The overline denotes the time average which for cosine squares is 1/2, thus:

$$F = \frac{1}{2}\sqrt{\frac{\epsilon}{\mu}}(a_v^2 + a_h^2) \tag{5.8}$$

Taking into account that for plane, monochromatic waves the time average always results in a factor $\frac{1}{2}$, we can also directly write the intensity using the electric field vector in complex notation (Equation 5.4).

$$\begin{aligned} F &= \frac{1}{2}\sqrt{\frac{\epsilon}{\mu}} \mathbf{E}(\mathbf{x}, t) \cdot \mathbf{E}^*(\mathbf{x}, t) \\ &= \frac{1}{2}\sqrt{\frac{\epsilon}{\mu}}(E_v E_v^* + E_h E_h^*) \end{aligned} \tag{5.9}$$

where the asterisk denotes complex conjugation.

In addition to the flux, three more intensity quantities are defined as in the following equations. They are called *Stokes parameters*:

$$I = \frac{1}{2}\sqrt{\frac{\epsilon}{\mu}}(E_v E_v^* + E_h E_h^*) \tag{5.10}$$

$$Q = \frac{1}{2}\sqrt{\frac{\epsilon}{\mu}}(E_v E_v^* - E_h E_h^*) \tag{5.11}$$

$$U = -\frac{1}{2}\sqrt{\frac{\epsilon}{\mu}}(E_v E_h^* + E_h E_v^*) \tag{5.12}$$

$$V = i\frac{1}{2}\sqrt{\frac{\epsilon}{\mu}}(E_h E_v^* - E_v E_h^*) \tag{5.13}$$

Written as a row or column vector, $(I, Q, U, V)$ is called *Stokes vector*. Note that sometimes, $S_0$, $S_1$, $S_2$, $S_3$ is used instead of $I$, $Q$, $U$, $V$. Using the amplitude/phase notation from Equation 5.5, we can rewrite the Stokes parameters as

$$I = \frac{1}{2}\sqrt{\frac{\epsilon}{\mu}}(a_v^2 + a_h^2) \tag{5.14}$$

$$Q = \frac{1}{2}\sqrt{\frac{\epsilon}{\mu}}(a_v^2 - a_h^2) \tag{5.15}$$

$$U = -\sqrt{\frac{\epsilon}{\mu}}a_v a_h \cos(\delta_v - \delta_h) \tag{5.16}$$

$$V = -\sqrt{\frac{\epsilon}{\mu}}a_v a_h \sin(\delta_v - \delta_h) \tag{5.17}$$

The Stokes parameters fully characterise the electromagnetic wave and therefore contain the same information as the electric field vector (except for one absolute phase). Since instruments generally measure intensities (fluxes), describing electromagnetic radiation by the Stokes parameters is more practical than describing it by the electric (or magnetic) field vector. Furthermore, the Stokes parameters are always real numbers. Note that the Stokes parameters are sometimes defined with different signs of $Q$, $U$, or $V$ (the definitions and signs used here are based on *Mishchenko et al.* [2000]). Moreover, their normalisation may vary. In particular, the Stokes parameters can be normalised to represent radiance or irradiance (instead of intensity), which is usually done in radiative transfer contexts.

In order understand what the Stokes parameters mean, we have to go back to the electric field vector and see what polarisation state it describes. To do so, we look at the curve that the tip of the physical electric field vector $\tilde{\mathbf{E}}$ describes with time at a fixed position $\mathbf{x_0}$:

$$\tilde{E}_v(t) = a_v \cos(\Delta_v - \omega t) \tag{5.18}$$

$$\tilde{E}_h(t) = a_h \cos(\Delta_h - \omega t) \tag{5.19}$$

where $\Delta_{v,h} = \mathbf{k x_0} + \delta_{v,h}$. To see that this is an ellipse, we first split the cosines using the addition theorem:

$$\tilde{E}_v(t) = a_v \cos\Delta_v \cos(\omega t) + a_v \sin\Delta_v \sin(\omega t) \tag{5.20}$$

$$\tilde{E}_h(t) = a_h \cos\Delta_h \cos(\omega t) + a_h \sin\Delta_h \sin(\omega t) \tag{5.21}$$

In order to have the tip of $\tilde{\mathbf{E}}$ describe an ellipse with semi-major axis $a_0 \cos\beta$ and semi-minor axis $a_0 \sin\beta$, where $a_0^2 = a_v^2 + a_h^2$, it should have the following form

$$\tilde{E}_v(t) = a_0 \sin\beta \cos(\omega t) \tag{5.22}$$

$$\tilde{E}_h(t) = a_0 \cos\beta \sin(\omega t) \tag{5.23}$$

Here $\beta$ must be between $-45°$ and $45°$: the tip of the vector $\tilde{\mathbf{E}}$ describes a circle for $\beta = \pm 45°$ (circular polarisation), oscillates along the $h$-axis for $\beta = 0$ (linear polarisation)

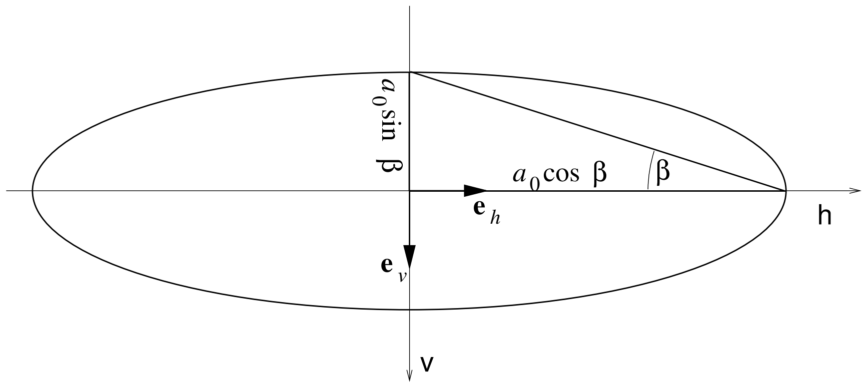


Figure 5.2: The ellipse that the electric field vector describes with time, with the major axis oriented along the $h$-axis.

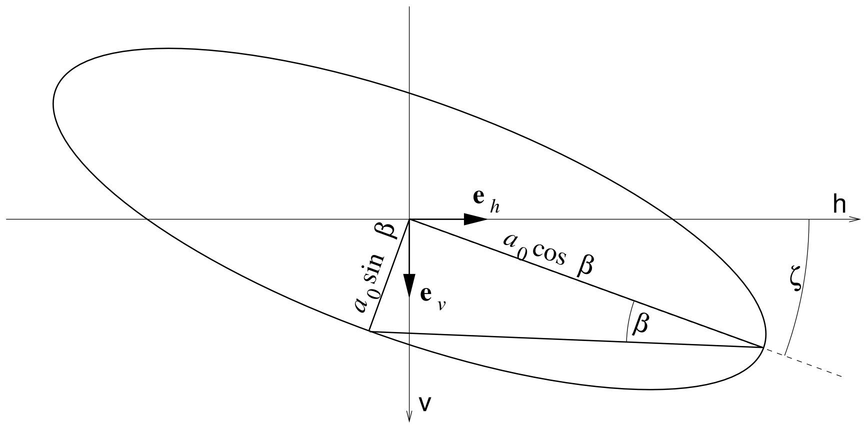


Figure 5.3: The ellipse that the electric field vector describes with time, with the major axis oriented arbitrarily.

and else describes an ellipse (cf. Figure 5.2). The sense of rotation is counterclockwise for positive $\beta$ (corresponding to left-circular or left-elliptic polarisation) and clockwise for negative $\beta$ (corresponding to right-circular or right-elliptic polarisation). Since $|\tan\beta|$ is the ratio of the semi-minor and semi-major axes of the ellipse (the ellipticity), $\beta$ is called the ellipticity angle. Note that the semi-major axis is oriented along the positive $h$-axis. To have the major axis of the ellipse enclose an arbitrary angle $\zeta$ ($0 \leq \zeta < 180°$) with the $h$-axis, we apply a rotation matrix and get the equation for an ellipse with arbitrary shape (ellipticity) and orientation (cf. Figure 5.3):

$$\tilde{E}_v(t) = a_0(\sin\beta\cos(\omega t)\cos\zeta + \cos\beta\sin(\omega t)\sin\zeta) \tag{5.24}$$

$$\tilde{E}_h(t) = a_0(-\sin\beta\cos(\omega t)\sin\zeta + \cos\beta\sin(\omega t)\cos\zeta) \tag{5.25}$$

With these definitions, horizontal polarisation corresponds to $\beta = 0°$ and $\zeta = 0°$; vertical polarisation to $\beta = 0°$ and $\zeta = 90°$; left-circular to $\beta = 45°$ and any value of $\zeta$; right-circular to $\beta = -45°$ and any value of $\zeta$.

Now we want to establish a direct connection between the parameters $\beta$ and $\zeta$ describing the shape (ellipticity) and orientation of the polarisation ellipse on the one hand, and the amplitudes $a_v$ and $a_h$ and phases $\delta_v$ and $\delta_h$ of the components of the electric field vector on the other hand. Comparing the $\sin(\omega t)$ and $\cos(\omega t)$ terms in Equations 5.24 to 5.25 with the corresponding terms in Equations 5.20 to 5.21, we get:

$$a_v \cos \Delta_v = a_0 \sin \beta \cos \zeta \tag{5.26}$$
$$a_v \sin \Delta_v = a_0 \cos \beta \sin \zeta \tag{5.27}$$

and

$$a_h \cos \Delta_h = -a_0 \sin \beta \sin \zeta \tag{5.28}$$
$$a_h \sin \Delta_h = a_0 \cos \beta \cos \zeta \tag{5.29}$$

Multiplying Equation 5.26 with Equation 5.28, and Equation 5.27 with Equation 5.29 and adding up the results, we get

$$a_v a_h (\cos \Delta_v \cos \Delta_h + \sin \Delta_v \sin \Delta_h) = a_0^2 \sin \zeta \cos \zeta (\cos^2 \beta - \sin^2 \beta) \tag{5.30}$$

Using the addition theorems for sinusoidals and taking into account that $\Delta_v - \Delta_h = \delta_v - \delta_h$:

$$\frac{a_v a_h}{a_0^2} \cos(\delta_v - \delta_h) = \tfrac{1}{2} \sin(2\zeta) \cos(2\beta) \tag{5.31}$$

In a similar way, subtracting the product of Equation 5.27 with Equation 5.28 from the product of Equation 5.26 with Equation 5.29 and adding up the results, we get

$$-\frac{a_v a_h}{a_0^2} \sin(\delta_v - \delta_h) = \tfrac{1}{2} \sin(2\beta) \tag{5.32}$$

The above two equations tell us how to translate the amplitudes ($a_v$, $a_h$) and phases ($\delta_v$, $\delta_h$) of the vertical and horizontal component of the electric field into the orientation and shape of the ellipse that the tip of the electric field vector describes with time. We can obtain one further relation by subtracting the sum of the squares of Equation 5.28 and Equation 5.29 from the sum of the squares of Equation 5.26 and Equation 5.27:

$$a_v^2 - a_h^2 = -a_0^2 \cos(2\zeta) \cos(2\beta) \tag{5.33}$$

Finally, we use the above 3 equations (5.31, 5.32 and 5.33) to rewrite the Stokes parameters (Equations 5.14 to 5.17) as

$$I = \tfrac{1}{2}\sqrt{\tfrac{\epsilon}{\mu}}\, a_0^2 \tag{5.34}$$
$$Q = -\tfrac{1}{2}\sqrt{\tfrac{\epsilon}{\mu}}\, a_0^2 \cos(2\zeta)\cos(2\beta) \tag{5.35}$$
$$U = -\tfrac{1}{2}\sqrt{\tfrac{\epsilon}{\mu}}\, a_0^2 \sin(2\zeta)\cos(2\beta) \tag{5.36}$$
$$V = -\tfrac{1}{2}\sqrt{\tfrac{\epsilon}{\mu}}\, a_0^2 \sin(2\beta) \tag{5.37}$$

FIXME: $\beta < 0$ is right-handed pol. (see above, consistent with Jackson and others); thus $V > 0$. This conflicts with Mishchenko's book (p.26).

Thus, we can get the orientation angle $\zeta$ of the ellipse from

$$\tan(2\zeta) = \frac{U}{Q} \tag{5.38}$$

Since $0 \leq 2\zeta < 360°$, there are 2 solutions for $\zeta$ for a given pair $U, Q$. This ambiguity is resolved by looking at Equation 5.35, taking into account that $|\beta| \leq 45°$ and thus $\cos(2\beta) \geq 0$: The sign of $\cos(2\zeta)$ must be the same as the sign of $-Q$.

We get the ellipticity angle $\beta$ from

$$\tan(2\beta) = -\frac{V}{(Q^2 + U^2)^{1/2}} \tag{5.39}$$

$I$ is the total intensity of the radiation, $Q$ is the difference in the intensity of the vertically and horizontally polarised components (cf. Section 5.3). $I$ is always non-negative, and $Q$, $U$, and $V$ are between $+I$ and $-I$, since they can be expressed as a product of $I$ with sines and/or cosines (Equations 5.35 to 5.37). Note also that the 4 Stokes parameters are not independent (for completely polarised radiation, see further Section 5.4), since the following equality applies:

$$I^2 = Q^2 + U^2 + V^2 \tag{5.40}$$

Some examples of Stokes parameters for specific polarisations are given at the end of the next section (page 55).

## 5.3 Measuring Stokes parameters

The three different ways given so far to write the Stokes parameters (Equations 5.10ff., Equations 5.14ff., Equations 5.34ff.) are not very helpful if we actually want to measure the Stokes parameters. So here we are going to rewrite them while keeping in mind that most instruments can just measure intensities of radiation.

We have seen above that the Stokes parameter $Q$ is the difference in the intensity of the vertically and horizontally polarised components (Equations 5.11, or 5.15)

$$Q = I_v - I_h \tag{5.41}$$

where

$$I_v = \tfrac{1}{2}\sqrt{\tfrac{\epsilon}{\mu}} E_v E_v^* \tag{5.42}$$

$$I_h = \tfrac{1}{2}\sqrt{\tfrac{\epsilon}{\mu}} E_h E_h^* \tag{5.43}$$

Thus if we measure $I_v$ and $I_h$ using – for optical wavelengths – a polariser aligned with the $v$- and the $h$-axis, respectively, or using – for microwaves – two appropriately aligned dipole antennas, we can directly obtain $I$ by taking their sum and $Q$ by taking their difference.

$U$ and $V$ can likewise be expressed as differences of intensities, but not with respect to the linear base $\mathbf{e}_v$and $\mathbf{e}_h$. We recall Equation 5.4, omitting the oscillatory term:

$$\mathbf{E} = (E_v \mathbf{e}_v + E_h \mathbf{e}_h) \tag{5.44}$$

Now we want to write $\mathbf{E}$ by two components along polarisation axes at $\pm 45°$ with respect to the $h$-axes. The basis vectors are thus (cf. Figure 5.4)

$$\mathbf{e}_{+45°} = \sqrt{\tfrac{1}{2}}\,(\mathbf{e}_h - \mathbf{e}_v) \tag{5.45}$$

$$\mathbf{e}_{-45°} = \sqrt{\tfrac{1}{2}}\,(\mathbf{e}_h + \mathbf{e}_v) \tag{5.46}$$

and we get the field vector in this modified linear basis:

$$\mathbf{E} = \underbrace{\sqrt{\tfrac{1}{2}}\,(E_v + E_h)}_{E_{-45°}}\,\mathbf{e}_{-45°} + \underbrace{\sqrt{\tfrac{1}{2}}\,(-E_v + E_h)}_{E_{+45°}}\,\mathbf{e}_{+45°} \tag{5.47}$$

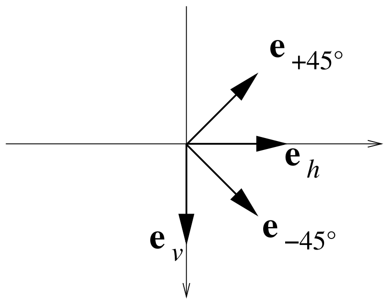


Figure 5.4: Two sets of basis vectors for the linear basis.

With the definitions of intensities of the components,

$$I_{-45^\circ} = \frac{1}{2}\sqrt{\frac{\epsilon}{\mu}}E_{-45^\circ}E^*_{-45^\circ} \tag{5.48}$$

$$I_{+45^\circ} = \frac{1}{2}\sqrt{\frac{\epsilon}{\mu}}E_{+45^\circ}E^*_{+45^\circ} \tag{5.49}$$

we get for their difference:

$$\begin{aligned} I_{-45^\circ} - I_{+45^\circ} &= \frac{1}{2}\sqrt{\frac{\epsilon}{\mu}}\left[\frac{1}{2}(E_v + E_h)(E_v^* + E_h^*) - \frac{1}{2}(-E_v + E_h)(-E_v^* + E_h^*)\right] \\ &= \frac{1}{2}\sqrt{\frac{\epsilon}{\mu}}(E_v E_h^* + E_h E_v^*) \end{aligned} \tag{5.50}$$

Therefore (cf. Equation 5.12)

$$U = I_{+45^\circ} - I_{-45^\circ} \tag{5.51}$$

Thus if we measure $I_{+45^\circ}$ and $I_{-45^\circ}$ using – for optical wavelengths – a polariser aligned at $+45^\circ$ and $-45^\circ$ with respect to the $h$-axis, respectively, or using – for microwaves – two appropriately aligned dipole antennas, we can directly obtain $U$ by taking their difference.

In order to see how to measure the fourth Stokes parameter, $V$, we have to transform to the circular basis, i.e., express $\mathbf{E}$ by a left-hand ($LH$) and a right-hand ($RH$) circularly polarised component. The relevant equations:

Basis vectors

$$\mathbf{e}_{LH} = \sqrt{\frac{1}{2}}\,(\mathbf{e}_v + i\mathbf{e}_h) \tag{5.52}$$

$$\mathbf{e}_{RH} = \sqrt{\frac{1}{2}}\,(\mathbf{e}_v - i\mathbf{e}_h) \tag{5.53}$$

Field vector in circular base

$$\mathbf{E} = \underbrace{\sqrt{\frac{1}{2}}\,(E_v - iE_h)}_{E_{LH}}\,\mathbf{e}_{LH} + \underbrace{\sqrt{\frac{1}{2}}\,(E_v + iE_h)}_{E_{RH}}\,\mathbf{e}_{RH} \tag{5.54}$$

Intensity of the components

$$I_{LH} = \frac{1}{2}\sqrt{\frac{\epsilon}{\mu}}E_{LH}E^*_{LH} \tag{5.55}$$

$$I_{RH} = \frac{1}{2}\sqrt{\frac{\epsilon}{\mu}}E_{RH}E^*_{RH} \tag{5.56}$$

Their difference

$$\begin{aligned} I_{LH} - I_{RH} &= \frac{1}{2}\sqrt{\frac{\epsilon}{\mu}}\left[\frac{1}{2}(E_v - iE_h)(E_v^* + iE_h^*) - \frac{1}{2}(E_v + iE_h)(E_v^* - iE_h^*)\right] \\ &= i\frac{1}{2}\sqrt{\frac{\epsilon}{\mu}}(E_v E_h^* - E_h E_v^*) \end{aligned} \tag{5.57}$$

Therefore (cf. Equation 5.13):

$$V = I_{RH} - I_{LH} \tag{5.58}$$

Thus if we measure $I_{RH}$ and $I_{LH}$ using – for microwaves – appropriate helical beam antennas, we can directly obtain $V$ by taking their difference. Unfortunately, for optical wavelengths, we cannot measure $I_{RH}$ and $I_{LH}$ directly with the help of filters like polarisers and retarders[1]. However, a combination of a retarder and a polarizer can be used to measure the sum of $I$ and $V$:

The light first passes through a retarder that delays the phase of the horizontally polarised component by 90° with respect to the phase of the vertically polarised component (a quarter-wave plate). A phase delay by 90°can be expressed as a multiplication of the horizontal component by $i$, so the resulting electric field vector $\mathbf{E}'$ is

$$\mathbf{E}' = (E_v \mathbf{e}_v + iE_h \mathbf{e}_h) \tag{5.59}$$

The light then passes through a polarizer that is aligned at $-45°$ with respect to the $h$-axis. This means we have to project $\mathbf{E}'$ onto $\mathbf{e}_{-45°}$, resulting in

$$\mathbf{E}'' = (\mathbf{E}' \cdot \mathbf{e}_{-45°})\mathbf{e}_{-45°} = \sqrt{\tfrac{1}{2}}\,(E_v + iE_h)\,\mathbf{e}_{-45°} \tag{5.60}$$

Measuring the intensity now, we get

$$\begin{aligned} I'' &= |\mathbf{E}''|^2 \qquad (5.61)\\ &= \tfrac{1}{2}\,(E_v + iE_h)\,(E_v^* - iE_h^*)\\ &= \tfrac{1}{2}\left(|E_v|^2 + |E_h|^2 - i(E_v E_h^* - E_h E_v^*)\right)\\ &= \tfrac{1}{2}(I + V) \end{aligned}$$

Here is a summary of the Stokes parameters in terms of intensities of orthogonal components:

$$\begin{aligned} I &= I_v + I_h = I_{-45°} + I_{+45°} = I_{RH} + I_{LH} \qquad (5.62)\\ Q &= I_v - I_h \qquad (5.63)\\ U &= I_{+45°} - I_{-45°} \qquad (5.64)\\ V &= I_{RH} - I_{LH} \qquad (5.65) \end{aligned}$$

We see that $Q$ and $U$ are both related to linear polarisation, while $V$ is related to circular polarisation.

Here are the Stokes parameters for some standard polarisations:

| polarisation | $(I,\ Q,\ U,\ V)$ |
|---|---|
| horizontal | $(I, -I,\ 0,\ 0)$ |
| vertical | $(I, +I,\ 0,\ 0)$ |
| linear $\pm 45°$ | $(I,\ 0, \mp I,\ 0)$ |
| right-circular | $(I,\ 0,\ 0,\ I)$ |
| left-circular | $(I,\ 0,\ 0, -I)$ |

[1] A retarder allows the phase of two orthogonal components of light to be varied with respect to each other.

## 5.4 Partial polarisation

The equality $I^2 = Q^2 + U^2 + V^2$ (Equation 5.40) is valid for the ideal case of a monochromatic plane wave that is completely polarised, i.e., where the amplitudes $a_v$ and $a_h$ and the phases $\delta_v$ and $\delta_v$ are fixed and do not vary with time. This means that the plane wave is emitted by one coherent source.

In reality, i.e., in the case of natural radiation, the amplitudes and phases fluctuate, since the radiation originates from several sources that do not emit radiation coherently, and since the emission from one source usually has very short coherence times. This means that we usually have a superposition of radiation from several incoherent sources, and that the polarisation state of the radiation from each source fluctuates as well[2]. Typically, such fluctuations have time scales that are longer than the period $(2\pi/\omega)$ of the oscillation, but that are still shorter than the integration time of the instrument that measures the radiation. Thus, the instrument measures an incoherent superposition of time averages over of the fluctuating polarisation. If the fluctuations are random for all the sources and if the different sources emit incoherently and are not in any way oriented, then there is no preferred orientation, ellipticity or handedness of the emitted radiation, which is then called unpolarised. This is the case for radiation from the sun. If the fluctuations are not completely random, the radiation is called partially polarised.

To quantify this rather heuristic argumentation, we express the above-mentioned ideas in the language of the Stokes parameters: The Stokes parameters $I$, $Q$, $U$, $V$ derived from measurements result from the superposition of radiation from many sources and/or the average over emission events with individual Stokes parameters $I_i$, $Q_i$, $U_i$, $V_i$. Since the different sources and/or emission events are incoherent, the Stokes parameters – which are intensity, not amplitude quantities – can simply be added up:

$$I = \sum_i I_i \,, \quad Q = \sum_i Q_i \,, \quad U = \sum_i U_i \,, \quad V = \sum_i V_i \tag{5.66}$$

In the case of unpolarised radiation, i.e., when the amplitudes and phases, or equivalently, the orientation angle $\zeta$ and the ellipticity angle $\beta$ are random (uniformly distributed), $Q$, $U$, and $V$ each cancel out.

The equality $I_i^2 = Q_i^2 + U_i^2 + V_i^2$ (cf. Equation 5.40) still holds for each contribution $i$, but for the resulting $I, Q, U, V$, we have in general the inequality

$$I^2 \geq Q^2 + U^2 + V^2 \tag{5.67}$$

To prove it, we must once again go back to the amplitude/phase notation (Equations 5.14ff.), also cf. *Chandrasekhar* [1960, chap. I.15], but we shall omit the factor $\frac{1}{2}\sqrt{\frac{\epsilon}{\mu}}$ on the right-hand sides, for the sake of better readability:

$$I = \sum_i I_i = \sum_i \left(a_v^{(i)}\right)^2 + \sum_i \left(a_h^{(i)}\right)^2 \tag{5.68}$$

$$Q = \sum_i Q_i = \sum_i \left(a_v^{(i)}\right)^2 - \sum_i \left(a_h^{(i)}\right)^2 \tag{5.69}$$

$$U = \sum_i U_i = -2 \sum_i a_v^{(i)} a_h^{(i)} \cos\delta^{(i)} \tag{5.70}$$

$$V = \sum_i V_i = 2 \sum_i a_v^{(i)} a_h^{(i)} \sin\delta^{(i)} \tag{5.71}$$

(5.72)

[2]This does, of course, not apply to coherent sources like lasers or coherent radars.

where $\delta^{(i)} = \delta_v^{(i)} - \delta_h^{(i)}$. We get

$$
\begin{aligned}
I^2 - Q^2 - U^2 - V^2 &= 4\sum_i \left(a_v^{(i)}\right)^2 \sum_i \left(a_h^{(i)}\right)^2 \\
&\quad -4\left(\sum_i a_v^{(i)} a_h^{(i)} \cos\delta^{(i)}\right)^2 \\
&\quad -4\left(\sum_i a_v^{(i)} a_h^{(i)} \sin\delta^{(i)}\right)^2
\end{aligned}
\tag{5.73}
$$

The first term on the right-hand side can be rearranged as

$$
\sum_i \left(a_v^{(i)} a_h^{(i)}\right)^2 + \sum_{\substack{i,j \\ i\neq j}} \left(a_v^{(i)} a_h^{(j)}\right)^2
\tag{5.74}
$$

The other two terms can be rearranged similarly to yield:

$$
\begin{aligned}
&-\sum_i \left(a_v^{(i)} a_h^{(i)}\right)^2 \left[\cos^2\delta^{(i)} + \sin^2\delta^{(i)}\right] \\
&-\sum_{\substack{i,j \\ i\neq j}} a_v^{(i)} a_h^{(i)} a_v^{(j)} a_h^{(j)} \left[\cos\delta^{(i)}\cos\delta^{(j)} + \sin\delta^{(i)}\sin\delta^{(j)}\right]
\end{aligned}
\tag{5.75}
$$

Putting this into Equation 5.73 (and dividing by 4), the sums over just $i$ cancel and we get:

$$
\begin{aligned}
(I^2 - Q^2 - U^2 - V^2)/4 &= \sum_{\substack{i,j \\ i\neq j}} \left(a_v^{(i)} a_h^{(j)}\right)^2 \\
&\quad -\sum_{\substack{i,j \\ i\neq j}} a_v^{(i)} a_h^{(i)} a_v^{(j)} a_h^{(j)} \cos(\delta^{(i)} - \delta^{(j)})
\end{aligned}
\tag{5.76}
$$

where the cosine addition theorem was used. In the summation, we now change from $i \neq j$ to $i < j$, so we have to symmetrise the first term (the second term is already symmetric with respect to $i$ and $j$ and therefore just gets a factor 2):

$$
\begin{aligned}
(I^2 - Q^2 - U^2 - V^2)/4 &= \sum_{\substack{i,j \\ i<j}} \Bigg[\left(a_v^{(i)} a_h^{(j)}\right)^2 + \left(a_v^{(j)} a_h^{(i)}\right)^2 \\
&\quad -2\left(a_v^{(i)} a_h^{(j)}\right)\left(a_v^{(j)} a_h^{(i)}\right)\cos(\delta^{(i)} - \delta^{(j)})\Bigg]
\end{aligned}
\tag{5.77}
$$

Each summand of the sum on the right-hand side is positive, since it is greater than or equal to $(a_v^{(i)} a_h^{(j)} - a_v^{(j)} a_h^{(i)})^2$, which completes the proof. The right-hand side vanishes only if $\delta^{(i)} = \delta^{(j)}$ and $a_v^{(i)}/a_h^{(i)} = a_v^{(j)}/a_h^{(j)}$ for all $i, j$, i.e., if the phase difference and amplitude ratio between the horizontal and vertical component of the electric field is the same for all contributions, in other words: if all contributions have the same polarisation.

For completeness, we shall now restate the definition of the Stokes component, extended to include natural radiation (i.e., including the case of partially polarised and unpolarised radiation). Instead of summing over the individual emission events, we use ensemble averages, denoted by angular brackets:

$$
I = \tfrac{1}{2}\sqrt{\tfrac{\epsilon}{\mu}}\,\langle E_v E_v^* + E_h E_h^* \rangle
\tag{5.78}
$$

$$Q = \frac{1}{2}\sqrt{\frac{\epsilon}{\mu}}\langle E_v E_v^* - E_h E_h^* \rangle \tag{5.79}$$

$$U = -\frac{1}{2}\sqrt{\frac{\epsilon}{\mu}}\langle E_v E_h^* + E_h E_v^* \rangle \tag{5.80}$$

$$V = i\frac{1}{2}\sqrt{\frac{\epsilon}{\mu}}\langle E_h E_v^* - E_v E_h^* \rangle \tag{5.81}$$

Except for the ensemble average $\langle .. \rangle$, the definition is identical to the one for monochromatic, plane waves (Equations 5.10 to 5.13). The same applies to the second and third definitions of the Stokes parameters (Equations 5.14 to 5.17 and Equations 5.34 to 5.37, respectively). Note that the fourth definition (Equations 5.62 to 5.65) which uses sums and differences of intensities, is equally valid for fully polarised, partially polarised and unpolarised radiation. The definition of intensities, however, has to include the ensemble average: $I_h = \langle E_h E_h^* \rangle$ etc.

Now we can define a measure for the degree of polarisation, $p$, as:

$$p = \frac{\sqrt{Q^2 + U^2 + V^2}}{I} \tag{5.82}$$

For completely polarised radiation, $Q^2 + U^2 + V^2 = I^2$, so $p = 1$, and for unpolarised radiation, $Q = U = V = 0$, so $p = 0$.

Furthermore, it can be convenient to define the polarised component of radiation by

$$I_p^2 = Q^2 + U^2 + V^2 \tag{5.83}$$

and the unpolarised component as

$$I_u = I - I_p \tag{5.84}$$

Thus, partially polarised radiation, described by a Stokes vector $(I, Q, U, V)$, can be regarded as as a superposition of completely polarised radiation described by the Stokes vector $(I_p, Q, U, V)$ and unpolarised radiation described by the Stokes vector $(I_u, 0, 0, 0)$. We see that the Stokes parameter formalism can conveniently deal with partially polarised and with unpolarised radiation, much in contrast to the formalism using the electric field (amplitude and phase).

In addition to the degree of polarisation, $p$, we can define measures for the circularity and the linearity of the polarisation. Recalling Equations 5.64 and 5.65, we can define the degree of linear polarisation, $p_{lin}$, as

$$p_{lin} = \frac{\sqrt{Q^2 + U^2}}{I} \tag{5.85}$$

and the the degree of circular polarisation, $p_{circ}$, as

$$p_{circ} = \frac{V}{I} \tag{5.86}$$

### 5.4.1 Polarisation of Radiation in the Atmosphere

The radiation encountered in atmospheric sounding (for which ARTS is intended) is natural radiation, coming from the sun, space (cosmic background), and/or the atmosphere and the Earth surface (thermal radiation, scattered radiation)[3]. Radiation from the sun is unpolarised, as already mentioned; the same applies for the cosmic background. In contrast,

[3]This is not so for active sounding techniques that use a coherent source, such as lidar.

radiation emitted by the ground can be polarised, dependent on material, texture and direction. Radiation emitted by the atmosphere (thermal radiation) is almost unpolarised because of the random orientation of the air molecules. An exception is caused by the Zeeman effect induced in oxygen molecules by the – anisotropic – Earth's magnetic field. Scattering of radiation by oriented particles, e.g. cirrus clouds, is sensitive to polarisation, and generally increases the degree of polarisation. Typically $I > |Q| > |U|, |V|$.

### 5.4.2 Antenna polarisation

Finally we want to know what an antenna of arbitrary polarisation response (antenna polarisation) measures if radiation of some other arbitrary polarisation is incident on it.

In order to clarify the concept, we first consider some trivial examples: We assume an antenna that receives only vertically polarised radiation.

- If the incident radiation is fully horizontally polarised, the antenna will measure nothing.
- If the incident radiation is fully vertically polarised, the antenna will measure the full intensity of the radiation.
- If the radiation is fully left- or right-circularly polarised, the antenna will measure half of the full intensity, for circularly polarised radiation is made up of equal portions of vertically and horizontally polarised radiation, superimposed with a phase lag of 90°.

In order to be able to describe the general case, we first have to formalise the description of the antenna polarisation. Polarised radiation is described by

1. the Jones vector, or
2. the Stokes vector, or
3. intensity, $I$, orientation angle, $\zeta$ (i.e., the angle between the major axis of the polarisation ellipse and the horizontal polarisation direction), and ellipticity angle, $\beta$ (see page 51).

Since the intensity of the radiation is the absolute square (the squared "length") of the complex Jones vector, or, in other words, the first Stokes component, $I$, the polarisation alone is defined by

1. a normalised Jones vector, or
2. three normalised Stokes components $Q$, $U$, and $V$ (where $Q^2 + U^2 + V^2 = 1$), or
3. the orientation angle $\zeta$ and the ellipticity angle $\beta$ (see Equation 5.38 to 5.39).

In the same way, the polarisation of the antenna can be described in one of three ways:

1. a normalised Jones vector

$$\mathbf{e} = \begin{bmatrix} e_v \\ e_h \end{bmatrix} \qquad \text{where} \quad \mathbf{e} \cdot \mathbf{e}^* = 1 \tag{5.87}$$

   (note that in the scalar product of two complex vectors, the second one has to be complex-conjugated.)

2. a normalised Stokes vector

$$\mathbf{i} = (1, q, u, v) \qquad \text{where} \quad q^2 + u^2 + v^2 = 1 \tag{5.88}$$

3. the two angles $\zeta$ and $\beta$. According to Equation 5.34 to 5.37, we have:

$$q = -\cos(2\zeta)\cos(2\beta) \tag{5.89}$$
$$u = -\sin(2\zeta)\cos(2\beta) \tag{5.90}$$
$$v = -\sin(2\beta) \tag{5.91}$$

Now we can calculate the intensity $I'$ the antenna measures. In terms of the electrical fields, i.e., Jones vectors, we just have to project the Jones vector $\mathbf{E}$ of the incident radiation onto the normalised Jones vector $\mathbf{e}$ of the antenna,

$$\mathbf{E}' = (\mathbf{E} \cdot \mathbf{e}^*)\mathbf{e} \tag{5.92}$$

(this is in effect like passing through a polarizer) and then take its absolute square

$$I' = \frac{1}{2}\sqrt{\frac{\epsilon}{\mu}}\,|\mathbf{E}'|^2 = \frac{1}{2}\sqrt{\frac{\epsilon}{\mu}}\,|(\mathbf{E} \cdot \mathbf{e}^*)|^2 \tag{5.93}$$

With some elementary algebra (mainly using that $\frac{1}{2}\sqrt{\frac{\epsilon}{\mu}}E_v E_v^* = (I+Q)/2$, $\frac{1}{2}\sqrt{\frac{\epsilon}{\mu}}E_h E_h^* = (I-Q)/2$, $\frac{1}{2}\sqrt{\frac{\epsilon}{\mu}}E_v E_h^* = -(U - \mathrm{i}V)/2$ which follow immediately from Equation 5.10 to 5.13 ) this can be rewritten in terms of the of the Stokes vector $\mathbf{I}$ of the incident radiation and the Stokes vector $\mathbf{i}$ of the antenna. It turns out to be just a scalar product:

$$I' = \frac{1}{2}\mathbf{i} \cdot \mathbf{I} \tag{5.94}$$

## 5.5 The scattering amplitude matrix

The electric field, $[E_v, E_h]^T$, originating from a single scattering event of an incident electric field $[E_v^0, E_h^0]^T$ may in the far field be written as (see further Equation 6.7)

$$\begin{bmatrix} E_v \\ E_h \end{bmatrix} = f(r) \begin{bmatrix} S_2 & S_3 \\ S_4 & S_1 \end{bmatrix} \begin{bmatrix} E_v^0 \\ E_h^0 \end{bmatrix}, \tag{5.95}$$

where $S_j$ are the scattering amplitude functions and all distance effects are put into the function $f(r)$. Using Stokes based nomenclature, the equation above becomes

$$\begin{bmatrix} I \\ Q \\ U \\ V \end{bmatrix} = g(r)\mathbf{F} \begin{bmatrix} I^0 \\ Q^0 \\ U^0 \\ V^0 \end{bmatrix}, \tag{5.96}$$

where all distance effects are put into the function $g(r)$ and the transformation matrix $\mathbf{F}$ can be expressed as [*Liou*, 2002, Sec. 5.4.3].

$$\mathbf{F} = \begin{bmatrix} \frac{1}{2}(M_2{+}M_3{+}M_4{+}M_1) & \frac{1}{2}(M_2{-}M_3{+}M_4{-}M_1) & S_{23}{+}S_{41} & -D_{23}{-}D_{41} \\ \frac{1}{2}(M_2{+}M_3{-}M_4{-}M_1) & \frac{1}{2}(M_2{-}M_3{-}M_4{+}M_1) & S_{23}{-}S_{41} & -D_{23}{+}D_{41} \\ S_{24}{+}S_{31} & S_{24}{-}S_{31} & S_{21}{+}S_{34} & -D_{21}{+}D_{34} \\ D_{24}{+}D_{31} & D_{24}{-}D_{31} & D_{21}{+}D_{34} & S_{21}{-}S_{34} \end{bmatrix}. \tag{5.97}$$

The elements of **F** are finally given by the following expressions:

$$M_k = |S_k|^2, \tag{5.98}$$

$$S_{kj} = S_{jk} = (S_j S_k^* + S_k S_j^*)/2, \tag{5.99}$$

$$-D_{kj} = D_{jk} = i(S_j S_k^* - S_k S_j^*)/2, \qquad j, k = 1, 2, 3, 4. \tag{5.100}$$

Depending on the properties of the scattering event, the structure of the matrix **F** differs. Two special cases are:

$$S_1 = S_2, \quad S_3 = S_4 = 0 \quad \rightarrow \quad \mathbf{F} = \begin{bmatrix} x & 0 & 0 & 0 \\ 0 & x & 0 & 0 \\ 0 & 0 & x & 0 \\ 0 & 0 & 0 & x \end{bmatrix}, \tag{5.101}$$

$$S_3 = S_4 = 0 \quad \rightarrow \quad \mathbf{F} = \begin{bmatrix} x & x & 0 & 0 \\ x & x & 0 & 0 \\ 0 & 0 & x & x \\ 0 & 0 & x & x \end{bmatrix}, \tag{5.102}$$

where $x$ indicates elements deviating from 0. Many (most?) natural materials have the property that $S_4$ is the complex conjugate of $S_3$ ($S_3 = S_4^*$) and this results in that **F** is a symmetric matrix (in general with all element positions filled).

# Chapter 6

# Basic radiative transfer theory

When dealing with atmospheric radiation a division can be made between two different wavelength ranges where the limit is found around 5 $\mu$m, i.e. one range consists of the near IR, visible and UV regions while the second range covers thermal and far IR and microwaves. The first reason to this division is the principal sources to the radiation in the two ranges, for wavelengths shorter than 5 $\mu$m the solar radiation is dominating while at longer wavelengths the thermal emission from the surface and the atmosphere is more important. A second reason is the importance of scattering but here it is impossible to give a fixed limit. Clouds are important scattering objects for most frequencies but at cloud free conditions scattering can in many cases be neglected for wavelengths $> 5$ $\mu$m. If the atmosphere can be assumed to be in local thermodynamic equilibrium the radiative transfer can be simplified considerably, and this is a valid assumption for the IR region and microwaves but not for e.g. UV frequencies.

The radiative transfer in the atmosphere must be adequately described in many situations, as when estimating rates of photochemical reactions, calculating radiative forcing in the atmosphere or evaluating a remote sensing observation. It is not totally straightforward to quantify the radiative transfer with good accuracy because the calculations can be very computationally demanding and many of the parameters needed are hard to determine. For example, situations when a great number of transitions or multiple scattering must be considered will cause long calculations while as a rule scattering is problematic to model because the shape and size distribution of the scattering particles are highly variable quantities.

This chapter introduces the theoretical background which is essential to develop a radiative transfer model including scattering. The theory is based on concepts of electrodynamics, starting from the Maxwell equations. An elementary book for electrodynamics is written by *Jackson* [1998]. For optics and scattering of radiation by small particles the reader may refer for instance to *van de Hulst* [1957] and *Bohren and Huffman* [1998]. The notation used in this chapter is mostly adapted from the book "Scattering, Absorption, and

---

**History**

| | |
|---|---|
| 120924 | Added discussion of the n2-law, mainly using text originally written for an ESA report by Bengt Rydberg (PE). |
| 110615 | Revised, and moved parts about surface from AUG (PE). |
| 050224 | Most text replaced by chapter 1 from Claudia Emde's phd-thesis. |
| 030305 | Copied from a compendium written by Patrick Eriksson. |

Emission of Light by Small Particles" by *Mishchenko et al.* [2002]. Several lengthy derivations of formulas, which are not shown in detail here, can also be found in this book. The purpose of this chapter is to provide definitions and give ideas, how these definitions can be derived using principles of electromagnetic theory. For the derivation of the radiative transfer equation an outline of the traditional phenomenological approach is given.

## 6.1 Basic definitions

From the Maxwell equations one can derive the formula for the electromagnetic field vector $\mathbf{E}$ of a plane electromagnetic wave propagating in a homogeneous medium without sources:

$$\mathbf{E}(\mathbf{r},t) = \mathbf{E}_0 \exp\left(-\frac{\omega}{c} m_\mathrm{I} \hat{\hat{\mathbf{n}}} \cdot \mathbf{r}\right) \exp\left(i\frac{\omega}{c} m_\mathrm{R} \hat{\hat{\mathbf{n}}} \cdot \mathbf{r} - i\omega t\right), \tag{6.1}$$

where $\mathbf{E}_0$ is the amplitude of the electromagnetic wave in vacuum, $c$ is the speed of light in vacuum, $\omega$ is the angular frequency, $\mathbf{r}$ is the position vector and $\hat{\hat{\mathbf{n}}}$ is a real unit vector in the direction of propagation. The complex refractive index $m$ is

$$m = m_\mathrm{R} + i m_\mathrm{I} = c\sqrt{\epsilon\mu}, \tag{6.2}$$

where $m_\mathrm{R}$ is the non-negative real part and $m_\mathrm{I}$ is the non-negative imaginary part. Furthermore $\mu$ is the permeability of the medium and $\epsilon$ the permittivity. For a vacuum, $m = m_\mathrm{R} = 1$. The imaginary part of the refractive index, if it is non-zero, determines the decay of the amplitude of the wave as it propagates through the medium, which is thus absorbing. The real part determines the phase velocity $v = c/m_\mathrm{R}$. The time-averaged Poynting vector $\mathbf{P}(\mathbf{r})$, which describes the flow of electromagnetic energy, is defined as

$$\mathbf{P}(\mathbf{r}) = \frac{1}{2}\mathrm{Re}(\langle\mathbf{E}(\mathbf{r})\rangle \times \langle\mathbf{H}^*(\mathbf{r})\rangle), \tag{6.3}$$

where $\mathbf{H}$ is the magnetic field vector and the $*$ denotes the complex conjugate. The Poynting vector for a homogeneous wave is given by

$$\langle\mathbf{P}(\mathbf{r})\rangle = \frac{1}{2}\mathrm{Re}\left(\sqrt{\frac{\epsilon}{\mu}}\right)|\mathbf{E}_0|^2 \exp\left(-2\frac{\omega}{c} m_\mathrm{I} \hat{\hat{\mathbf{n}}} \cdot \mathbf{r}\right)\hat{\hat{\mathbf{n}}}. \tag{6.4}$$

Equation 6.4 shows that the energy flows in the direction of propagation and its absolute value $I(\mathbf{r}) = |\langle\mathbf{P}(\mathbf{r})\rangle|$, which is usually called intensity (or irradiance), is exponentially attenuated. Rewriting Equation 6.4 gives

$$I(\mathbf{r}) = I_0 \exp(-\alpha^p \hat{\hat{\mathbf{n}}} \cdot \mathbf{r}), \tag{6.5}$$

where $I_0$ is the intensity for $\mathbf{r} = \mathbf{0}$. The absorption coefficient $\alpha^p$ is

$$\alpha^p = 2\frac{\omega}{c} m_\mathrm{I} = \frac{4\pi m_\mathrm{I}}{\lambda} = \frac{4\pi m_\mathrm{I}\nu}{c}, \tag{6.6}$$

where $\lambda$ is the free-space wavelength and $\nu$ the frequency. Intensity has the dimension of monochromatic flux $[\mathrm{energy}/(\mathrm{area} \times \mathrm{time})]$.

## 6.2 Scattering, absorption and thermal emission by a single particle

A parallel monochromatic beam of electromagnetic radiation propagates in vacuum without any change in its intensity or polarization state. A small particle, which is interposed into the beam, can cause several effects:

**Absorption:** The particle converts some of the energy contained in the beam into other forms of energy.

**Elastic scattering:** Part of the incident energy is extracted from the beam and scattered into all spatial directions at the frequency of the incident beam. Scattering can change the polarization state of the radiation.

**Inelastic scattering:** As above, but the frequency is changed by the scattering. This process is neglected below.

**Extinction:** The energy of the incident beam is reduced by an amount equal to the sum of absorption and scattering.

**Dichroism:** The change of the polarization state of the beam as it passes a particle.

**Thermal emission:** If the temperature of the particle is non-zero, the particle emits radiation in all directions over a large frequency range.

The beam is an oscillating plane magnetic wave, whereas the particle can be described as an aggregation of a large number of discrete elementary electric charges. The incident wave excites the charges to oscillate with the same frequency and thereby radiate secondary electromagnetic waves. The superposition of these waves gives the total elastically scattered field.

One can also describe the particle as an object with a refractive index different from that of the surrounding medium. The presence of such an object changes the electromagnetic field that would otherwise exist in an unbounded homogeneous space. The difference of the total field in the presence of the object can be thought of as the field *scattered* by the object. The angular distribution and the polarization of the scattered field depend on the characteristics of the incident field as well as on the properties of the object as its size relative to the wavelength and its shape, composition and orientation.

### 6.2.1 Definition of the amplitude matrix

For the derivation of a relation between the incident and the scattered electric field we consider a finite scattering object in the form of a single body or a fixed aggregate embedded in an infinite homogeneous, isotropic and non-absorbing medium. We assume that the individual bodies forming the scattering object are sufficiently large that they can be characterized by optical constants appropriate to bulk matter, not to optical constants appropriate for single atoms or molecules. Solving the Maxwell equations for the internal volume, which is the interior of the scattering object, and the external volume one can derive a formula, which expresses the total electric field everywhere in space in terms of the incident field and the field inside the scattering object. Applying the far field approximation gives a relation between incident and scattered field, which is that of a spherical wave. The amplitude matrix $\mathbf{S}(\hat{\mathbf{n}}^{\mathrm{sca}}, \hat{\mathbf{n}}^{\mathrm{inc}})$ includes this relation:

$$\begin{bmatrix} E_{\psi}^{\mathrm{sca}}(r\hat{\mathbf{n}}^{\mathrm{sca}}) \\ E_{\omega}^{\mathrm{sca}}(r\hat{\mathbf{n}}^{\mathrm{sca}}) \end{bmatrix} = \frac{e^{ikr}}{r}\mathbf{S}(\hat{\mathbf{n}}^{\mathrm{sca}}, \hat{\mathbf{n}}^{\mathrm{inc}}) \begin{bmatrix} E_{0\psi}^{\mathrm{inc}} \\ E_{0\omega}^{\mathrm{inc}} \end{bmatrix}. \tag{6.7}$$

The amplitude matrix depends on the directions of incident $\hat{\mathbf{n}}^{\mathrm{inc}}$ and scattering $\hat{\mathbf{n}}^{\mathrm{sca}}$ as well as on size, morphology, composition, and orientation of the scattering object with respect to the coordinate system. The distance between the origin and the observation point is denoted by $r$ and the wave number of the external volume is denoted by $k$.

The amplitude matrix provides a complete description of the scattering pattern in the far field zone. The amplitude matrix explicitly depends on $\omega^{\mathrm{inc}}$ and $\omega^{\mathrm{sca}}$ even when $\psi^{\mathrm{inc}}$ and/or $\psi^{\mathrm{sca}}$ equal 0 or $\pi$.

### 6.2.2 Phase matrix

The phase matrix $\mathbf{Z}$ describes the transformation of the Stokes vector of the incident wave into that of the scattered wave for scattering directions away from the incidence direction ($\hat{\mathbf{n}}^{\mathrm{sca}} \neq \hat{\mathbf{n}}^{\mathrm{inc}}$),

$$\mathbf{s}^{\mathrm{sca}}(r\hat{\mathbf{n}}^{\mathrm{sca}}) = \frac{1}{r^2}\mathbf{Z}(\hat{\mathbf{n}}^{\mathrm{sca}}, \hat{\mathbf{n}}^{\mathrm{inc}})\mathbf{s}^{\mathrm{inc}}. \tag{6.8}$$

The $4 \times 4$ phase matrix can be written in terms of the amplitude matrix elements for single particles [*Mishchenko et al.*, 2002]. All elements of the phase matrix have the dimension of area and are real. As the amplitude matrix, the phase matrix depends on $\omega^{\mathrm{inc}}$ and $\omega^{\mathrm{sca}}$ even when $\psi^{\mathrm{inc}}$ and/or $\psi^{\mathrm{sca}}$ equal 0 or $\pi$. In general, all 16 elements of the phase matrix are non-zero, but they can be expressed in terms of only seven independent real numbers. Four elements result from the moduli $|S_{ij}|$ $(i, j = 1, 2)$ and three from the phase-differences between $S_{ij}$. If the incident beam is unpolarized, i.e., $\mathbf{s}^{\mathrm{inc}} = (I^{\mathrm{inc}}, 0, 0, 0)^T$, the scattered light generally has at least one non-zero Stokes parameter other than intensity:

$$I^{\mathrm{sca}} = Z_{11}I^{\mathrm{inc}}, \tag{6.9}$$
$$Q^{\mathrm{sca}} = Z_{21}I^{\mathrm{inc}}, \tag{6.10}$$
$$U^{\mathrm{sca}} = Z_{31}I^{\mathrm{inc}}, \tag{6.11}$$
$$V^{\mathrm{sca}} = Z_{41}I^{\mathrm{inc}}. \tag{6.12}$$

This is the phenomena is traditionally called “polarization”. The non-zero degree of polarization Equation 5.82 can be written in terms of the phase matrix elements

$$p = \frac{\sqrt{Z_{21}^2 + Z_{31}^2 + Z_{41}^2}}{Z_{11}}. \tag{6.13}$$

### 6.2.3 Extinction matrix

In the special case of the exact forward direction ($\hat{\mathbf{n}}^{\mathrm{sca}} = \hat{\mathbf{n}}^{\mathrm{inc}}$) the attenuation of the incoming radiation is described by the extinction matrix $\mathbf{K}$. In terms of the Stokes vector we get

$$\mathbf{s}(r\hat{\mathbf{n}}^{\mathrm{inc}})\Delta S = \mathbf{s}^{\mathrm{inc}}\Delta S - \mathbf{K}(\hat{\mathbf{n}}^{\mathrm{inc}})\mathbf{s}^{\mathrm{inc}} + O(r^{-2}). \tag{6.14}$$

Here $\Delta S$ is a surface element normal to $\hat{\mathbf{n}}^{\text{inc}}$. The extinction matrix can also be expressed explicitly in terms of the amplitude matrix. It has only seven independent elements. Again the elements depend on $\omega^{\text{inc}}$ and $\omega^{\text{sca}}$ even when the incident wave propagates along the $z$-axis.

### 6.2.4 Absorption vector

The particle also emits radiation if its temperature $T$ is above zero Kelvin. According to Kirchhoff's law of radiation the emissivity equals the absorptivity of a medium under thermodynamic equilibrium. The energetic and polarization characteristics of the emitted radiation are described by a four-component Stokes emission column vector $\mathbf{a}(\hat{\mathbf{r}}, T, \omega)$. The emission vector is defined in such a way that the net rate, at which the emitted energy crosses a surface element $\Delta S$ normal to $\hat{\mathbf{r}}$ at distance $r$ from the particle at frequencies from $\omega$ to $\omega + \Delta\omega$, is

$$W^e = \frac{1}{r^2}\mathbf{a}(\hat{\mathbf{r}}, T, \omega)B(T, \omega)\Delta S \Delta\omega, \tag{6.15}$$

where $W^e$ is the power of the emitted radiation and $B$ is the Planck function. In order to calculate $\mathbf{a}$ we assume that the particle is placed inside an opaque cavity of dimensions large compared to the particle and any wavelengths under consideration. We have thermodynamic equilibrium if the cavity and the particle is maintained at the constant temperature $T$. The emitted radiation inside the cavity is isotropic, homogeneous, and unpolarized. We can represent this radiation as a collection of quasi-monochromatic, unpolarized, incoherent beams propagating in all directions characterized by the Planck blackbody radiation

$$B(T, \omega)\Delta S \Delta\Omega = \frac{\hbar\omega^3}{2\pi^2 v^2 \left[\exp\left(\frac{\hbar\omega}{k_B T}\right) - 1\right]}\Delta S\, \Delta\Omega, \tag{6.16}$$

where $\Delta\Omega$ is a small solid angle about any direction, $\hbar$ is the Planck constant divided by $2\pi$, and $k_B$ is the Boltzmann constant. With respect to the $\mathrm{n}^2$-law discussed below, it could be noticed that the Planck law is governed by the local phase velocity, $v$, [see e.g. *Thomas and Stamnes*, 2002], and not the vacuum speed.

The blackbody Stokes vector is

$$\mathbf{s}_b(T, \omega) = \begin{bmatrix} B(T, \omega) \\ 0 \\ 0 \\ 0 \end{bmatrix}. \tag{6.17}$$

For the Stokes emission vector, which we also call particle absorption vector, we can derive

$$a_i^p(\hat{\mathbf{r}}, T, \omega) = K_{i1}(\hat{\mathbf{r}}, \omega) - \int_{4\pi} \mathrm{d}\hat{\mathbf{r}}' Z_{i1}(\hat{\mathbf{r}}, \hat{\mathbf{r}}', \omega), \quad i = 1, \ldots, 4. \tag{6.18}$$

This relation is a property of the particle only, and it is valid for any particle, in thermodynamic equilibrium or non-equilibrium.

### 6.2.5 Optical cross sections

The optical cross-sections are defined as follows: The product of the scattering cross section $C_{\text{sca}}$ and the incident monochromatic energy flux gives the total monochromatic power removed from the incident wave as a result of scattering into all directions. The product of the absorption cross section $C_{\text{abs}}$ and the incident monochromatic energy flux gives the power which is removed from the incident wave by absorption. The extinction cross section $C_{\text{ext}}$ is the sum of scattering and absorption cross section. One can express the extinction cross sections in terms of extinction matrix elements

$$C_{\text{ext}} = \frac{1}{I^{\text{inc}}} ( \quad K_{11}(\hat{\mathbf{n}}^{\text{inc}})I^{\text{inc}} + K_{12}(\hat{\mathbf{n}}^{\text{inc}})Q^{\text{inc}} + \tag{6.19}$$

$$K_{13}(\hat{\mathbf{n}}^{\text{inc}})U^{\text{inc}} + K_{14}(\hat{\mathbf{n}}^{\text{inc}})V^{\text{inc}}), \tag{6.20}$$

and the scattering cross section in terms of phase matrix elements

$$C_{\text{sca}} = \frac{1}{I^{\text{inc}}} \int_{4\pi} \mathrm{d}\hat{\mathbf{r}}( \quad Z_{11}(\hat{\mathbf{r}}, \hat{\mathbf{n}}^{\text{inc}})I^{\text{inc}} + Z_{12}(\hat{\mathbf{r}}, \hat{\mathbf{n}}^{\text{inc}})Q^{\text{inc}} + \tag{6.21}$$

$$Z_{13}(\hat{\mathbf{r}}, \hat{\mathbf{n}}^{\text{inc}})U^{\text{inc}} + Z_{14}(\hat{\mathbf{r}}, \hat{\mathbf{n}}^{\text{inc}})V^{\text{inc}}). \tag{6.22}$$

The absorption cross section is the difference between extinction and scattering cross section:

$$C_{\text{abs}} = C_{\text{ext}} - C_{\text{sca}}. \tag{6.23}$$

The single scattering albedo $\omega_0$, which is a commonly used quantity in radiative transfer theory, is defined as the ratio of the scattering and the extinction cross section:

$$\omega_0 = \frac{C_{\text{sca}}}{C_{\text{ext}}} \leq 1. \tag{6.24}$$

All cross sections are real-valued positive quantities and have the dimension of area.

The phase function is generally defined as

$$p(\hat{\mathbf{r}}, \hat{\mathbf{n}}^{\text{inc}}) = \frac{4\pi}{C_{\text{sca}} I^{\text{inc}}} ( \quad Z_{11}(\hat{\mathbf{r}}, \hat{\mathbf{n}}^{\text{inc}})I^{\text{inc}} + Z_{12}(\hat{\mathbf{r}}, \hat{\mathbf{n}}^{\text{inc}})Q^{\text{inc}} + \tag{6.25}$$

$$Z_{13}(\hat{\mathbf{r}}, \hat{\mathbf{n}}^{\text{inc}})U^{\text{inc}} + Z_{14}(\hat{\mathbf{r}}, \hat{\mathbf{n}}^{\text{inc}})V^{\text{inc}}). \tag{6.26}$$

The phase function is dimensionless and normalized:

$$\frac{1}{4\pi} \int_{4\pi} p(\hat{\mathbf{r}}, \hat{\mathbf{n}}^{\text{inc}}) \, \mathrm{d}\hat{\mathbf{r}} = 1. \tag{6.27}$$

## 6.3 Scattering, absorption and emission by ensembles of independent particles

The formalism described in the previous chapter applies only for radiation scattered by a single body or a fixed cluster consisting of a limited number of components. In reality, one normally finds situations, where radiation is scattered by a very large group of particles forming a constantly varying spatial configuration. Clouds of ice crystals or water droplets are a good example for such a situation. A particle collection can be treated at each given moment as a fixed cluster, but as a measurement takes a finite amount of time, one measures a statistical average over a large number of different cluster realizations.

Solving the Maxwell equations for a whole cluster, like a collection of particles in a cloud, is computationally too expensive. Fortunately, particles forming a random group can often be considered as independent scatterers. This approximation is valid under the following assumptions:

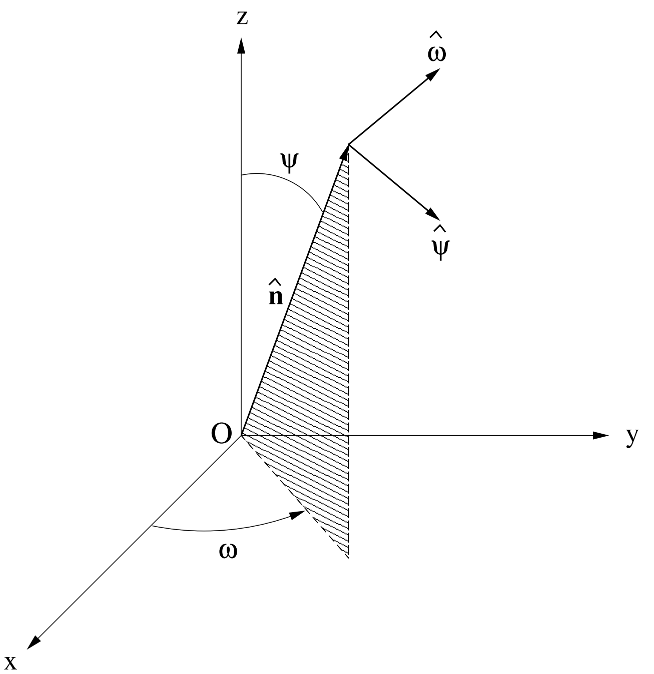


Figure 6.1: Coordinate system to describe the direction of propagation and the polarization state of a plane electromagnetic wave (adapted from Mishchenko).

1. Each particle is in the far-field zone of all other particles.
2. Scattering by the individual particles is incoherent.

As a consequence of assumption 2, the Stokes parameters of the partial waves can be added without regard to the phase. If the particle number density is sufficiently small, the single scattering approximation can be applied. The scattered field in this approach is obtained by summing up the fields generated by the individual particles in response to the external field in isolation from all other particles. If the particle positions are random, one can show, that the phase matrix, the extinction matrix and the absorption vector are obtained by summing up the respective characteristics of all constituent particles.

### 6.3.1 Single scattering approximation

We consider a volume element containing $N$ particles. We assume that $N$ is sufficiently small, so that the mean distance between the particles is much larger than the incident wavelength and the average particle size. Furthermore we assume that the contribution of the total scattered signal of radiation scattered more than once is negligibly small. This is equivalent to the requirement

$$\frac{N \langle C_{\mathrm{sca}} \rangle}{l^2} \ll 1, \tag{6.28}$$

where $\langle C_{\mathrm{sca}} \rangle$ is the average scattering cross section per particle and $l$ is the linear dimension of the volume element. The electric field scattered by the volume element can be written as the vector sum of the partial scattered fields scattered by the individual particles:

$$\mathbf{E}^{\text{sca}}(\mathbf{r}) = \sum_{n=1}^{N} \mathbf{E_n}^{\text{sca}}(\mathbf{r}). \tag{6.29}$$

As we assume single scattering the partial scattered fields are given according to Equation 6.7:

$$\begin{bmatrix} [E_n^{\text{sca}}(\mathbf{r})]_\psi \\ [E_n^{\text{sca}}(\mathbf{r})]_\omega \end{bmatrix} = \frac{e^{ikr}}{r} \mathbf{S}(\hat{\mathbf{r}}, \hat{\mathbf{n}}^{\text{inc}}) \begin{bmatrix} E_{0\psi}^{\text{inc}} \\ E_{0\omega}^{\text{inc}} \end{bmatrix}, \tag{6.30}$$

where $\mathbf{S}$ is the total amplitude scattering matrix given by:

$$\mathbf{S}(\hat{\mathbf{r}}, \hat{\mathbf{n}}^{\text{inc}}) = \sum_{n=1}^{N} e^{i\Delta_n} \mathbf{S}_n(\hat{\mathbf{r}}, \hat{\mathbf{n}}^{\text{inc}}). \tag{6.31}$$

$\mathbf{S}_n(\hat{\mathbf{r}}, \hat{\mathbf{n}}^{\text{inc}})$ are the individual amplitude matrices and the phase $\Delta_n$ is given by

$$\Delta_n = k\mathbf{r}_{\text{On}} \cdot (\hat{\mathbf{n}}^{\text{inc}} - \hat{\mathbf{r}}), \tag{6.32}$$

where the vector $\mathbf{r}_{\text{On}}$ connects the origin of the volume element $O$ with the $n$th particle origin (see Figure 6.2). Since $\Delta_n$ vanishes in forward direction and the individual extinction matrices can be written in terms of the individual amplitude matrix elements, the total extinction matrix is given by

$$\mathbf{K} = \sum_{n=1}^{N} \mathbf{K}_n = N \langle \mathbf{K} \rangle, \tag{6.33}$$

where $\langle \mathbf{K} \rangle$ is the average extinction matrix per particle. One can derive the analog equation for the phase matrix

$$\mathbf{Z} = \sum_{n=1}^{N} \mathbf{Z}_n = N \langle \mathbf{Z} \rangle, \tag{6.34}$$

where $\langle \mathbf{Z} \rangle$ is the average phase matrix per particle. In almost all practical situations, radiation scattered by a collection of independent particles is incoherent, as a minimal displacement of a particle or a slight change in the scattering geometry changes the phase differences entirely. It is important to note, that the ensemble averaged phase matrix and the ensemble averaged extinction matrix have in general 16 independent elements. The relations between the matrix elements, which can be derived for single particles, do not hold for particle ensembles.

## 6.4 Phenomenological derivation of the radiative transfer equation

When the scattering medium contains a very large number of particles the single scattering approximation is no longer valid. In this case we have to take into account that each particle scatters radiation that has already been scattered by another particle. This means that the radiation leaving the medium has a significant multiple scattered component. The observation point is assumed to be in the far-field zone of each particle, but it is not necessarily in the far-field zone of the scattering medium as a whole. A traditional method in this case is to

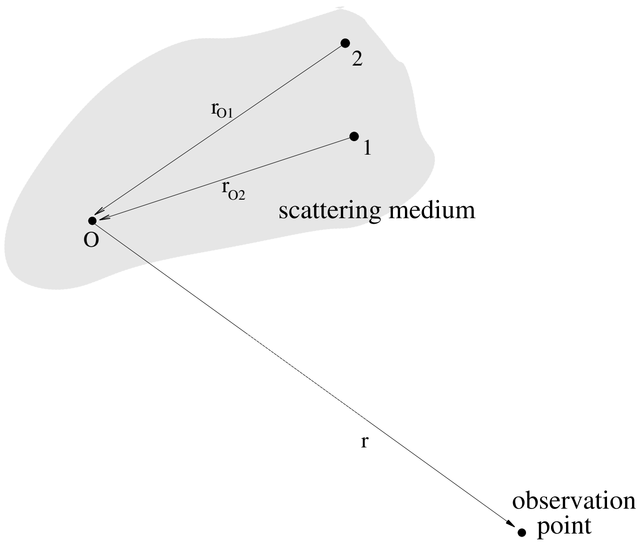


Figure 6.2: A volume element of a scattering medium conststing of a particle ensemble. $O$ is the origin of the volume element, $r_{O1}$ connects the origin with particle 1 and $r_{O2}$ with particle 2. The observation point is assumed to be in the far-field zone of the volume element.

solve the radiative transfer equation. This approach still assumes, that the particles forming the scattering medium are randomly positioned and widely separated and that the extinction and the phase matrices of each volume element can be obtained by incoherently adding the respective characteristics of the constituent particles. In other words the scattering media is assumed to consist of a large number of discrete, sparsely and randomly distributed particles and is treated as continuous and locally homogeneous. Radiative transfer theory is originally a phenomenological approach based on considering the transport of energy through a medium filled with a large number of particles and ensuring energy conservation. *Mishchenko* [2002] has demonstrated that it can be derived from electromagnetic theory of multiple wave scattering in discrete random media under certain simplifying assumptions.

In the phenomenological radiative transfer theory, the concept of single scattering by individual particles is replaced by the assumption of scattering by a small homogeneous volume element. It is furthermore assumed that the result of scattering is not the transformation of a plane incident wave into a spherical scattered wave, but the transformation of the specific intensity vector, which includes the Stokes vectors from all waves contributing to the electromagnetic radiation field.

The vector radiative transfer equation (VRTE) is

$$\begin{aligned}\frac{\mathrm{d}\mathbf{s}(\nu,\mathbf{r},\hat{\mathbf{n}})}{\mathrm{d}s} = & -\mathbf{K}(\nu,\mathbf{r},\hat{\mathbf{n}})\mathbf{s}(\nu,\mathbf{r},\hat{\mathbf{n}}) + \mathbf{a}(\nu,\mathbf{r},\hat{\mathbf{n}})B(\nu,\mathbf{r}) \\ & + \int_{4\pi} \mathrm{d}\hat{\mathbf{n}}'\mathbf{Z}(\nu,\mathbf{r},\hat{\mathbf{n}},\hat{\mathbf{n}}')\mathbf{s}(\nu,\mathbf{r},\hat{\mathbf{n}}'),\end{aligned} \tag{6.35}$$

where $\mathbf{s}$ is the specific intensity vector, $\mathbf{K}$ is the total extinction matrix, $\mathbf{a}$ is the total absorption vector, $B$ is the Planck function and $\mathbf{Z}$ is the total phase matrix. Furthermore $\nu$ is the frequency of the radiation, $\mathrm{d}s$ is a path-length-element of the propagation path, $\mathbf{r}$ represents the atmospheric position and $\hat{\mathbf{n}}$ the propagation direction. Equation 6.35 is valid for monochromatic or quasi-monochromatic radiative transfer. We can use this equation for simulating microwave radiative transfer through the atmosphere, as the scattering events do not change the frequency of the radiation.

The four-component specific intensity vector $\mathbf{s} = (I, Q, U, V)^T$ fully describes the radiation and it can directly be associated with the measurements carried out by a radiometer used for remote sensing. For the definition of the components of the specific intensity vector refer to Section 5, where the Stokes components are described.

The three terms on the right hand side of Equation 6.35 describe physical processes in an atmosphere containing different particle types and different trace gases. The first term represents the extinction of radiation traveling through the scattering medium, $\mathbf{K}$. For microwave radiation in cloudy atmospheres, extinction is caused by gaseous absorption, particle absorption and particle scattering. Therefore $\mathbf{K}$ can be written as a sum of two matrices, the particle extinction matrix $\mathbf{K}^p$ and the gaseous extinction matrix $\mathbf{K}^g$:

$$\mathbf{K}(\nu, \mathbf{r}, \hat{\mathbf{n}}) = \mathbf{K}^p(\nu, \mathbf{r}, \hat{\mathbf{n}}) + \mathbf{K}^g(\nu, \mathbf{r}, \hat{\mathbf{n}}). \tag{6.36}$$

The particle extinction matrix is the sum over the individual specific extinction matrices $\mathbf{K}_i^p$ of the $N$ different particles types contained in the scattering medium weighted by their particle number densities $n_i^p$:

$$\mathbf{K}^p(\nu, \mathbf{r}, \hat{\mathbf{n}}) = \sum_{i=1}^{N} n_i^p \mathbf{K}_i^p(\nu, \mathbf{r}, \hat{\mathbf{n}}). \tag{6.37}$$

The gaseous extinction matrix can normally be derived from the scalar gas absorption. This as there is no polarization due to gas absorption at cloud altitudes, and the off-diagonal elements of the gaseous extinction matrix are zero. On the other hand, at very high altitudes above approximately 40 km there is polarization due to the Zeeman effect, mainly due to oxygen molecules. In addition, in the toposphere and stratosphere molecular scattering can be neglected in the microwave frequency range. Hence the coefficients on the diagonal correspond to the gas absorption coefficient:

$$\begin{aligned} \mathbf{K}_{l,m}^g(\nu, \mathbf{r}) = \alpha^g(\nu, \mathbf{r}) \quad & \text{if } l = m \\ 0 \quad & \text{if } l \neq m. \end{aligned} \tag{6.38}$$

where $\alpha^g$ is the total scalar gas absorption coefficient, which is calculated from the individual absorption coefficients of all $M$ trace gases $\alpha_i^g$ and their volume mixing ratios $n_i^g$ as:

$$\alpha^g(\nu, \mathbf{r}) = \sum_{i=1}^{M} n_i^g \alpha_i^g(\nu, \mathbf{r}). \tag{6.39}$$

The second term in Equation 6.35 is the thermal source term. It describes thermal emission by gases and particles in the atmosphere. The absorption vector $\mathbf{a}$ is

$$\mathbf{a}(\nu, \mathbf{r}, \hat{\mathbf{n}}) = \mathbf{a}^p(\nu, \mathbf{r}, \hat{\mathbf{n}}) + \mathbf{a}^g(\nu, \mathbf{r}, \hat{\mathbf{n}}), \tag{6.40}$$

where $\mathbf{a}^p$ and $\mathbf{a}^g$ are the particle absorption vector and the gas absorption vector, respectively. The particle absorption vector is a sum over the individual absorption vectors $\mathbf{a}_i^p$, again weighted with $n_i^p$:

$$\mathbf{a}^p(\nu, \mathbf{r}, \hat{\mathbf{n}}) = \sum_{i=1}^{N} n_i^p \mathbf{a}_i^p(\nu, \mathbf{r}, \hat{\mathbf{n}}). \tag{6.41}$$

The gas absorption vector is simply (if no Zeeman splitting)

$$\mathbf{a}^g = [\alpha^p, 0, 0, 0]^T. \tag{6.42}$$

The last term in Equation 6.35 is the scattering source term. It adds the amount of radiation which is scattered from all directions $\hat{\mathbf{n}}'$ into the propagation direction $\hat{\mathbf{n}}$. The phase matrix $\mathbf{Z}$ is the sum of the individual phase matrices $\mathbf{Z}_i$ weighted with $n_i^p$:

$$\mathbf{Z}(\nu, \mathbf{r}, \hat{\mathbf{n}}) = \sum_{i=1}^{N} n_i^p \mathbf{Z}_i(\nu, \mathbf{r}, \hat{\mathbf{n}}). \tag{6.43}$$

The scalar radiative transfer equation (SRTE)

$$\begin{aligned}\frac{\mathrm{d}I(\nu, \mathbf{r}, \hat{\mathbf{n}})}{\mathrm{d}s} &= -K_{11}(\nu, \mathbf{r}, \hat{\mathbf{n}})I(\nu, \mathbf{r}, \hat{\mathbf{n}}) + a_1(\nu, \mathbf{r}, \hat{\mathbf{n}})B(\nu, \mathbf{r}) \\ &\quad + \int_{4\pi} \mathrm{d}\hat{\mathbf{n}}' Z_{11}(\nu, \mathbf{r}, \hat{\mathbf{n}}, \hat{\mathbf{n}}')I(\nu, \mathbf{r}, \hat{\mathbf{n}}')\end{aligned} \tag{6.44}$$

can be used presuming that the radiation field is unpolarized. This approximation is reasonable if the scattering medium consists of spherical or completely randomly oriented particles, where $\mathbf{K}^p$ is diagonal and only the first element of $\mathbf{a}^p$ is non-zero.

## 6.5 The n$^2$-law of radiance

### 6.5.1 Introduction

The radiance, $\mathbf{s}$, is unchanged for propagation in "free space". The term free space implies a refractive index of unity and that extinction is zero. However, it is possible to define a slightly different quantity that is conserved also for propagation with a varying refractive index. This quantity is here denoted as, $\mathbf{s}_{n2}$, and is defined as [*Mobley*, 1994; *Mätzler and Melsheimer*, 2006]:

$$\mathbf{s}_{n2} \equiv \frac{\mathbf{s}}{n^2}. \tag{6.45}$$

That is, for radiation propagating without extinction or any sources, $\mathbf{s}_{n2}$ is constant along the propagation path. This is denoted as the $n^2$-law for radiance. This impact of $n$ can, for different reasons, normally be neglected. As a consequency and to keep the nomenclature simple, the n2-law is in general ignored in the ARTS documentation.

### 6.5.2 Treatment in ARTS

As mentioned, the quantity defined by Equation 6.45 is constant for propagation without attenuation. Further, it can be shown that the radiance corresponding to some emission is independent on the refractive index along the propagation path, only the refractive indexes at the emission and measurement points matter. This is also valid with attenuation along the propagation path [*Mobley*, 1994, Eq. 4.23]:

$$\frac{I_m}{n_m^2} = e^{-\tau} \frac{I_e}{n_e^2}, \tag{6.46}$$

where $I_m$ is measured radiance, $n_m$ the refractive index where the measurement is performed, $I_e$ emitted radiance, $n_e$ the refractive index at the emission point, and $\tau$ is the optical thickness between the two points.

As long as LTE applies, the emission is proportional to the Planck function, $B$ (Eq. 6.16). Hence, using an emissivity, $\varepsilon$, we have

$$\frac{I_e}{n_e^2} = \frac{\varepsilon B(T_e)}{n_e^2} = \varepsilon B_{n2}(T_e), \tag{6.47}$$

where $T_e$ is the temperature of the emitting substance, and

$$B_{n2}(T_B) \equiv \frac{B(T_B)}{n^2} = \frac{2h\nu^3}{c^2(exp(h\nu/k_bT_B)-1)}. \tag{6.48}$$

That is, it turns out that by consistently apply $c$ in the Planck function (instead of $v$), the dependency of $n_e$ is removed. What remains to obtain the correct radiance to output, $I$, is to consider the impact of $n_m$:

$$I = n_m^2 I', \tag{6.49}$$

where $I'$ is the radiance calculated ignoring the n$^2$-law.

As discussed by *Mätzler and Melsheimer* [2006], it can be deduced from basic principles that the brightness temperature must be a preserved quantity, even in light of the n$^2$-law. This statement can also be understood from Equation 6.48. In simple terms, the brightness temperature is defined with respect to the local Planck function and the impact of refractive index variations vanishes if the radiance is measured in terms of brightness temperature.

## 6.6 Simple solution without scattering and polarization

If scattering can be neglected and the atmosphere is assumed to be in local thermodynamic equilibrium, the radiative transfer equation gets unusually simple. These assumptions will be made below and they are normally valid for the infrared region and longer wavelengths as in the microwave region. For these conditions the atmospheric absorption and emission are linked and the basic problem to determine the radiative transfer is to calculate the absorption. At the wavelengths considered rotational and vibrational transitions are the dominating absorbing processes.

The basic equation describing radiative transfer along a specific direction is

$$\frac{dI(\nu)}{dl} = -k(l,\nu)(I(\nu) + B(l,\nu)) \tag{6.50}$$

where $I$ is the intensity per unit area, $\nu$ the frequency, $l$ the distance along the propagation path, $k$ the total absorption coefficient (summed over all species and transitions) and $B$ the Planck function. This differential equation can be solved:

$$I(\nu) = I_0(\nu)e^{-\int_0^h k(l',\nu)dl'} + \int_0^h k(l,\nu)B(T(l),\nu)e^{-\int_0^l k(l',\nu)dl'}dl \tag{6.51}$$

where the receiver is assumed to be placed at $l = 0$ and $h$ is the distance along the path to the limit of the media. $I_0$ is the intensity at the point $h$ which can represent thermal emission from the surface, solar radiation at top of the atmosphere or cosmic background radiation depending on the observation geometry. When discussing radiative transfer the quantity optical depth, $\tau$, is commonly used and it is defined as

$$\tau(l,\nu) = \int_0^l k(l',\nu)dl' \tag{6.52}$$

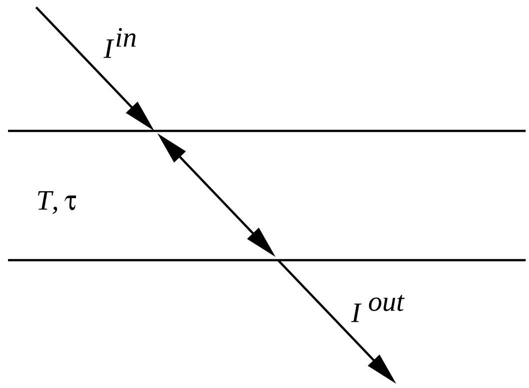


Figure 6.3: Schematic picture of the radiative transfer through a medium with constant temperature.

and Equation 6.51 can be written as

$$I(\nu) = I_0(\nu)e^{-\tau(h,\nu)dl'} + \int_0^h k(l,\nu)B(T(l),\nu)e^{-\tau(l',\nu)}dl \tag{6.53}$$

The terms inside the integral found in this equation have a simple physical meaning, the radiation emitted at one point is $kBdl$ and this quantity is attenuated by the factor $e^{-\tau}$ before it reaches the observation point.

## 6.7 Special solutions

If the total emission along the propagation path can be neglected compared to the transmitted part of the incoming radiation, the radiative transfer equation is simplified to the well known Beer-Lambert law:

$$I(\nu) = I_0(\nu)e^{-\tau(h,\nu)} \tag{6.54}$$

This equation can for example be used when evaluating solar occultation observations.

If the temperature is constant through the medium studied (Fig. 6.3) the integral in Equation 6.51 can be solved analytically:

$$I^{out} = I^{in}e^{-\tau} + B(T,\nu)(1 - e^{-\tau}) \tag{6.55}$$

where is $\tau$ the total optical thickness of the medium. Two special cases can be distinguished. If the layer is totally optically thick ($\tau \to \infty$) then $I^{in}$ is totally absorbed and $I^{out} = B$, the medium emits as a blackbody. If the layer has no absorption ($\tau = 0$) then Equation 6.55 gives $I^{out} = I^{in}$ as expected.

In microwave radiometry the measured intensity is normally presented by means of the brightness temperature, $T_b$. This quantity is derived from the Rayleigh-Jeans approximation of the Planck function:

$$B(T,\nu) \approx \frac{2\nu^2 k_b T}{c^2} = \frac{2k_b T}{\lambda^2} \tag{6.56}$$

This equation is valid when $h\nu \ll kT$ which is the case in the microwave region due to the relatively low frequencies. If the temperature is 50 K, $hv$ equals $kT$ at 1.04 THz. The

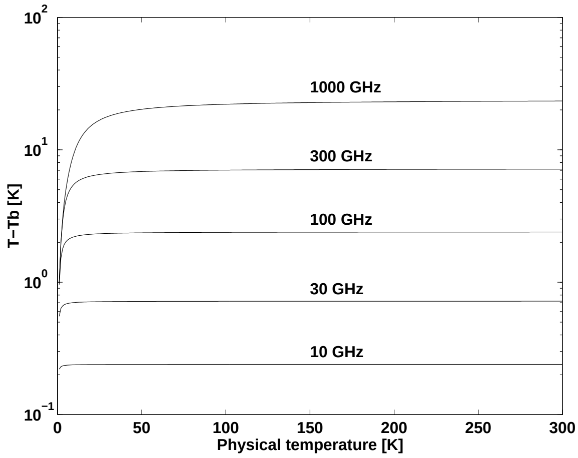


Figure 6.4: The difference between the physical temperarature of a blackbody and the equivalent brightness temperature calculated using the Rayleight-Jeans approximation.

important aspect of Equation 6.56 is the linear relationship between the intensity and the physical temperature. The natural definition of brightness temperature, $T_b$, is then

$$T_b(\nu) = \frac{\lambda^2}{2k_bT}I(\nu) \tag{6.57}$$

The difference between the brightness temperature and the physical temperature (corresponding to the actual intensity) increases with frequency which is exemplified in Figure 6.4. The differences for higher frequencies are certainly not negligible and the brightness temperature shall not be mistaken for the physical temperature. The important fact is that the brightness temperature has a linear relationship to the intensity and gives a more intuitive understanding of the magnitude of the emission. In the Rayleigh-Jeans limit Equation 6.51 can be written as

$$T_b(\nu) = T_{b0}(\nu)e^{-\tau(h,\nu)dl'} + \int_0^h k(l,\nu)T(l)e^{-\tau(l',\nu)}dl \tag{6.58}$$

## 6.8 Surface emission and reflection

### 6.8.1 The dielectric constant and the refractive index

The properties of a material can be reported either as the relative dielectric constant, $\epsilon$, or the refractive index, $n$. Both these quantities can be complex and are related as

$$n = \sqrt{\epsilon}. \tag{6.59}$$

### 6.8.2 Relating reflectivity and emissivity

Thermodynamic equilibrium can be assumed for natural surfaces, as long as there exist no strong temperature gradients. The Kirchoff law can then be used to relate the reflectivity and emissivity of a surface. For rough surfaces the scattering properties must be integrated to determine the emissivity (Equation 6.77). For specular reflections (defined below) and scalar radiative transfer calculations, the emissivity $e$ is

$$e = 1 - r, \tag{6.60}$$

where $r$ is the reflective (power reflection coefficient) of the surface. Equation 6.60 is valid for each polarisation state individually [*Ulaby et al.*, 1981, Eq. 4.190a].

We have then that

$$I^{\mathrm{up}} = I^{\mathrm{down}} r + (1-r)B, \tag{6.61}$$

where $I^{\mathrm{up}}$ is upwelling radiation, $I^{\mathrm{down}}$ is downwelling radiation and $B$ is the magnitude of blackbody radiation. As expected, if $I^{\mathrm{down}} = B$, also $I^{\mathrm{up}}$ equals $B$. Expressing the last observation using vector nomenclature gives

$$\begin{bmatrix} B \\ 0 \\ 0 \\ 0 \end{bmatrix} = \mathbf{R} \begin{bmatrix} B \\ 0 \\ 0 \\ 0 \end{bmatrix} + \mathbf{b}, \tag{6.62}$$

where $\mathbf{R}$ is the matrix (4 x 4) correspondence to the scalar reflectivity, describing the properties of the surface reflection. The vector $\mathbf{b}$ is the surface emission, that can be expressed as

$$\mathbf{b} = (\mathbf{1} - \mathbf{R}) \begin{bmatrix} B \\ 0 \\ 0 \\ 0 \end{bmatrix}, \tag{6.63}$$

where $\mathbf{1}$ is the identity matrix.

### 6.8.3 Specular reflections

If the surface is sufficiently smooth, radiation will be reflected/scattered only in the complementary angle, specular reflection. Required smoothness for assuming specular reflection is normally estimated by the Rayleigh criterion:

$$\Delta h < \frac{\lambda}{8\cos\theta_1} \tag{6.64}$$

where $\Delta h$ is the root mean square variation of the surface height, $\lambda$ the wavelength and $\theta_1$ the angle between the surface normal and the incident direction of the radiation. The criterion can also be defined with the factor 8 replaced with a higher number.

The complex reflection coefficient for the amplitude of the electromagnetic wave for vertical ($R_v$) and horizontal ($R_v$) polarisation is for a flat surface (if the relative magnetic permeability ($\mu_r$) of both media is 1) given by the Fresnel equations:

$$R_v = \frac{n_2\cos\theta_1 - n_1\cos\theta_2}{n_2\cos\theta_1 + n_1\cos\theta_2} \tag{6.65}$$

$$R_h = \frac{n_1\cos\theta_1 - n_2\cos\theta_2}{n_1\cos\theta_1 + n_2\cos\theta_2} \tag{6.66}$$

where $n_1$ is refractive index for the medium where the reflected radiation is propagating, $\theta_1$ is the incident angle (measured from the local surface normal) and $n_2$ is the refractive index of the reflecting medium. The angle $\theta_2$ is the propagation direction for the transmitted part, and is (approximately) given by Snell's law:

$$\mathrm{Re}(n_1)\sin\theta_1 = \mathrm{Re}(n_2)\sin\theta_2, \tag{6.67}$$

where $\mathrm{Re}(\cdot)$ denotes the real real part. Equation 6.67 is theoretically correct only if both $n_1$ and $n_2$ have no imaginary part. For cases where medium 1 is air, $n_1$ can (in this context) be set to 1, and an expression allowing $n_2$ to be complex is found in Section 5.4.1.3 of *Liou* [2002]. We are not awere of any expression for the case when both $n_1$ and $n_2$ are complex.

The power reflection coefficients are converted to an intensity reflection coefficient as

$$r = |R|^2, \tag{6.68}$$

where $|\cdot|$ denotes the absolute value. Note that $R$ can be complex, while $r$ is always real.

The surface reflection can be seen as a scattering event and Section 5.5 can be used to derive the reflection matrix values. The scattering amplitude functions of Equation 5.95 are simply

$$\begin{aligned} S_2 &= R_v, && (6.69)\\ S_1 &= R_h, && (6.70)\\ S_3 = S_4 &= \; = 0. && (6.71) \end{aligned}$$

This leads to that the transformation matrix for a specular surface reflection is (compare to *Liou* [2002, Sec. 5.4.3])

$$\mathbf{R} = \begin{bmatrix} \frac{r_v+r_h}{2} & \frac{r_v-r_h}{2} & 0 & 0 \\ \frac{r_v-r_h}{2} & \frac{r_v+r_h}{2} & 0 & 0 \\ 0 & 0 & \frac{R_hR_v^*+R_vR_h^*}{2} & i\frac{R_hR_v^*-R_vR_h^*}{2} \\ 0 & 0 & i\frac{R_vR_h^*-R_hR_v^*}{2} & \frac{R_hR_v^*+R_vR_h^*}{2} \end{bmatrix}. \tag{6.72}$$

For the case of $R_v = R_h$ the matrix in Equation 6.72 is strictly diagonal and all the diagonal elements have the same value, $(r_v + r_h)/2$. If the downwelling radiation is unpolarised, the reflected part of the upwelling radiation is

$$\mathbf{R}\begin{bmatrix} I \\ 0 \\ 0 \\ 0 \end{bmatrix} = \begin{bmatrix} I(r_v + r_h)/2 \\ I(r_v - r_h)/2 \\ 0 \\ 0 \end{bmatrix}. \tag{6.73}$$

as expected.

If $\mathbf{R}$ is given by Equation 6.72, Equation 6.63 gives that the surface emission is

$$\mathbf{b} = \begin{bmatrix} B\left(1 - \frac{r_v+r_h}{2}\right) \\ B\frac{r_h-r_v}{2} \\ 0 \\ 0 \end{bmatrix}. \tag{6.74}$$

### 6.8.4 Rough surfaces

The scattering of rough surfaces is normally described by the bidirectional reflectance distribution function, BRDF. With the BRDF, $f(\theta_0, \phi_0, \theta_1, \phi_1)$, the scattered radiance in the direction $(\theta_1, \phi_1)$ can be written as (see e.g. *Rees* [2001] or *Petty* [2006])

$$I'(\theta_1, \phi_1) = \int_0^{\pi/2}\int_0^{2\pi} I(\theta, \phi)\cos(\theta) f(\theta, \phi, \theta_1, \phi_1)\sin(\theta)\,\mathrm{d}\phi\,\mathrm{d}\theta, \tag{6.75}$$

where $I(\theta, \phi)$ is the downwelling radiance for incidance angle $\theta$ and azimuth angle $\phi$. One important property of the BRDF is

$$f(\theta_0, \phi_0, \theta_1, \phi_1) = f(\theta_1, \phi_1, \theta_0, \phi_0). \tag{6.76}$$

The reflectivity is the half-sphere integral of the BRDF

$$r(\theta_1, \phi_1) = \int_0^{\pi/2} \int_0^{2\pi} f(\theta_1, \phi_1, \theta, \phi) \cos(\theta) \sin(\theta) \, \mathrm{d}\phi \, \mathrm{d}\theta. \tag{6.77}$$

An ideally rough surface is denoted as Lambertian. The BRDF is for this case constant, and normally expressed using the the diffuse reflectivity, $r_d$ [e.g. *Petty*, 2006]:

$$f = \frac{r_d}{\pi}. \tag{6.78}$$

From Eq. 6.77 it follows that $r = r_d$.

# Chapter 7

# Propagation paths

## 7.1 Structure of implementation

The workspace method for calculating propagation paths is ppathCalc, but this is just a getaway function for `ppath_calc`. The main use of ppathCalc is to debug and test the path calculations, and that WSM should normally not be part of the control file.

### 7.1.1 Main functions for clear sky paths

The master function to calculate full clear sky propagation paths is `ppath_calc`. This function is outlined in Algorithm 1. The function can be divided into three main parts, initialisation (handled by `ppath_start_stepping`), a repeated call of ppath_step_agenda and putting data into the return structure (ppath).

**Algorithm 1** Outline of the function `ppath_calc`.

check consistency of function input
call `ppath_start_stepping` to set ppath_step
**while** radiative background not reached **do**
  call ppath_step_agenda
  **if** path is at the highest pressure surface **then**
    radiative background is space
  **else if** path is at either end point of latitude or longitude grid **then**
    this is not allowed, issue an runtime error
  **end if**
  **if** cloud box is active **then**
    **if** path is at the surface of the cloud box **then**
      radiative background is the cloud box surface
    **end if**
  **end if**
**end while**
initialise the WSV ppath to hold found number of path points

**History**

120227 Created by splitting and revising the corresponding chapter in *ARTS User Guide* (Patrick Eriksson).

The main task of the function `ppath_start_stepping` is to set up ppath_step for the first call of ppath_step_agenda, which means that the practical starting point for the path calculations must be determined. As the propagation path is followed in the backward direction, the calculation starting points equals the end point of the path. If the sensor is placed inside the model atmosphere, the sensor position gives directly the starting point. For cases when the sensor is found outside the atmosphere, the point where the path exits the atmosphere must be determined. The exit point can be determined by pure geometrical calculations (see Sections 7.2 and 7.3) as the refractive index is assumed to have the constant value of 1 outside the atmosphere. The problem is accordingly to find the geometrical crossing between the limit of the atmosphere and the sensor line-of-sight (LOS). The function performs further some other tasks, which include:

- If the sensor is placed inside the model atmosphere
  - Checks that the sensor is placed above the surface level. If not, an error is issued.
  - If the sensor and surface altitudes are equal, and the sensor LOS is downward, the radiative background is set to be the surface. For 2D and 3D, the tilt of the surface radius is considered when determining if the LOS is downward.
  - If the cloud box is active and the sensor position is inside the cloud box, the radiative background is set to be "cloud box interior".
- If the sensor is placed outside the model atmosphere
  - If it is found for 2D and 3D that the exit point of the path not is at the top of the atmosphere, but is either at a latitude or longitude end face of the atmosphere, an error is issued. This problem can not appear for 1D.

For further details, see the code.

### 7.1.2 Main functions for propagation path steps

Example on workspace methods to calculate propagation path steps are ppath_stepGeometric and ppath_stepRefractionBasic. All such methods adapt automatically to the atmospheric dimensionality, but the different dimensionalities are handled by separate internal functions. For example, the sub-functions to ppath_stepGeometric are `ppath_step_geom_1d`, `ppath_step_geom_2d` and `ppath_step_geom_3d`. See `m_ppath.cc` to get the names of the sub-functions for other propagation path step workspace methods.

Many tasks are independent of the algorithm for refraction that is used, or if refraction is considered at all. These tasks are solved by two functions for each atmospheric dimensionality. For 1D the functions are `ppath_start_1d` and `ppath_end_1d`, and the corresponding functions for 2D and 3D are named in the same way. The functions to calculate geometrical path steps are denoted as `do_gridrange_1d`, `do_gridcell_2d` and `do_gridcell_3d_byltest`. Paths steps passing a tangent point are handled by a recursive call of the step function. Algorithm 2 summarises this for geometrical 2D steps.

## 7.2 Some basic geometrical relationships for 1D and 2D

This section gives some expressions to determine positions along a propagation path when refraction is neglected. The expressions deal only with propagation path inside a plane,

**Algorithm 2** Outline of the function `ppath_step_geom_2d`.

call `ppath_start_2d`
**if** `ppath_step.ppc` $< 1$ **then**
  calculate the path constant (this is then first path step)
**end if**
call `do_gridcell_2d`
call `ppath_end_2d`
**if** calculated step ends with tangent point **then**
  call `ppath_step_geom_2d` with temporary `Ppath` structure
  append temporary `Ppath` structure to `ppath_step`
**end if**

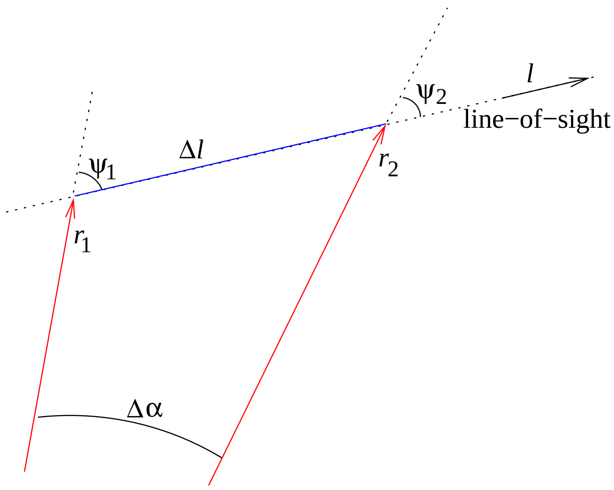


Figure 7.1: The radius ($r$) and zenith angle ($\psi$) for two points along the propagation path, and the distance along the path ($\Delta l$) and the latitude difference ($\Delta\alpha$) between these points.

where the latitude angle is the angular distance from an arbitrary point. This means that the expressions given here can be directly applied for 1D and 2D. Some of the expression are also of interest for 3D. The ARTS method for making the calculation of concern is given inside parenthesis above each equation, if not stated explicitly. A part of a geometrical propagation path is shown in Figure 7.1.

The law of sines gives that the product must $r\sin(\psi)$ be constant along the propagation path:

$$p_c = r\sin(\psi), \tag{7.1}$$

where the absolute value is taken for 2D zenith angles as they can for such cases be negative. The propagation path constant, $p_c$, is determined by the position and line-of-sight of the sensor, a calculation done by the function `geometrical_ppc`. The constant equals also the radius of the tangent point of the path (that is found along an imaginary prolongation of the path behind the sensor if the viewing direction is upwards). The expressions below are based on $p_c$ as the usage of a global constant for the path should decrease the sensitivity to numerical inaccuracies. If the calculations are based solely on the values for the neighbouring point, a numerical inaccuracy can accumulate when going from one point to next. The propagation path constant is stored in the field `constant` of ppath and ppath_step.

The relationship between the distance along the path for an infinitesimal change in radius is here denoted as the geometrical factor, $g$. If refraction is neglected, valid expressions for the geometrical factor are

$$g = \frac{\mathrm{d}l}{\mathrm{d}r} = \frac{1}{\cos(\psi)} = \frac{1}{\sqrt{1-\sin^2(\psi)}} = \frac{r}{\sqrt{r^2-p_c^2}}. \tag{7.2}$$

For the radiative transfer calculations, only the distance between the points, $\Delta l$, is of interest, but for the internal propagation path calculations the length from the tangent point (real or imaginary), $l$, is used. By integrating Equation 7.2, we get that (`geomppath_l_at_r`)

$$l(r) = \sqrt{r^2 - p_c^2}. \tag{7.3}$$

As refraction is here neglected, the tangent point, the point of concern and the centre of the coordinate system make up a right triangle and Equation 7.3 corresponds to the Pythagorean relation where $p_c$ is the radius of the tangent point. The distance between two points ($\Delta l$) is obtained by taking the difference of Equation 7.3 for the two radii.

The radius for a given $l$ is simply (`geomppath_r_at_l`)

$$r(l) = \sqrt{l^2 + p_c^2}. \tag{7.4}$$

The radius for a given zenith angle is simply obtained by rearranging Equation 7.1 (`geomppath_r_at_za`)

$$r(\psi) = \frac{p_c}{sin(\psi)}. \tag{7.5}$$

The zenith angle for a given radius is (`geomppath_za_at_r`)

$$\psi(r) = \begin{cases} 180 - \sin^{-1}(p_c/r) & \text{for} \quad 90^\circ < \psi_a \leq 180^\circ, \\ \sin^{-1}(p_c/r) & \text{for} \quad 0^\circ \leq \psi_a \leq 90^\circ, \\ -\sin^{-1}(p_c/r) & \text{for} \quad -90^\circ \leq \psi_a < 0^\circ, \\ \sin^{-1}(p_c/r) - 180 & \text{for} \quad -180^\circ \leq \psi_a < -90^\circ, \end{cases} \tag{7.6}$$

where $\psi_a$ is any zenith angle valid for the path on the same side of the tangent point. For example, for a 1D case, the part of the path between the tangent point and the sensor has zenith angles $90^\circ < \psi_a \leq 180^\circ$.

The latitude for a point (`geomppath_lat_at_za`) is most easily determined by its zenith angle

$$\alpha(\psi) = \alpha_0 + \psi_0 - \psi \tag{7.7}$$

where $\psi_0$ and $\alpha_0$ are the zenith angle and latitude of some other point of the path. Equation 7.7 is based on the fact that the quantities $\psi_1$, $\psi_2$ and $\Delta\alpha$ fulfil the relationship

$$\Delta\alpha = \psi_1 - \psi_2, \tag{7.8}$$

this independently of the sign of the zenith angles. The definitions used here result in that the absolute value of the zenith angle always decreases towards zero when following the path in the line-of-sight direction, that is, when going away from the sensor. It should then be remembered that the latitudes for 1D measures the angular distance to the sensor, and for 2D a positive zenith angle means observation towards higher latitudes.

The radius for a given latitude (`geomppath_r_at_lat`) is obtained by combining Equations 7.7 and 7.5.

## 7.3 Calculation of geometrical propagation paths

This section describes the calculation of geometrical propagation paths for different atmospheric dimensionalities. That is, the effect of refraction is neglected. These calculations are performed by the workspace method ppath_stepGeometric. This method, as all methods for propagation path steps, adjust automatically to the atmospheric dimensionality, but the actual calculations are performed a sub-function for each dimensionality.

### 7.3.1 1D

The core function for this case is `do_gridrange_1d`. The lowest and highest radius value along the path step is first determined. If the line-of-sight is upwards ($\psi \leq 90°$), then the start point of the step gives the lowest radius, and the radius of the pressure surface above gives the highest value. In the case of a downwards line-of-sight, the lowest radius is either the tangent point, the pressure surface below or the surface. The needed quantities to describe the propagation path between the two found radii are calculated by the function `geompath_from_r1_to_r2`, that has the option to introduce more points to fulfil a length criterion between the path points. The mathematics of `geompath_from_r1_to_r2` are given by Equations 7.1–7.7.

### 7.3.2 2D

The definitions given in Chapter 3 of *ARTS User Guide* results in that for a 2D case the radius of a pressure surface varies linearly from one point of the latitude grid to next. Compared to the 1D case, this is the main additional problem to solve, handled by `plevel_crossing_2d`. A two step procedure is applied. In the first step the propagation path is moved towards the pressure level as far as exact expressions can be used. For example, if the level is approached from above the path is moved down to the maximum radius of the level inside the gridbox. An approximative solution is needed for the second step. Figure 7.2 gives a schematic description of the problem at hand, which is handled by the internal function `rslope_crossing`. The law of sine gives the following relationship for the crossing point:

$$\frac{\sin \Theta_p}{r_0 + c\alpha} = \frac{\sin(\pi - \alpha - \Theta_p)}{r_p}, \tag{7.9}$$

which can be re-written to

$$r_p \sin(\Theta_p) = (r_0 + c\alpha)(\sin \Theta_p \cos \alpha + \cos \Theta_p \sin \alpha). \tag{7.10}$$

This equation has no analytical solution. A first step to find an approximate solution is to note that $\alpha$ is limited to relatively small values. For example, if it shall be possible for the angular distance $\alpha$ to reach the value of 3°, the vertical distance between $r_p$ and $r$ must be about 8 km. For angles $\alpha \leq 3°$, the sine and cosine terms can be replaced with the three first (non-constant) terms of their Taylor expansions maintaining a high accuracy. That is,

$$\begin{aligned}\cos \alpha &\approx 1 - \alpha^2/2 + \alpha^4/24 + \alpha^6/720 \\ \sin \alpha &\approx \alpha - \alpha^3/6 + \alpha^5/120\end{aligned}$$

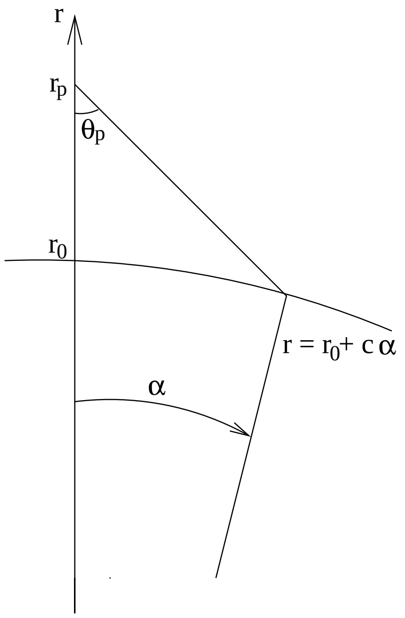


Figure 7.2: Quantities used to describe how to find the crossing between a geometrical propagation path and a tilted pressure surface. The angle $\alpha$ is the angular distance from a reference point on the path. The problem at hand is to find $\alpha$ for the crossing point. The radius of the pressure surface at $\alpha = 0$ is denoted as $r_0$. The tilt of the pressure surface is $c$.

Equation 7.10 becomes with these replacements a polynomial equation of order 6:

$$\begin{aligned}
0 &= p_0 + p_1\alpha + p_2\alpha^2 + p_3\alpha^3 + p_4\alpha^4 + p_5\alpha^5 + p_6\alpha^6, \qquad (7.11)\\
p_0 &= (r_0 - r_p)\sin(\Theta_p)\\
p_1 &= r_0\cos(\Theta_p) + c\sin(\Theta_p),\\
p_2 &= -r_0\sin(\Theta_p)/2 + c\cos(\Theta_p),\\
p_3 &= -r_0\cos(\Theta_p)/6 - c\sin(\Theta_p)/2,\\
p_4 &= r_0\sin(\Theta_p)/24 - c\cos(\Theta_p)/6,\\
p_5 &= r_0\cos(\Theta_p)/120 + c\sin(\Theta_p)/24,\\
p_6 &= -r_0\sin(\Theta_p)/720 + c\cos(\Theta_p)/120.
\end{aligned}$$

This equation is solved numerically with the root finding algorithm implemented in the function `poly_root_solve`. Solutions of interest shall not be imaginary. Several issues associated with numerical accuracy must be considered, see the code (`rslope_crossing2d`) for details.

Geometrical 2D propagation path steps are determined by `do_gridcell_2d`. This function uses `plevel_crossing_2d` to calculate the latitude distance to a crossing of the pressure surface below and above the present path point, as well as the planets surface if it is found inside the grid box. If the closest crossing point with the pressure surfaces is outside the latitude range of the grid cell, it is the crossing of the path with the end latitude (in the viewing direction) that is of interest (Figure 7.3).

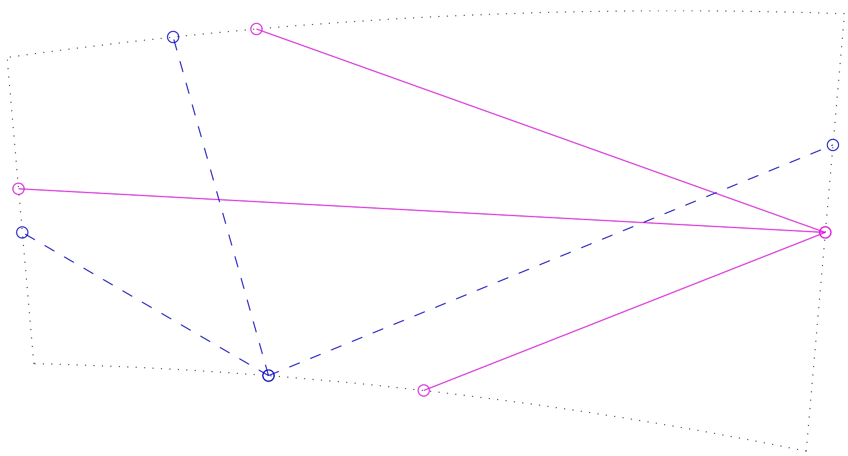

Figure 7.3: Example on propagation path steps starting from a latitude end face (solid lines), or the lower pressure surface (dashed lines), to all other grid cell faces. The distortion of the grid cell from cylinder segment is highly exaggerated compared to a real case. The relationship between vertical and horizontal size deviates also from normal real cases. Typical values for the vertical extension is around 500 m, while the horizontal length is normally $>$10 km.

### 7.3.3 3D

**Conversion between polar and Cartesian coordinates**

The Cartesian coordinate system used follows the (standard?) Earth-centred earth-fixed (ECEF) system (`http://en.wikipedia.org/wiki/ECEF`), with the axes defined as:

**x-axis** is along latitude 0°and longitude 0°

**y-axis** is along latitude 0°and longitude +90°

**z-axis** is along latitude +90°

This definition results in the following relationships between the spherical $(r, \alpha, \beta)$ and Cartesian $(x, y, z)$ coordinates

$$\begin{aligned} x &= r\cos(\alpha)\cos(\beta) \\ y &= r\cos(\alpha)\sin(\beta) \\ z &= r\sin(\alpha) \end{aligned} \tag{7.12}$$

and

$$\begin{aligned} r &= \sqrt{x^2+y^2+z^2} \\ \alpha &= \arcsin(z/r) \\ \beta &= \arctan(y/x) \qquad \text{(implemented by the atan2 function)} \end{aligned} \tag{7.13}$$

The functions performing these transformations are `sph2cart` and `cart2sph`.

The first step to transform a line-of-sight, given by the zenith ($\psi$) and the azimuth ($\omega$) angle, to Cartesian coordinates is to determine the corresponding vector with unit length in the spherical coordinate system:

$$\begin{bmatrix} \mathrm{d}r \\ \mathrm{d}\alpha \\ \mathrm{d}\beta \end{bmatrix} = \begin{bmatrix} \cos(\psi) \\ \sin(\psi)\cos(\omega)/r \\ \sin(\psi)\sin(\omega)/(r\cos(\alpha)) \end{bmatrix} \tag{7.14}$$

This vector is then translated to the Cartesian coordinate system as

$$\begin{bmatrix} \mathrm{d}x \\ \mathrm{d}y \\ \mathrm{d}z \end{bmatrix} = \begin{bmatrix} \cos(\alpha)\cos(\beta) & -r\sin(\alpha)\cos(\beta) & -r\cos(\alpha)\sin(\beta) \\ \cos(\alpha)\sin(\beta) & -r\sin(\alpha)\sin(\beta) & r\cos(\alpha)\cos(\beta) \\ \sin(\alpha) & r\cos(\alpha) & 0 \end{bmatrix} \begin{bmatrix} \mathrm{d}r \\ \mathrm{d}\alpha \\ \mathrm{d}\beta \end{bmatrix} \tag{7.15}$$

Note that the radial terms ($r$) in Equations 7.14 and 7.15 cancel each other. These calculations are performed in `poslos2cart`. Special expressions must be used for positions at the north and south pole (see the code) as the azimuth angle has there a special definition (see Section 5.2.2 of *ARTS User Guide*).

The Cartesian position of a point along the geometrical path at a distance $l$ is then simply

$$\begin{bmatrix} x_2 \\ y_2 \\ z_2 \end{bmatrix} = \begin{bmatrix} x_1 + l\mathrm{d}x \\ y_1 + l\mathrm{d}y \\ z_1 + l\mathrm{d}z \end{bmatrix} \tag{7.16}$$

The Cartesian viewing vector $[\mathrm{d}x, \mathrm{d}y, \mathrm{d}z]^T$ is constant along a geometrical path. The new position is converted to spherical coordinates by Equation 7.13 and the new spherical viewing vector is calculated as

$$\begin{bmatrix} \mathrm{d}r \\ \mathrm{d}\alpha \\ \mathrm{d}\beta \end{bmatrix} = \begin{bmatrix} \cos(\alpha)\cos(\beta) & \cos(\alpha)\sin(\beta) & \sin(\alpha) \\ -\sin(\alpha)\cos(\beta)/r & -\sin(\alpha)\sin(\beta)/r & \cos(\alpha)/r \\ -\sin(\beta)/(r\cos(\alpha)) & \cos(\beta)/(r\cos(\alpha)) & 0 \end{bmatrix} \begin{bmatrix} \mathrm{d}x \\ \mathrm{d}y \\ \mathrm{d}z \end{bmatrix} \tag{7.17}$$

which is converted to a zenith and azimuth angle as

$$\begin{aligned} \psi &= \arccos(\mathrm{d}r) \\ \omega &= \arccos(r\mathrm{d}\alpha/\sin(\psi)), \qquad \text{for} \quad \mathrm{d}\beta >= 0 \\ \omega &= -\arccos(r\mathrm{d}\alpha/\sin(\psi)), \qquad \text{for} \quad \mathrm{d}\beta < 0 \end{aligned} \tag{7.18}$$

These calculations are performed in `cart2poslos`. Again special expressions must be used for positions at the north and south pole (see the code).

### Finding the crossing of a specified $r$, $\alpha$ or $\beta$

The starting point in for all three cases is the following equation system:

$$\begin{aligned} r\cos(\alpha)\cos(\beta) &= x + l\mathrm{d}x, \\ r\cos(\alpha)\sin(\beta) &= y + l\mathrm{d}y, \\ r\sin(\alpha) &= z + l\mathrm{d}z, \end{aligned} \tag{7.19}$$

where $(x, y, z)$ is the position of the sensor, $(\mathrm{d}x, \mathrm{d}y, \mathrm{d}z)$ the sensor LOS, and either $r$, $\alpha$ or $\beta$ is given.

The distance $l$ to a given $r$ is found by adding the square of all three equations:

$$r^2 = (x + l\mathrm{d}x)^2 + (y + l\mathrm{d}y)^2 + (z + l\mathrm{d}z)^2. \tag{7.20}$$

Once $l$ is determined, the latitude and longitude can easily be calculated by Equations 7.16 and 7.13. These calculations are implemented in the function `r_crossing_3d`.

If instead $\alpha$ is given, the length to the point of interest can found by again squaring the three equations, but now summing the x- and y-terms and diving with the z-term:

$$\tan^2(\alpha) = \frac{(z + l\mathrm{d}z)^2}{(x + l\mathrm{d}x)^2 + (y + l\mathrm{d}y)^2}. \tag{7.21}$$

The solution of this quadratic equation is implemented in the function `lat_crossing_3d`[1]. The solution for $\alpha = 0°$ is particularly simple ($l = -z/\mathrm{d}z$). The case of $\alpha = 90°$ is set to have no solution ($\tan(90°) = \infty$), and is instead assumed to be picked up as a crossing with one of the two longitudes defining the grid box. Another complication is that, as the tan-term is squared, both $\pm\alpha$ can show up as possible solutions, and it must be tested that the found length gives a $\alpha$ with the correct sign.

For a given longitude, the x- and y-equations can be combined to give:

$$l = \frac{y - x\tan(\beta)}{\mathrm{d}x\tan(\beta) - \mathrm{d}y}. \tag{7.22}$$

This case is handled by `lon_crossing_3d`[2]. If the zenith or azimuth angle equals 0° or 180°, or if the start and target longitudes are equal, there is no valid solution.

### Finding the crossing with a pressure level

The same approach as for 2D is applied. The difference is that for 3D the additional dimension gives a more complex variation of the radius of the pressure level. For 2D, the variation can be expressed as a first order polynomial ($r = r_0 + c\alpha$), while for 3D a second order polynomial must be used

$$r = r_0 + c_1\alpha + c_2\alpha^2. \tag{7.23}$$

The coefficients $c_1$ and $c_2$ are detwermined in a purely numerical way, by `plevel_slope_3d`. The change in radius, $\Delta r_1$ and $\Delta r_2$, at a distance of $\Delta\alpha$ and $2\Delta\alpha$, respectively, are determined. These values give

$$c_1 = \frac{4\Delta r_1 - \Delta r_2}{2\Delta\alpha} \tag{7.24}$$

and

$$c_2 = \frac{4\Delta r_1 - c_1\Delta\alpha}{(\Delta\alpha)^2}. \tag{7.25}$$

The polynomial to solve becomes (cf. Eq. 7.27)

$$\begin{aligned}
0 &= p_0 + p_1\alpha + p_2\alpha^2 + p_3\alpha^3 + p_4\alpha^4 + p_5\alpha^5 + p_6\alpha^6, \qquad (7.26)\\
p_0 &= (r_0 - r_p)\sin(\Theta_p),\\
p_1 &= r_0\cos(\Theta_p) + c_1\sin(\Theta_p),
\end{aligned}$$

[1] This function is presently not used. The source code can be found in `ppath_NotUsed.cc`

[2] This function is presently not used. The source code can be found in `ppath_NotUsed.cc`

$$
\begin{aligned}
p_2 &= -r_0 \sin(\Theta_p)/2 + c_1 \cos(\Theta_p) + c_2 \sin(\Theta_p), \\
p_3 &= -r_0 \cos(\Theta_p)/6 - c_1 \sin(\Theta_p)/2 + c_2 \cos(\Theta_p), \\
p_4 &= r_0 \sin(\Theta_p)/24 - c_1 \cos(\Theta_p)/6 - c_2 \sin(\Theta_p)/2, \\
p_5 &= r_0 \cos(\Theta_p)/120 + c_1 \sin(\Theta_p)/24 - c_2 \cos(\Theta_p)/6, \\
p_6 &= -r_0 \sin(\Theta_p)/720 + c_1 \cos(\Theta_p)/120 + c_2 \sin(\Theta_p)/24.
\end{aligned}
$$

The solution of this polynomial is handled by `rslope_crossing3d`[3].

### A robust 3D algorithm

**Algorithm 3** The method applied in `do_gridcell_3d_byltest` to find the total length of the path step to be calculated. The symbol $S$ signifies here conversion from Cartesian to spherical coordinates (Equation 7.13).

calculate the spherical position $(x_0, y_0, z_0)$ and LOS vector $(\mathrm{d}x, \mathrm{d}y, \mathrm{d}z)$
calculate $(r_c, \alpha_c, \beta_c) = S(x_0, y_0, z_0) - (r_0, \alpha_0, \beta_0)$, the position correction term
set $l_{in} = 0$
**if** $l_s > 0$ **then**
  $l_{out} = l_s$ ($l_s$ is a function input)
**else**
  set $l_s$ to 3*vertical thickness of gid cell
**end if**
**while** $S(x_0 + l_{out}\mathrm{d}x, y_0 + l_{out}\mathrm{d}y, z_0 + l_{out}\mathrm{d}z) - (r_c, \alpha_c, \beta_c)$ is inside grid cell **do**
  $l_{out} \leftarrow 5 * l_{out}$
**end while**
set $l_{end} = (l_{in} + l_{out})/2$
set accuracy flag to false
**while** accuracy flag is false **do**
  calculate $(r, \alpha, \beta) = S(x_0 + l_{end}\mathrm{d}x, y_0 + l_{end}\mathrm{d}y, z_0 + l_{end}\mathrm{d}z) - (r_c, \alpha_c, \beta_c)$
  **if** $(r, \alpha, \beta)$ is inside grid cell **then**
    $l_{in} = l_{end}$
  **else**
    $l_{out} = l_{end}$
  **end if**
  **if** $(l_{out} - l_{in})$ smaller than specified accuracy **then**
    set accuracy flag to true
  **else**
    $l_{end} = (l_{in} + l_{out})/2$
  **end if**
**end while**
$(r, \alpha, \beta) \leftarrow (r, \alpha, \beta) + (r_c, \alpha_c, \beta_c)$
A recursive call can be neeeded, see the text.

Some of the expressions presented above, for finding the crossing of a specified $r$, $\alpha$ or $\beta$, wehre found to be sensitive to numerical inaccuracy and an algorith that avoids those expressions have been devised. It applies a straightforward "length-search" algorithm (Algorithm 3 and Figure 7.4). The main advantage of the algorithm is that a correction for the

[3] This function is presently not used. The source code can be found in `ppath_NotUsed.cc`

shift in position caused by the transformations back and fourth to the Cartesian coordinate system can be applied. The correction term assures that the position is not changed for a step of zero length, and is not moved outside the grid cell due to the numerical problems. The algorithm was further found to be sufficiently fast to be accepted. A simple bisection search to find the length of the propagation path step is used. Both the position and the line-of-sight for the other end point of the path step are calculated using a transformation to Cartesian coordinates. This algorithm is implemented by the function `do_gridcell_3d_byltest`.

The core task is to find the length of the path step. The search algorithm is safe with respect to all grid cell boundaries, except the lower pressure level where it can fail for zenith angles around 90°. In this case, the path can pass the lower pressure level and re-enter the grid cell after a short distance. For 1D cases, the part inside the lower cell would hold the tangent point, but for a non-spherical reference ellipsoid and "titled" pressure levels the tangent point can be found elsewhere.

The bisection algorithm can miss such excursions to the lower grid cell. Analytic approaches to handle this was rejected due to numerical problems. Instead, all final points of the path step are checked with respect to this issue and if any point is found to be below the lower pressure level, the function is called recursively with the distance to the problematic point as maximum search length ($l_s$ in Algorithm 3).

## 7.4 Basic treatment of refraction

Refraction affects the radiative transfer in several ways. The distance through a layer of a fixed vertical thickness will be changed, and for a limb sounding observation the tangent point is moved both vertically and horizontally. If the atmosphere is assumed to be horizontally stratified (1D), a horizontal displacement is of no importance but for 2D and 3D calculations this effect must be considered. For limb sounding and a fixed zenith angle, the tangent point is moved downwards compared to the pure geometrical case (Figure 7.5), resulting in that inclusion of refraction in general gives higher intensities.

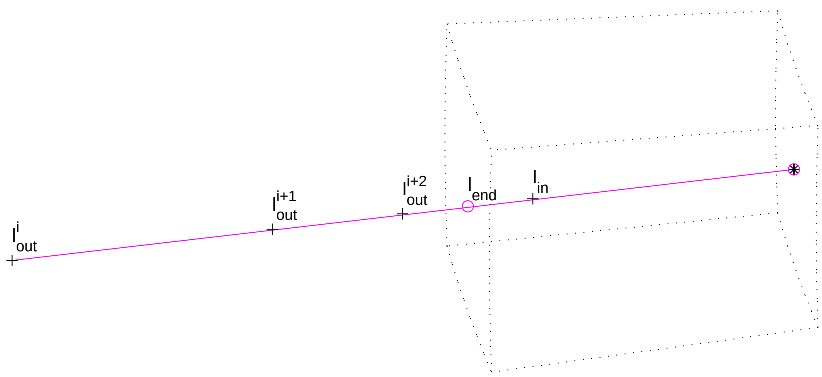


Figure 7.4: Schematic of Algorithm 3. The figure shows two iterations of the algorithm to search for the total length of the path step. The asterisk $(*)$ gives the start point for the calculations and the circles $(\circ)$ are the final end points of the path step. The plus signs $(+)$ shows the position of the different lengths tested during the iterations.

The refraction causes a bending of the path, which gives a deviation from the geometrical approximation of propagation along a straight line. The bending of the path is obtained by the relationship

$$\frac{\mathrm{d}x}{\mathrm{d}l} = \frac{1}{n}\left(\frac{\partial n}{\partial y}\right)_x \tag{7.27}$$

where $x$ is the direction of propagation, $l$ the distance along the path, $n$ the refractive index[4], and $y$ is the coordinate perpendicular to the path. See further Section 9.4 in *Rodgers* [2000].

The workspace method ppath_stepRefractionBasic takes refraction into consideration by probably the most simple (from the viewpoint of implementation) algorithm possible.

The approach taken in ppath_stepRefractionBasic is to take a geometrical ray tracing step from the present point of the path (and in the direction of present line-of-sight). Refraction is considered only when the line-of-sight at the new point is determined (Figure 7.6). The found line-of-sight is used to calculate the next ray tracing step etc. The main difference between handling 1D, 2D or 3D cases is how the line-of-sight for the new point is corrected to compensate for the bending due to refraction. The calculation of propagation paths including the effect of refraction is often denoted as ray tracing.

The length of the calculation steps is set by the generic input `lraytrace`. This length shall not be confused with the final distance between the points that define the path, which is controlled by `lmax`. The path is first determined in steps of `lraytrace`. The normal situation is that the ray tracing step length is considerably shorter than the final spacing between the path points. Suitable values for `lraytrace` have not yet been investigated in detail, but for limb sounding values in around 1–10 km should be appropriate. Shorter ray tracing steps (down to a level where rounding errors will start to have an impact) will of course give a propagation path more accurately determined, but on the cost of more time consuming calculations.

### 7.4.1 1D

When determining the propagation path through the atmosphere geometrical optics can be applied because the change of the refractive index over a wavelength can be neglected. Applying Snell's law to the geometry shown in Figure 7.7 gives

$$n_i \sin(\psi_i) = n_{i+1} \sin(\psi_{i'}) \tag{7.28}$$

Using the same figure, the law of sines gives the relationship

$$\frac{\sin(\psi_{i+1})}{r_i} = \frac{\sin(180^\circ - \psi'_{i+1})}{r_{i+1}} = \frac{\sin(\psi_{i'})}{r_{i+1}} \tag{7.29}$$

By combining the two equations above, the Snell's law for a spherical atmosphere (that is, 1D cases) is derived [e.g. *Kyle*, 1991; *Balluch and Lary*, 1997]:

$$p_c = r_i n_i \sin(\psi_i) = r_{i+1} n_{i+1} \sin(\psi_{i+1}) \tag{7.30}$$

where $p_c$ is a constant. With other words, the Snell's law for spherical atmospheres states that the product of $n$, $r$ and $\sin(\psi)$ is constant along the propagation path. It is noteworthy that with $n = 1$, Equations 7.1 and 7.30 are identical.

[4]The refractive index is here assumed to have no imaginary part

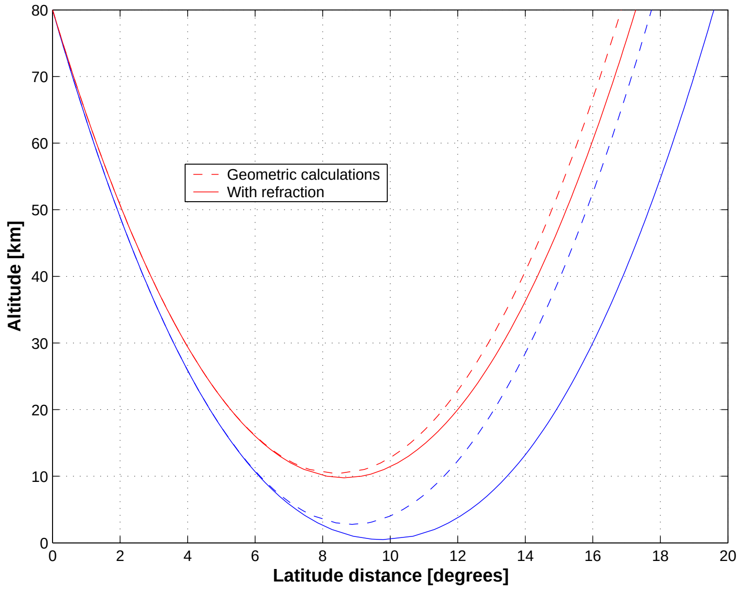


Figure 7.5: Comparison of propagation paths calculated geometrically and with refraction considered, for the same zenith angle of the sensor line-of-sight. The figure include two pair of paths, with refracted tangent altitude of about 0 and 10 km, respectively. The horizontal coordinate is the latitude distance from the point where the path exits the model atmosphere (at 80 km). The model atmosphere used had a spherical symmetry (that is, 1 D case, but the calculations were performed in 2D mode).

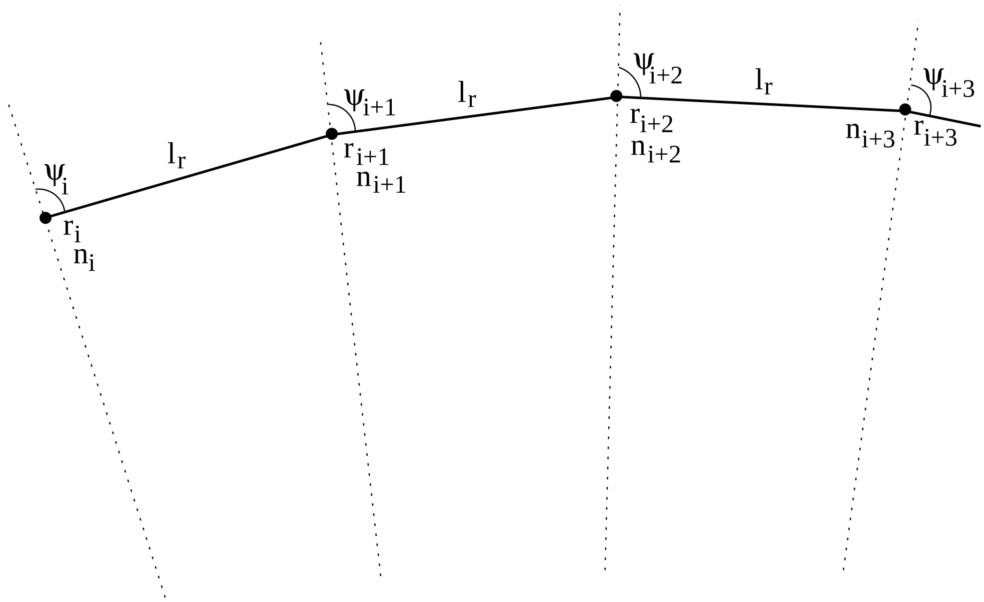


Figure 7.6: Schematic of the “basic” ray tracing scheme. The ray tracing step length is $l_r$.

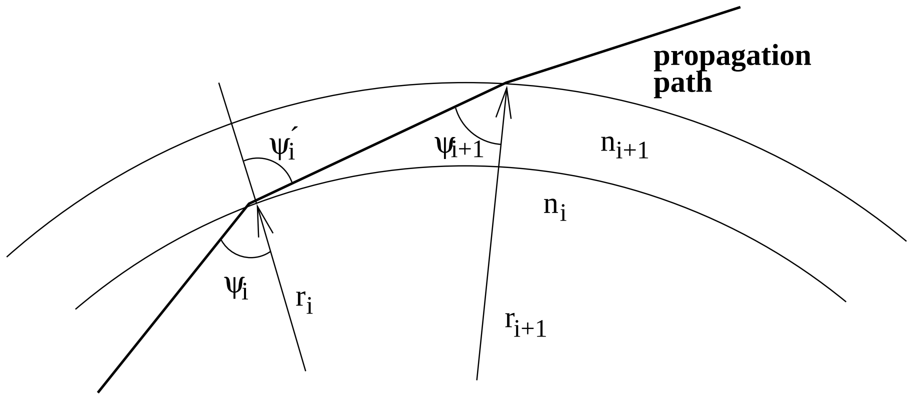


Figure 7.7: Geometry to derive Snell's law for a spherical atmosphere.

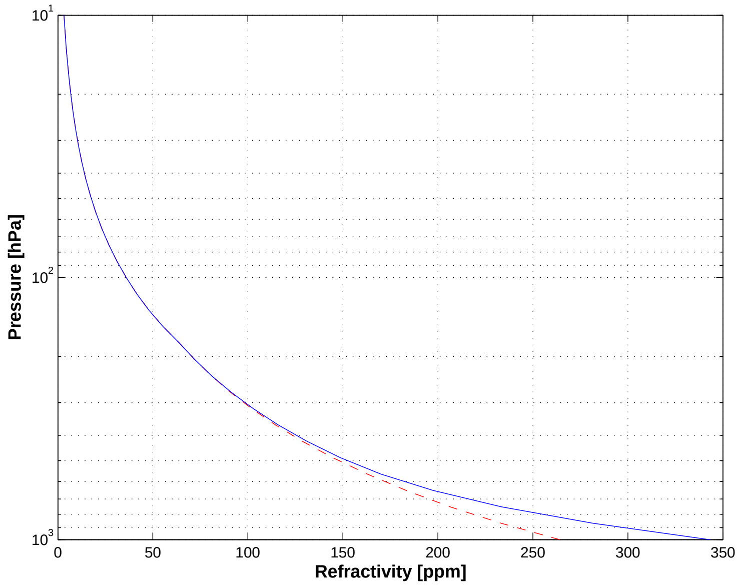


Figure 7.8: Vertical variation of refractivity $(n-1)\cdot 10^6$. Calculated for a mid-latitude summer climatology (FASCODE), where the dashed line is for a completely dry atmosphere, and the solid line includes also contribution from water vapour.

The Snell's law for a spherical atmosphere makes it very easy to determine the zenith angle of the path for a given radius. A rearrangement of Equation 7.30 gives

$$\psi = \arcsin(rn/p_c) \tag{7.31}$$

This relationship makes it possible to handle refraction for 1D without calculating any gradients of the refractive index, which is needed for 2D and 3D. These calculations are implemented in the function `raytrace_1d_linear_euler`. Figure 7.8 shows the vertical variation of the refractive index.

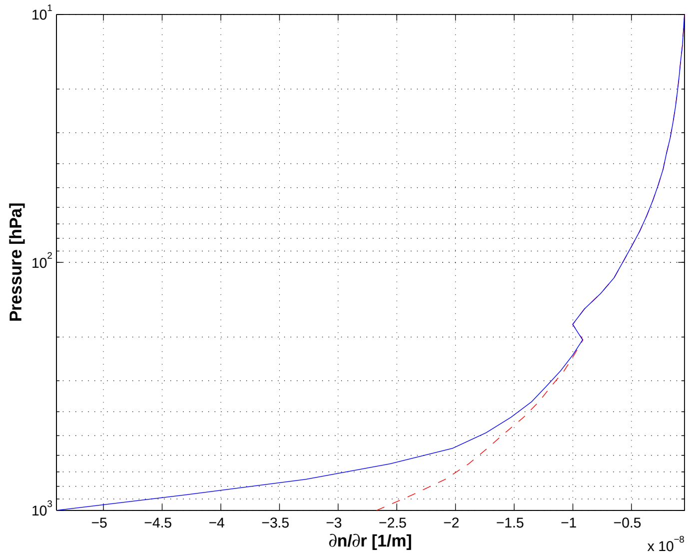


Figure 7.9: Vertical gradient of the refractive index. Calculated for a mid-latitude summer climatology (FASCODE), where the dashed line is for a completely dry atmosphere, and the solid line includes also contribution from water vapour.

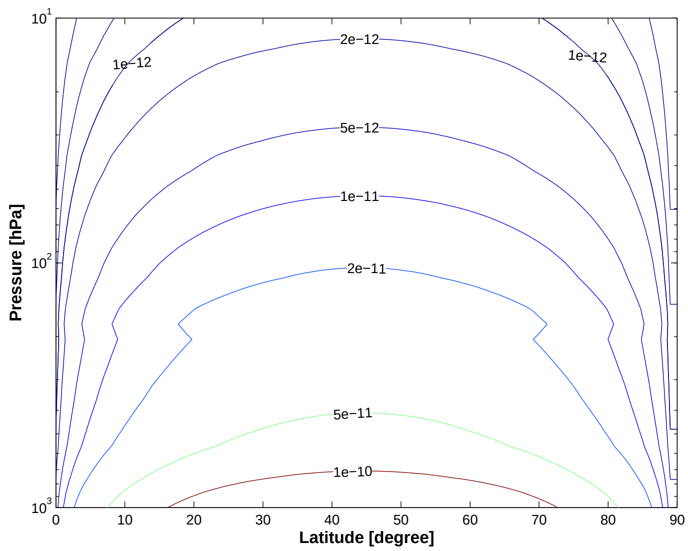


Figure 7.10: Latitude gradient of the refractive index due to varying radius of the geoid. The gradient is given as the change in refractive index over 1 m, which allows direct comparison with the values in Figure 7.9e. The wet atmosphere from Figure 7.9 was used for all latitudes, and the the plotted gradient is only caused by the fact that the radius of the geoid is not constant. The gradient is positive on the southern hemisphere (shown), and negative on the northern hemisphere.

### 7.4.2 2D

Equation 7.27 expressed in polar coordinates is [*Rodgers*, 2000, Eq. 9.30]

$$\frac{\mathrm{d}(\alpha+\psi)}{\mathrm{d}l} = -\frac{\sin\psi}{n}\left(\frac{\partial n}{\partial r}\right)_{\alpha} + \frac{\cos\psi}{nr}\left(\frac{\partial n}{\partial \alpha}\right)_{r} \tag{7.32}$$

If the gradients are zero (corresponding to the geometrical case) we find that the sum of the zenith angle and the latitude is constant along a 2D geometrical path, which is also made clear by Equation 7.7. The geometrical zenith angle at ray tracing point $i+1$ is accordingly $\psi_{i+1} = \psi_i - (\alpha_{i+1} - \alpha_i)$. If then also the refraction is considered, we get the following expression:

$$\psi_{i+1} = \psi_i - (\alpha_{i+1} - \alpha_i) + \frac{l_g}{n_i}\left[-\sin\psi_i\left(\frac{\partial n}{\partial r}\right)_{\alpha_i} + \frac{\cos\psi_i}{r_i}\left(\frac{\partial n}{\partial \alpha}\right)_{r_i}\right] \tag{7.33}$$

These calculations are handled by `raytrace_2d_linear_euler`.

The gradients of the refractive index for 2D are calculated by the function `refr_gradients_2d`. The radial and latitudinal gradients of the refractive index are calculated in pure numerical way, by shifting the position slightly from the position of concern. Figures 7.9 and 7.10 show example on gradients of the refractive index. This function returns both gradients as the change of the refractive index over 1 m. The conversion for the latitude gradient, from rad$^{-1}$ to m$^{-1}$, corresponds to the $1/r$ term found in Equation 7.33, and this term is accordingly left out in `raytrace_2d_linear_euler`.

### 7.4.3 3D

For 3D, the geometrical expressions are used to calculate the geometrical zenith and azimuth angles at the end of the ray tracing step. Following the methodology for 2D, the geometrical zenith and azimuth angles are then corrected to incorporate the influence of refraction. The zenith angle is calculated as

$$\begin{aligned}\psi_{i+1} &= \psi_g - \frac{l_g\sin\psi_i}{n_i}\left(\frac{\partial n}{\partial r}\right)_{(\alpha_i,\beta_i)} + \\ &\quad + \frac{l_g\cos\psi_i}{r_i n_i}\left[\cos\omega_i\left(\frac{\partial n}{\partial \alpha}\right)_{(r_i,\beta_i)} + \frac{\sin\omega_i}{\cos\alpha_i}\left(\frac{\partial n}{\partial \beta}\right)_{(r_i,\alpha_i)}\right]\end{aligned} \tag{7.34}$$

where $\psi_g$ is the zenith angle obtained from the geometrical expressions. In similar manner, the geometrical azimuth angle, $\omega_g$, is corrected as

$$\omega_{i+1} = \omega_g + \frac{l_g\sin\psi_i}{r_i n_i}\left[-\sin\omega_i\left(\frac{\partial n}{\partial \alpha}\right)_{(r_i,\beta_i)} + \frac{\cos\omega_i}{\cos\alpha_i}\left(\frac{\partial n}{\partial \beta}\right)_{(r_i,\alpha_i)}\right] \tag{7.35}$$

This expression, slightly modified, is found in `raytrace_3d_linear_euler`. The terms of Equation 7.35 missing in that function, are part of `refr_gradients_3d` to convert the gradients to the same unit. The longitude gradient is converted to the unit [1/m] by multiplication with the term $1/(r\cos\alpha)$.

# Chapter 8

# Reversed Monte Carlo Scattering: ARTS-MC

## 8.1 Introduction

The ARTS Monte Carlo scattering module (ARTS-MC) offers an efficient method for polarized radiative transfer calculations in arbitrarily complex 3D cloudy cases. The algorithm solves the integral form of the Vector Radiative Transfer Equation (VRTE), by applying Monte Carlo integration with importance sampling (MCI) (e.g. [*Press et al.*, 1997]). As described in [*Battaglia et al.*, 2007], when compared to other techniques for solving the VRTE in 3D domains the ARTS-MC algorithm has the following advantages:

- All computational effort is dedicated to calculating the Stokes vector at the location of interest and in the direction of interest. This is in contrast to forward Monte Carlo and discrete ordinate methods where the whole radiation field is calculated.
- CPU and memory cost scale more slowly than discrete ordinate methods with grid size, so that large or detailed 3D scenarios are not a problem.
- Only parts of the atmosphere that significantly contribute to the observed radiance are considered in the computation. Where the medium is optically thick, only the parts of the atmosphere closest to the sensor are visited by the algorithm. This contrasts with DOM methods, where the whole radiation field is computed, and in particular with forward Monte Carlo methods, where added optical thickness further restricts the number of photons reaching the sensor.

The Monte Carlo integration of the VRTE is over infinite dimensions, where for each scattering order there is a dimension representing: path-lengths, the choice between emission and scattering, and the choice between reflection or emission at the earth's surface. In practice the integrand is always calculated for a finite scattering order, as the dimensionality of the integral is truncated by photon emission or the boundary of the domain. Thus, the algorithm can be pictured as tracing a large number of photons backwards from sensor, in

---

**History**

| | |
|---|---|
| 120410 | Moved from user guide to theory document. |
| 300504 | Created and written by Cory Davis. |

randomly selected multiply scattered propagation paths to either their point of emission, or entry into the scattering domain. This physical picture is identical to the Backward-Forward Monte Carlo algorithm described by [*Liu et al.*, 1996]. However, BFMC did not account for dichroism, which is correctly accounted for in ARTS-MC by importance sampling.

The description of reversed Monte Carlo as tracing photon paths backwards from the sensor gives a useful first-order physical picture for understanding the algorithm, but can lead to difficulty understanding the veracity of the method with regard to polarization. These difficulties are not apparent in the scalar radiative transfer case[1]. Specifically, questions I have been asked that highlight the difficulty have included:

- how can you sample a single reversed pathlength when the medium is dichroic? (i.e. different extinction for the different polarized components)
- when reverse tracing, how can you decide on a scattering or emission event when the single scattering albedo depends on the polarization state of the incoming photon?
- How can you sample a single reverse scattered (i.e. incoming) direction when the scattered polarization state depends on the polarization state of the incoming photon?

The answer in each case is to forget the physical picture, focus on the mathematical solution to the VRTE, and realise that MCI permits some freedom in the choice of probability density functions (PDFs), provided the sampled integrand is properly weighted. In the model presented here we choose PDFs that aim to minimise the variance in the 1st element of the Stokes vector. This issue does not arise in the scalar case because it is possibile to perfectly sample the phase function to choose new incoming directions, and perfectly sample the transmission function to choose pathlengths, so no weighting terms appear. With the above difficulties in mind, in comparison with [*Davis et al.*, 2005], the algorithm description presented here is more in the context of MCI and with less reference to reversed traced photons. What were referred to as photons in [*Davis et al.*, 2005] we now call Stokes Vector Evaluations (SVE).

The current implementation of the algorithm differs slightly from the description in [*Davis et al.*, 2005]; changes include:

- the initial line of sight is no longer treated differently than the scattered paths
- the algorithm is no longer confined to the 'cloudbox',
- MCI is now used for convolving the simulated Stokes vector with a 2D antenna response ([*Davis et al.*, 2005] discusses only pencil beam calculations)
- MCI is now used to treat emission or reflection from the earth's surface.

These changes make the algorithm simpler and more general.

## 8.2 Model

The radiative transfer model solves the vector radiative transfer equation (VRTE), here written as (cf. Eq. 6.35)

$$\frac{d\mathbf{I}(\mathbf{n})}{ds} = -\mathbf{K}(\mathbf{n})\mathbf{I}(\mathbf{n}) + \mathbf{K_a}(\mathbf{n})I_b(T) +$$

[1] Although this physical picture of reversed Monte Carlo radiative transfer in the scalar case makes intuitive sense, the mathematical demonstration of how this method solves the Schwarzchild equation is often neglected

$$\int_{4\pi} \mathbf{Z}(\mathbf{n},\mathbf{n}')\mathbf{I}(\mathbf{n}')d\mathbf{n}' \tag{8.1}$$

where $\mathbf{I}$ is the 4 element column vector of radiances $\mathbf{I} = [I, Q, U, V]^T$ with units (Wm$^{-2}\mu$m$^{-1}$sr$^{-1}$). This will be referred to as the Stokes vector, although normally the Stokes vector is expressed in units of intensity. $s$ is distance along direction $\mathbf{n}$ and $I_b$ is the Planck radiance. $\mathbf{K}(\mathbf{n})$, $\mathbf{K_a}(\mathbf{n})$, and $\mathbf{Z}(\mathbf{n},\mathbf{n}')$ are the bulk extinction matrix, absorption coefficient vector and phase matrix of the medium respectively. For brevity these have been expressed as bulk optical properties, where individual single scattering properties have been multiplied by particle number density and averaged over all orientations and particle types. The argument $\mathbf{n}$ has been retained to signify that in general these properties depend on the direction of propagation.

To apply Monte Carlo integration to the problem, the VRTE needs to be expressed in integral form. (e.g. *Hochstadt* [1964])

$$\begin{aligned}&\mathbf{I}(\mathbf{n},\mathbf{s_0}) = \mathbf{O}(\mathbf{u_0},\mathbf{s_0})\mathbf{I}(\mathbf{n},\mathbf{u_0}) + \\ &\quad \textstyle\int_{u_0}^{s_0} \mathbf{O}(\mathbf{s}',\mathbf{s_0})\left(\mathbf{K_a}(\mathbf{n})I_b(T) + \int_{4\pi}\mathbf{Z}(\mathbf{n},\mathbf{n}')\mathbf{I}(\mathbf{n}')d\mathbf{n}'\right)ds'\end{aligned} \tag{8.2}$$

, where $\mathbf{O}(\mathbf{s}',\mathbf{s})$ is the evolution operator defined by *Degl'Innocenti and Degl'Innocenti* [1985]. $\mathbf{u_0}$ is the point where the line of sight intersects the far boundary of the scattering domain, and $\mathbf{s_0}$ is the exit point where the outgoing Stokes vector is calculated.

### 8.2.1 Integration over the antenna response function

If we consider a scalar antenna response function, $\psi = \psi(\theta,\phi) = \psi(\mathbf{n})$, where $\psi(\mathbf{n})$ is normalised such that $\int_{4\pi}\psi(\mathbf{n})dn = 1$, then the observed Stokes vector $\mathbf{I_{ant.}}(\mathbf{n},\mathbf{s_0})$ will be

$$\mathbf{I}_\psi(\mathbf{n},\mathbf{s_0}) = \int_{4\pi}\psi(\mathbf{n}')\mathbf{I}(\mathbf{n}',\mathbf{s_0})d\mathbf{n}' \tag{8.3}$$

If we apply Monte Carlo integration with importance sampling to Eq. 8.3 and sample $\mathbf{n}'$ according to a probability density function (PDF) equal to $\psi(\mathbf{n}')$, an unbiased estimate of Eq. 8.3 is given by (e.g. *Press et al.* [1992])

$$\mathbf{I}_\psi(\mathbf{n},\mathbf{s_0}) = \int_{4\pi}\mathbf{I}(\mathbf{n}',\mathbf{s_0})\psi(\mathbf{n}')d\mathbf{n}' \tag{8.4}$$

$$\approx \langle\mathbf{I}(\mathbf{n}',\mathbf{s_0})\rangle_\psi \tag{8.5}$$

, where the angled brackets indicate the arithmetic mean, and the $\psi$ subscript indicates the sampled PDF. Eq. 8.5 has an estimated error for each Stokes index, $j$, of

$$\delta I_j = \sqrt{\frac{\langle I_j^2\rangle - \langle I_j\rangle^2}{N}}. \tag{8.6}$$

### 8.2.2 The path integral

We now require a Monte Carlo estimate of the integrand in Eq. 8.5, which is given by Eq. 8.2. First, we re-express 8.2 as a single integral, for simplicity dropping the prime on $\mathbf{n}'$,

$$\mathbf{I}(\mathbf{n},\mathbf{s_0}) = \int_{\infty}^{s_0} \begin{cases} \mathbf{O}(\mathbf{s}',\mathbf{s_0})\left(\mathbf{K_a}(\mathbf{n})I_b(T) + \int_{4\pi}\mathbf{Z}(\mathbf{n},\mathbf{n}')\mathbf{I}(\mathbf{n}')d\mathbf{n}'\right) & s' < s'_{boundary} \\ \frac{\mathbf{O}(\mathbf{u_0},\mathbf{s_0})\mathbf{I}(\mathbf{n},\mathbf{u_0})g}{\int_{u_0}^{\infty} g ds} & s' \geq s'_{boundary} \end{cases} ds' \quad (8.7)$$

, where $g$ is the PDF we will eventually use to sample pathlength, $\Delta s$. $s'_{boundary}$ represents the pathlength corresponding to the boundary of the domain opposite the line of sight. The integrand Eq. 8.7 is a piecewise function of the path distance, where path distances corresponding to positions outside the modelled domain give a boundary radiance attenuated by the evolution operator over the length of the path within the model domain, and path distances corresponding to points within the modelled atmosphere give a sum of emission and scattering attenuated by the evolution operator over the distance between the point and the atmosphere exit. The reader could easily verify that evaluating Eq. 8.7 is equivalent Eq. 8.2.

The aim in importance sampling is to choose probability density functions (PDFs) for the independent variables that are as close as possible to being proportional to the integrand *Liu* [2001]. This concentrates computational effort on regions where the integrand is most significant and also reduces the variance in the Stokes Vector evalations (SVE), thus reducing the number of SVEs and hence CPU time required to give a prescribed accuracy. Eq. 8.2 suggests that the PDF for sampling path length, where path length is the distance traced backwards from the sensor, $\Delta s = |\mathbf{s} - \mathbf{s}'|$, should be proportional in some way to the evolution operator $\mathbf{O}(\mathbf{s}',\mathbf{s})$.

In general there is no closed form expression for $\mathbf{O}(\mathbf{s}',\mathbf{s})$. However, in cases where the extinction matrix is constant along a propagation path

$$\mathbf{O}(\mathbf{s}',\mathbf{s}) = \exp\left(-\mathbf{K}\Delta s\right) \quad (8.8)$$

In ARTS a propagation path consists of a set of coordinates indicating where the path intersects with grid surfaces. If the extinction matrix in the path segment between two such points is considered constant, $\mathbf{K} = (\mathbf{K_j} + \mathbf{K_{j+1}})/2$, the evolution operator between two arbitrary points $\mathbf{s_0}$ and $\mathbf{s}_N$ is

$$\begin{aligned}\mathbf{O}(\mathbf{s}_0,\mathbf{s}_N) = \mathbf{O}(\mathbf{s}_{N-1},\mathbf{s}_N)\mathbf{O}(\mathbf{s}_{N-2},\mathbf{s}_{N-1})\ldots \\ \mathbf{O}(\mathbf{s}_1,\mathbf{s}_2)\mathbf{O}(\mathbf{s}_0,\mathbf{s}_1),\end{aligned} \quad (8.9)$$

, where $\mathbf{O}(\mathbf{s_i},\mathbf{s_{i+1}})$ is given by Eq. 8.8.

Since PDFs are scalar functions, and that we consider the first element of the Stokes vector most important, we choose the pathlength PDF to be proportional to the (1,1) element of $\mathbf{O}(\mathbf{s}',\mathbf{s})$,

$$g(\Delta s) = \tilde{k}\tilde{O_{11}}(\Delta s) \quad (8.10)$$

, where $\tilde{O_{11}}(\Delta s)$, is the piecewise exponential function that includes $O_{11}(\mathbf{s}',\mathbf{s})$ values at points where the line of sight intersects with grid surfaces. Between two such adjacent intersections, $A$ and $B$, the function $\tilde{O_{11}}(\Delta s)$ is given by

$$\tilde{O_{11}}(\Delta s) = O_{11}(\Delta s_A)\exp\left(-\tilde{k}\left(\Delta s - \Delta s_A\right)\right) \quad (8.11)$$

, and

$$\tilde{k} = \frac{1}{(\Delta s_B - \Delta s_A)} \ln\left(\frac{O_{11}^A}{O_{11}^B}\right) \tag{8.12}$$

, which, for cases where the extinction matrix is diagonal, is equal to $K_{11} = (K_{11}^A + K_{11}^B)/2$. Eq. 8.10 is sampled by drawing a random number (from the uniform distribution [0,1]), $r$, and solving

$$\tilde{O_{11}}(\Delta s) = r. \tag{8.13}$$

for $\Delta s$. In practise this is done by stepping backwards over grid boundaries until $O_{11} <= r$, and solving Eqs. 8.11 and 8.13 within the final grid step,

$$\Delta s = \Delta s_A + \frac{1}{\tilde{k}} \ln\left(\frac{O_{11}^A}{r}\right) \tag{8.14}$$

With pathlength sampled according to Eq. 8.13, the Monte Carlo estimate for Eq. 8.7 becomes

$$\begin{aligned}
\mathbf{I}(\mathbf{n},\mathbf{s_0}) &= \int_\infty^{s_0} \begin{cases} \frac{\mathbf{O}(\mathbf{s}',\mathbf{s_0})}{g(\Delta s)} \left(\mathbf{K_a}(\mathbf{n}) I_b(T) + \int_{4\pi} \mathbf{Z}(\mathbf{n},\mathbf{n}')\mathbf{I}(\mathbf{n}')d\mathbf{n}'\right) & s' < s'_{boundary} \\ \frac{\mathbf{O}(\mathbf{u_0},\mathbf{s_0})\mathbf{I}(\mathbf{n},\mathbf{u_0})}{1-\tilde{O_{11}}(\Delta s)} & s' \geq s'_{boundary} \end{cases} g(\Delta s) ds' \\
&\approx \left\langle \begin{cases} \frac{\mathbf{O}(\mathbf{s}',\mathbf{s_0})}{g(\Delta s)} \left(\mathbf{K_a}(\mathbf{n}) I_b(T) + \int_{4\pi} \mathbf{Z}(\mathbf{n},\mathbf{n}')\mathbf{I}(\mathbf{n}')d\mathbf{n}'\right) & s' < s'_{boundary} \\ \frac{\mathbf{O}(\mathbf{u_0},\mathbf{s_0})\mathbf{I}(\mathbf{n},\mathbf{u_0})}{1-\tilde{O_{11}}(\Delta s)} & s' \geq s'_{boundary} \end{cases} \right\rangle_{g(\Delta s)}
\end{aligned} \tag{8.15}$$

So if the sampled pathlength corresponds to a point outside the atmosphere, or below the earth' surface, the SVE is given by $\frac{\mathbf{O}(\mathbf{u_0},\mathbf{s_0})\mathbf{I}(\mathbf{n},\mathbf{u_0})}{1-\tilde{O_{11}}(\Delta s)}$. In the top of atmosphere cases, this can be immediately calculated: $\mathbf{O}(\mathbf{u_0},\mathbf{s_0})$ from Eq. 8.9, and $\mathbf{I}(\mathbf{n},\mathbf{u_0})$ from the background radiation from space. As shown in Figure 8.2.8, in this event, we have our SVE and we can begin the calculation for the next one. If however the reversed traced path passes the earth's surface, the calculation of $\mathbf{I}(\mathbf{n},\mathbf{u_0})$ requires more steps.

### 8.2.3 Emission and scattering

If the sampled pathlength corresponds to a point within the atmosphere then the emission and scattering terms in the top term in Eq. 8.15, must be calculated. We also treat this as Monte Carlo integration:

$$\begin{aligned}
\mathbf{K_a}(\mathbf{n}) I_b(T) + \int_{4\pi} \mathbf{Z}(\mathbf{n},\mathbf{n}')\mathbf{I}(\mathbf{n}')d\mathbf{n}' &= \int_0^1 \begin{cases} \frac{1}{\tilde{\omega}} \int_{4\pi} \mathbf{Z}(\mathbf{n},\mathbf{n}')\mathbf{I}(\mathbf{n}')d\mathbf{n}' & r \leq \tilde{\omega} \\ \frac{\mathbf{K_a}(\mathbf{n}) I_b(T)}{1-\tilde{\omega}} & r > \tilde{\omega} \end{cases} dr \\
&\approx \left\langle \begin{cases} \frac{1}{\tilde{\omega}} \int_{4\pi} \mathbf{Z}(\mathbf{n},\mathbf{n}')\mathbf{I}(\mathbf{n}')d\mathbf{n}' & r \leq \tilde{\omega} \\ \frac{\mathbf{K_a}(\mathbf{n}) I_b(T)}{1-\tilde{\omega}} & r > \tilde{\omega} \end{cases} \right\rangle
\end{aligned} \tag{8.16}$$

. Here we are using a uniform random deviate $r$, and an albedo-like quantity,

$$\tilde{\omega} = 1 - \frac{K_{a1}(\mathbf{n_0},\mathbf{s_1})}{K_{11}(\mathbf{n_0},\mathbf{s_1})} \tag{8.17}$$

, to choose between emission and scattering contributions. Note: we can't use the actual single-scattering albedo as this depends on the polarization state of the incident radiation. If

$r > \tilde{\omega}$, then the event is considered to be emission. In this case we have all the information required to calculate the SVE,

$$\mathbf{I}^{\mathbf{i}}(\mathbf{n}, \mathbf{s_0}) = \frac{\mathbf{Q_k O}(\mathbf{s_{k+1}}, \mathbf{s_k})\mathbf{K_a}(\mathbf{n_k}, \mathbf{s_{k+1}})I_b(T, \mathbf{s_{k+1}})}{g(\Delta s)(1-\tilde{\omega})} \tag{8.18}$$

, where $\mathbf{O}(\mathbf{s_{k+1}}, \mathbf{s_k})$ is the evolution operator pertaining to the preceding pathlength sample, and $g(\Delta s)$, the corresponding importance sampling weight, as indicated in Eq. 8.15. The matrix $\mathbf{Q_k}$, whose calculation will be described below, holds the multiplicative effect of previous evolution operators, phase matrices, surface reflection matrices, and importance sampling weighting factors, acting on the reversed traced multiply scattered propagation path.

### 8.2.4 The scattering integral

If, in Eq. 8.16 our sampled $r \leq \tilde{\omega}$ , we have sampled a scattering event. In this case we need to evaluate the scattering integral $\int_{4\pi} \mathbf{Z}(\mathbf{n}, \mathbf{n}')\mathbf{I}(\mathbf{n}')d\mathbf{n}'$. Again we apply Monte Carlo integration with importance sampling to this integral.

$$\int_{4\pi} \mathbf{Z}(\mathbf{n}, \mathbf{n}')\mathbf{I}(\mathbf{n}')d\mathbf{n}' = \int_0^{2\pi}\int_0^{\pi} \frac{\mathbf{Z}(\mathbf{n}, \mathbf{n}')\mathbf{I}(\mathbf{n}')}{g(\theta_{inc}, \phi_{inc})} g(\theta_{inc}, \phi_{inc}) \sin\theta_{inc} d\theta_{inc} d\phi_{inc} \tag{8.19}$$

$$\approx \left\langle \frac{\sin\theta_{inc}\mathbf{Z}(\mathbf{n}, \mathbf{n}')\mathbf{I}(\mathbf{n}')}{g(\theta_{inc}, \phi_{inc})} \right\rangle_{g(\theta_{inc}, \phi_{inc})} \tag{8.20}$$

Given the desire to use a PDF proportional to the integrand, we choose to sample incoming directions, $\mathbf{n}' = (\theta_{inc}, \phi_{inc})$ from a PDF proportional to $\sin\theta_{inc}\mathbf{Z}(\theta_{scat}, \phi_{scat}, \theta_{inc}, \phi_{inc})$. At the scattering point sample a new incident direction $(\theta_{inc}, \phi_{inc})$ according to

$$g(\theta_{inc}, \phi_{inc}) = \frac{Z_{11}(\theta_{scat}, \phi_{scat}, \theta_{inc}, \phi_{inc})\sin(\theta_{inc})}{K_{11}(\theta_{scat}, \phi_{scat}) - K_{a1}(\theta_{scat}, \phi_{scat})} \tag{8.21}$$

, which is sampled by the rejection method as described in *Liu* [2001]. This sampling of the new incoming direction for the evaluation of Eq. 8.20 leads to the calculation of the incoming stokes vector $\mathbf{I}(\mathbf{n}', \mathbf{s})$ at the point of scattering $\mathbf{s}$ in the new incident direction $\mathbf{n}'$. We thus return to pathlength sampling and evaluation of Eq. 8.15.

### 8.2.5 Applying the Mueller matrices

The influence of the phase matrix and the preceding evolution operator, along with the importance samping weights, are stored by calculating the matrix

$$\mathbf{Q_k} = \mathbf{Q_{k-1}q_k} \tag{8.22}$$

, where

$$\mathbf{q_k} = \frac{\sin(\theta_{inc})_k\mathbf{O}(\mathbf{s_k}, \mathbf{s_{k-1}})\mathbf{Z}(\mathbf{n_{k-1}}, \mathbf{n_k})}{g(\Delta s)\, g(\theta_{inc}, \phi_{inc})\tilde{\omega}}, \tag{8.23}$$

and $\mathbf{Q_0} = 1$. The index $k$ represents the scattering order. The $\mathbf{Q_k}$ is updated through precedent scattering events and finally applied to an emission contribution (Eq. 8.18) if an emission event is sampled in Eq. 8.16.

### 8.2.6 Boundary contributions

If the $k^{\text{th}}$ pathlength sampled in Eq. 8.15 is beyond the top of the atmosphere or below the earth surface, $\mathbf{Q_k}$ is applied in

$$\mathbf{I^i}(\mathbf{n},\mathbf{s_0})=\frac{\mathbf{Q_k}\mathbf{O}(\mathbf{u_k},\mathbf{s_k})\mathbf{I}(\mathbf{n_k},\mathbf{u_k})}{O_{11}(\mathbf{u_k},\mathbf{s_k})} \tag{8.24}$$

, where $\mathbf{I}(\mathbf{n_k},\mathbf{u_k})$ is the incoming radiance at boundary point $\mathbf{u}_k$. For the top of atmosphere case, $\mathbf{I}(\mathbf{n_k},\mathbf{u_k})=I_{space}$. In ARTS it is possible to set $I_{space}$ to any value, but in most cases this is set to the cosmic background radiance associated with a Planck temperature of 2.735K.

For the surface case, if we choose to treat the surface as a blackbody, i.e. there is no reflection, in Eq. 8.24 we set $\mathbf{I}(\mathbf{n_k},\mathbf{u_k})=I_{surf}$, where $I_{surf}$ is the Planck radiance associated with the surface temperature, $I_{surf}=I_b\left(T_{surf}\right)$.

### 8.2.7 Surface reflection

Currently ARTS-MC can only consider specular reflection. Mostly ARTS-MC has been applied where surface reflections have a small or negligible effect on simulated remote sensing observations.*It would be a straightforward development to handle more complicated reflections. In the same way that the phase matrix is sampled to choose new incoming directions for scattering events, we could sample the Bidirectional reflection distribution (BDRF) for surface reflection events.* In analogy with scattering and emission in Eq. 8.16, $\mathbf{I_{surf}}$ is given by the sum of reflected and emitted radiation:

$$\begin{aligned}
\mathbf{I_{surf}}(\mathbf{n_k},\mathbf{u_k}) &= \mathbf{B}(\mathbf{n_k},\mathbf{u_k})+\mathbf{R}(\mathbf{n_k},\mathbf{n_{k+1}},\mathbf{u_k})\mathbf{I}(\mathbf{n_{k+1}},\mathbf{u_k})\\
&= \int_0^1\left\{\begin{array}{rl}\frac{1}{R_{11}}\mathbf{R}(\mathbf{n_k},\mathbf{n_{k+1}},\mathbf{u_k})\mathbf{I}(\mathbf{n_{k+1}},\mathbf{u_k}) & r\le R_{11}\\ \frac{\mathbf{B}(\mathbf{n_k},\mathbf{u_k})}{1-R_{11}} & r>R_{11}\end{array}\right. dr\\
&\approx \left\langle\left\{\begin{array}{rl}\frac{1}{R_{11}}\mathbf{R}(\mathbf{n_k},\mathbf{n_{k+1}},\mathbf{u_k})\mathbf{I}(\mathbf{n_{k+1}},\mathbf{u_k}) & r\le R_{11}\\ \frac{\mathbf{B}(\mathbf{n_k},\mathbf{u_k})}{1-R_{11}} & r>R_{11}\end{array}\right.\right\rangle_r
\end{aligned} \tag{8.25}$$

The reflection matrix $\mathbf{R}(\mathbf{n_k},\mathbf{n_{k+1}},\mathbf{u_k})$ and related surface emission, $\mathbf{B}(\mathbf{n_k},\mathbf{u_k})$ are calculated in one of several ways, as described in section **[FIXME: that stuff should be in this document but it isn't yet]**. As in Eq. 8.16, we use a uniform random deviate $r$; if $r>R_{11}$, where $R_{11}$ is the (1,1) element of $\mathbf{R}(\mathbf{n_k},\mathbf{n_{k+1}},\mathbf{u_k})$, then the event is considered to be surface emission. In this case we have all the information required to calculate the SVE in Eq.8.24 becomes,

$$\mathbf{I^i}(\mathbf{n},\mathbf{s_0})=\frac{\mathbf{Q_k}\mathbf{O}(\mathbf{u_k},\mathbf{s_k})\mathbf{B}(\mathbf{n_k},\mathbf{u_k})}{O_{11}(\mathbf{u_k},\mathbf{s_k})(1-R_{11})}. \tag{8.26}$$

If our sampled $r\le R_{11}$ in Eq. 8.25, then we have a surface reflection contribution, and the incoming (downward) stokes vector $\mathbf{I}(\mathbf{n_{k+1}},\mathbf{u_k})$ remains unknown. As in the scattering case we record the effect the evolution and reflection operators in the matrix $\mathbf{Q_k}=\mathbf{Q_{k-1}}\mathbf{q_k}$, where

$$\mathbf{q_k}=\frac{\mathbf{O}(\mathbf{s_k},\mathbf{s_{k-1}})\mathbf{R}(\mathbf{n_{k-1}},\mathbf{n_k})}{O_{11}(\mathbf{u_k},\mathbf{s_k})R_{11}} \tag{8.27}$$

, and continue with another path integral (Eq. 8.15) in the direction $\mathbf{n_{k+1}}$. Since the refection is specular, $\mathbf{n_{k+1}}$ is described by zenith and azimuthal angles $\theta_{k+1} = \pi - \theta_k$ and $\phi_{k+1} = \phi_k$. With regard to the scattering order $k$, surface reflection is considered the same as scattering.

### 8.2.8 Summary

Summarizing sections 8.2.2 to 8.2.7 we see that successively nested Monte Carlo integrals are calculated until atmospheric emission, surface emission, or top of atmosphere contributions are sampled. Mueller matrices encountered in each nested integral (evolution operators, phase matrices, reflection matrices), along with Monte Carlo weights, are recorded in the matrix $\mathbf{Q_k}$. This matrix applies the Mueller matrices in the correct 'forward' order to each emission or top of atmosphere contribution (Eq.s 8.18, 8.26, and 8.24). The algorithm summarized graphically in Figure 8.2.8.

## 8.3 Practical considerations regarding optical properties

### 8.3.1 Particle orientation and the evolution operator

The calculation of the evolution operator in Eqs. 8.8 and 8.9 requires evaluation of the matrix exponential. If the scattering particles are spheres (P10), or randomly orientated (p20), as described in Section [**FIXME**], then Eq. 8.8 is simply

$$O_{jj}(s', s) = \exp\left(-K_{jj}\Delta s\right) \tag{8.28}$$

If scattering particles have rotational symmetry, and the axis of symmetry is oriented vertically, or if the particles are have random azimuthal orientation (p30), as described in Section [**FIXME**], then the extinction matrix has a block diagonal form with 3 independent elements, $K_{jj}$, $K_{12}$, and $K_{34}$ (See section [**FIXME**]).

### 8.3.2 Particle orientation and the phase matrix

## 8.4 Variations on the ARTS-MC algorithm

### 8.4.1 The original ARTS-MC and forcing the original pathlength sample to be within the 3D box

### 8.4.2 1D clear sky variables and clear sky radiance look up

### 8.4.3 MCIPA

### 8.4.4 optical path and ice water path calculations

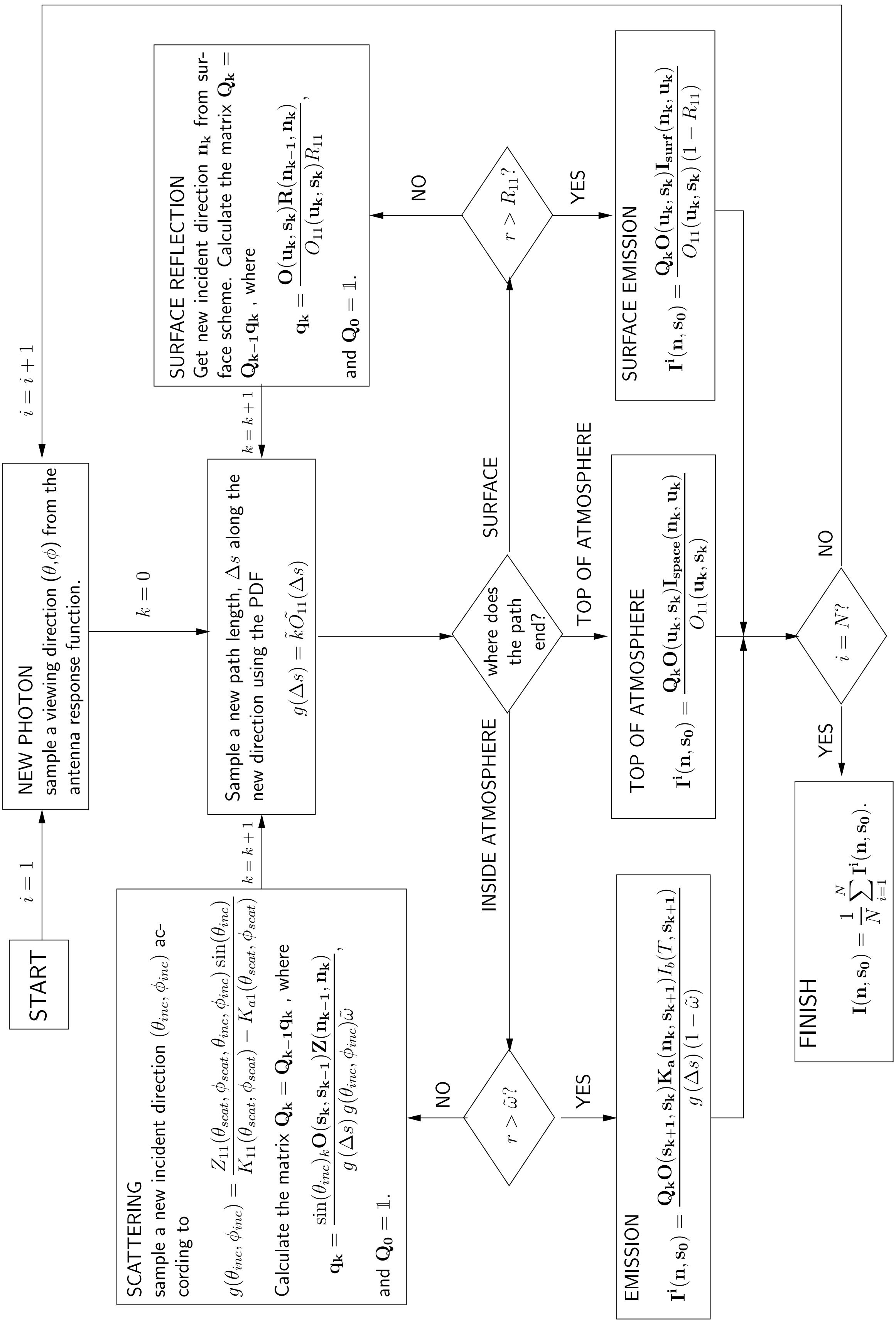


Figure 8.1: Flowchart illustrating MCGeneral algorithm

# Part I

# Bibliography and Appendices

# Bibliography

Balluch, M., and D. Lary, Refraction and atmospheric photochemistry, *Journal of Geophysical Research*, *102*, 8845–8854, 1997.

Battaglia, A., C. P. Davis, C. Emde, and C. Simmer, Microwave radiative transfer intercomparison study for 3-D dichroic media, *Journal of Quantitative Spectroscopy and Radiative Transfer*, *105*, 55–67, 2007.

Bauer, A., M. Godon, M. Kheddar, and J. M. Hartmann, Temperature and perturber dependence of water vapor line broadening: Experiments at 183 GHz; calculations below 1000 GHz, *Journal of Quantitative Spectroscopy and Radiative Transfer*, *41*, 49–54, 1989.

Bauer, A., M. Godon, J. Carlier, Q. Ma, and R. H. Tipping, Absorption by $H_2O$ and $H_2O$-$N_2$ mixtures at 153 GHz, *Journal of Quantitative Spectroscopy and Radiative Transfer*, *50*, 463–475, 1993.

Bauer, A., M. Godon, J. Carlier, and Q. Ma, Water vapor absorption in the atmospheric window at 239 GHz, *Journal of Quantitative Spectroscopy and Radiative Transfer*, *53*, 411–423, 1995.

Becker, G. E., and S. H. Autler, Water vapor absorption of electromagnetic radiation in the centimeter wavelength range, *Phys. Rev.*, *70*, 300–307, 1946.

Bernath, P., *Spectra of Atoms and Molecules*, Oxford University Press, 1995, ISBN 0-195-07598-6.

Berton, R. P. H., Statistical distribution of water content and sizes for clouds above Europe, *Ann. Geophys.*, *18*, 385–397, 2000.

Bohren, C., and D. R. Huffman, *Absorption and Scattering of Light by Small Particles*, Wiley Science Paperback Series, 1998.

Borysow, A., and L. Frommhold, Collision induced rototranslational absorption spectra of $N_2$–$N_2$ pairs for temperatures from 50 to 300 K, *Astrophysical Journal*, *311*, 1043–1057, 1986.

Brussaard, G., and P. A. Watson, *Atmospheric Modelling and Millimetre Wave Propagation*, Chapman & Hall, 1995, ISBN 0-412-56230-8.

Buehler, S. A., P. Eriksson, T. Kuhn, A. von Engeln, and C. Verdes, ARTS, the Atmospheric Radiative Transfer Simulator, *Journal of Quantitative Spectroscopy and Radiative Transfer*, *91*, 65–93, 2005.

Chandrasekhar, S., *Radiative Transfer*, Dover Publications, New York, 1960.

Clough, S. A., F. X. Kneizys, and R. W. Davis, Line shape and water vapor continuum, *Atmospheric Research*, *23*, 229–241, 1989.

Costa, A. A., G. P. Almeida, and A. J. C. Sampaio, A bin-microphysics cloud model with high-order, positive-definite advection, *Atmospheric Research*, *55*, 225–255, 2000.

Cruz Pol, S. L., C. S. Ruf, and S. J. Keihm, Improved 20– to 32–GHz atmospheric absorption model, *Radio Science*, *33*, 1319–1333, 1998, updated version can be downloaded from `http://ece.uprm.edu/~pol/Atmosphere.html`.

Dagg, I. R., G. E. Reesor, and J. L. Urbaniak, Collision induced absorption in $N_2$, $CO_2$, and $H_2$ at $2\,\mathrm{cm}^{-1}$, *Canadian Journal of Physics*, *53*, 1764–1776, 1975.

Dagg, I. R., G. E. Reesor, and M. Wong, A microwave cavity measurement of collision-induced absorption in $N_2$ and $CO_2$ at $4.6\,\mathrm{cm}^{-1}$, *Can. J. Phys.*, *56*, 1037–1045, 1978.

Davis, C., C. Emde, and R. Harwood, A 3D polarized reversed monte carlo radiative transfer model for mm and sub-mm passive remote sensing in cloudy atmospheres, *IEEE Transactions on Geoscience and Remote Sensing*, *43*, 1096–1101, 2005.

Degl'Innocenti, E. L., and M. L. Degl'Innocenti, On the solution of the radiative-transfer equations for polarized radiation, *Solar Physics*, *97*, 239–250, 1985.

Drayson, S. R., Rapid computation of the Voigt profile, *Journal of Quantitative Spectroscopy and Radiative Transfer*, *16*, 611, 1976.

English, S. J., C. Guillou, C. Prigent, and D. C. Jones, Aircraft measurements of water vapor continuum absorption at millimeter wavelengths, *Quarterly Journal of the Royal Meteorological Society*, *120*, 603–625, 1994.

Eriksson, P., Microwave radiometric observations of the middle atmosphere: Simulations and inversions, Ph.D. thesis, School of Electrical and Computer Engineering, Chalmers University of Technology, Sweden, 1999.

Eriksson, P., F. Merino, D. Murtagh, P. Baron, P. Ricaud, and J. de La Noë, Studies for the Odin sub-millimetre radiometer: 1. Radiative transfer and instrument simulation, *Canadian Journal of Physics*, *80*, 321–340, 2002.

Eriksson, P., M. Ekström, S. Bühler, and C. Melzheimer, Efficient forward modelling by matrix representation of sensor responses, *International Journal of Remote Sensing*, *27*, 1793–1808, 2006.

Godon, M., J. Carlier, and A. Bauer, Laboratory studies of water vapor absorption in the atmospheric window at 213 GHz, *Journal of Quantitative Spectroscopy and Radiative Transfer*, *47*, 275–285, 1992.

Goody, R. M., *Principles of atmospheric physics and chemistry*, Oxford University Press, 1995.

Goody, R. M., and Y. L. Yung, *Atmospheric radiation, theoretical basis*, Oxford University Press, 1989, second edition.

Gordy, W., and R. Cook, *Microwave Molecular Spectra*, Interscience Publishers, 1970, SBN 471 93161 6.

Herzberg, G., *Infrared and Raman Spectra of Polyatomic Mollecules*, Van Nostrand Reinhold Company, 1945, ISBN 0-442-03386-9.

Hess, M., P. Koepke, and I. Schult, Optical properties of aerosols and clouds: The software package OPAC, *Bulletin of the American Meteorological Society*, *79*, 831–844, 1998.

Ho, W., I. A. Kaufman, and P. Thaddeus, Laboratory measurement of microwave absorption in models of the atmosphere of Venus, *Journal of Geophysical Research*, *71*, 5091–5108, 1966.

Hochstadt, H., *Differential Equations: A Modern Approach*, Holt, Rinehart, and Winston, 1964.

Hufford, G. A., A model for the complex permittivity of ice at frequencies below 1 thz, *Interntl. J. Infrared & Millimeter Waves*, *12*, 677–682, 1991.

Hui, A. K., B. H.Armstrong, and A. A. Wray, Rapid computation of the voigt and complex error functions, *Journal of Quantitative Spectroscopy and Radiative Transfer*, *19*, 509–516, 1978.

Jackson, J. D., *Classical electrodynamics*, John Wiley & Sons, New York, 1998.

Kneizys, F. X., et al., The MODTRAN2/3 report and LOWTRAN7 model laboratory studies and propagation modelling, *Tech. Rep. 1/11/96*, Phillips Laboratory, Geophysical Directorate, PL/GPOS, 1996, editors: L. W. Abreu and G. P. Anderson.

Kuntz, M., and M. Höpfner, Efficient line-by-line calculation of absorption coefficients, *Journal of Quantitative Spectroscopy and Radiative Transfer*, *63*, 97–114, 1999.

Kyle, T., *Atmospheric transmission, emission and scaterring*, Pergamon Press, 1991.

Larsen, H., J.-F. Gayet, G. Febvre, H. Chepfer, and G. Brogniez, Measurement errors in cirrus cloud microphysical properties, *Ann. Geophys.*, *16*, 266–276, 1998.

Larsson, R., S. A. Buehler, P. Eriksson, and J. Mendrok, A treatment of the Zeeman effect using Stokes formalism and its implementation in the Atmospheric Radiative Transfer Simulator (ARTS), *Journal of Quantitative Spectroscopy and Radiative Transfer*, *133*, 445–453, 2014.

Li, L., J. Vivekanandan, C. H. Chan, and L. Tsang, Microwave radiometric technique to retrieve vapor; liquid and ice; part I – developement of a neural network-based inversion method, *IEEE Transactions on Geoscience and Remote Sensing*, *35*, 224–235, 1997.

Liebe, H. J., Modelling attenuation and phase of radio waves in air at frequencies below 1000 ghz, *Radio Science*, *16*, 1183–1199, 1981.

Liebe, H. J., The atmospheric water vapor continuum below 300 GHz, *Interntl. J. Infrared & Millimeter Waves*, *5(2)*, 207–227, 1984.

Liebe, H. J., MPM – an atmospheric millimeter–wave propagation model, *Interntl. J. Infrared & Millimeter Waves*, *10*, 631–650, 1989.

Liebe, H. J., and D. H. Layton, Millimeter-wave properties of the atmosphere: Laboratory studies and propagation modelling, *Tech. Rep. 87224*, U.S. Dept. of Commerce, National Telecommunications and Information Administration, Institute for Communication Sciences, 1987, 80p.

Liebe, H. J., T. Manabe, and G. A. Hufford, Millimeter–wave attenuation and delay rates due to fog/cloud conditions, *IEEE Trans. Antennas Propag.*, *37*, 1617–1623, 1989.

Liebe, H. J., G. A. Hufford, and T. Manabe, A model for the complex permittivity of water at frequencies below 1 thz, *Interntl. J. Infrared & Millimeter Waves*, *12*, 659–675, 1991.

Liebe, H. J., P. W. Rosenkranz, and G. A. Hufford, Atmospheric 60-GHz oxygen spectrum: new laboratory measurements and line parameters, *Journal of Quantitative Spectroscopy and Radiative Transfer*, *48*, 629–643, 1992.

Liebe, H. J., G. A. Hufford, and M. G. Cotton, Propagation modeling of moist air and suspended water/ice particles at frequencies below 1000 GHz., in *AGARD 52nd Specialists Meeting of the Electromagnetic Wave Propagation Panel, Palma de Mallorca, Spain*, 1993, `ftp://ftp.its.bldrdoc.gov/pub/mpm93/`.

Liou, K. N., *An introduction to atmospheric radiation*, 2nd ed., Academic Press, 2002.

Lipton, A. E., M. K. Griffin, and A. G. Ling, Microwave transfer model differences in remote sensing of cloud liquid water at low temperatures, *IEEE Transactions on Geoscience and Remote Sensing*, *37*, 620–623, 1999.

Liu, J. S., *Monte Carlo Strategies in Scientific Computing*, Springer-Verlag, 2001.

Liu, Q., C. Simmer, and E. Ruprecht, Three-dimensional radiative transfer effects of clouds in the microwave spectral range, *Journal of Geophysical Research*, *101*, 4289–4298, 1996.

Ludlam, F. H., and B. J. Mason, The physics of clouds, in *Encyclopedia of Physics*, edited by S. Flg̈ge, vol. 48, Springer, Berlin, 1957.

Ma, Q., and R. H. Tipping, Water vapor continuum in the millimeter spectral region, *Journal of Chemical Physics*, *93*, 6127–6139, 1990.

Mätzler, C., and C. Melsheimer, Radiative transfer and microwave radiometry, in *Thermal microwave radiation: applications for remote sensing*, edited by C. Mätzler, The institution of engineering and technology, UK, 2006.

Mishchenko, M. I., Vector radiative transfer equation for arbitrarily shaped and arbitrarily oriented particles: a microphysical derivation from statistical electromagnetics, *Applied Optics*, *41*, 7114–7134, 2002.

Mishchenko, M. I., J. W. Hovenier, and L. D. Travis, eds., *Light Scattering by Nonspherical Particles*, Academic Press, 2000, ISBN 0-12-498660-9.

Mishchenko, M. I., L. D. Travis, and A. A. Lacis, *Scattering, Absorption and Emission of Light by Small Particles*, Cambridge University Press, 2002, ISBN 0-521-78252.

Mobley, C. D., *Light and water: radiative transfer in natural waters*, chap. Across the surface, Academic Press, USA, 1994.

Newell, A. C., and R. C. Baird, Absolute determination of refractive indices of gases at 47.7 Gigahertz, *J. Appl. Phys.*, *36*, 1965.

Oliveiro, J. J., and R. L. Longbothum, Empirical fits to voight line width: A brief review, *Journal of Quantitative Spectroscopy and Radiative Transfer*, *17*, 233–236, 1977.

Pawlowska, H., J. L. Brenguier, and F. Burnet, Microphysical properties of stratocumulus clouds, *Atmospheric Research*, *55*, 15–33, 2000.

Petty, G. W., *A first course in atmospheric radiation*, Sundog Publishing, 2006.

Press, W., S. Teukolsky, W. Vetterling, and B. Flannery, *Numerical recipes in FORTRAN*, 2nd ed., Cambridge University Press, 1992.

Press, W., S. Teukolsky, W. Vetterling, and B. Flannery, *Numerical recipes in C*, 2nd ed., Cambridge University Press, 1997.

Ray, P., Broadband complex refractive indices of ice and water, *Appl. Opt.*, *11*, 1836–1844, 1972.

Rees, W. G., *Physical principles of remote sensing*, 2nd ed., Cambridge University Press, 2001.

Rodgers, C., *Inverse methods for atmospheric sounding: Theory and practise*, 1st ed., World Scientific Publishing, 2000.

Rodgers, C. D., Characterization and error analysis of profiles retrieved from remote sounding measurements, *Journal of Geophysical Research*, *95*, 5587–5595, 1990.

Rosenkranz, P. W., Absorption of microwaves by atmospheric gases, in *Atmospheric remote sensing by microwave radiometry*, edited by M. A. Janssen, pp. 37–90, John Wiley & Sons, Inc., 1993, `ftp://mesa.mit.edu/phil/lbl_rt`.

Rosenkranz, P. W., Water vapor microwave continuum absorption: A comparison of measurements and models, *Radio Science*, *33*, 919–928, 1998, (correction in 34, 1025, 1999), `ftp://mesa.mit.edu/phil/lbl_rt`.

Rothman, L. S., et al., The HITRAN molecular database: editions of 1991 and 1992, *Journal of Quantitative Spectroscopy and Radiative Transfer*, *48*, 469–507, 1992.

Rothman, L. S., et al., The HITRAN molecular spectroscopic database and HAWKS (HITRAN atmospheric workstation): 1996 edition, *Journal of Quantitative Spectroscopy and Radiative Transfer*, *60*, 665–710, 1998.

Rybicki, G. B., and A. P. Lightman, *Radiative processes in astrophysics*, chap. Plasma effects, John Wiley and Sons, Inc., USA, 1979.

Salby, M. L., *Fundamentals of Atmospheric Physics*, vol. 61 of *International Geophysics Series*, Academic Press, 1996, ISBN 0-12-615160-1.

Seinfeld, J. H., and S. N. Pandis, *Atmospheric Chemistry and Physics : from Air Pollution to Climate Change*, Wiley, 1998, ISBN 0-471-17816-0.

Shupe, M. D., T. Uttal, S. Y. Matrosov, and A. S. Frisch, Cloud water content and hydrometeor sizes during the FIRE-Arctic Clouds Experiment, *Journal of Geophysical Research*, *106*, 15015–15028, 2000.

Stankevich, K. S., Absorption of sub–millimeter–range radio waves in a dry atmosphere, *Radiophys. Quantum Electron. (Engl. Transl.)*, *17*, 579–581, 1974.

Stone, N. W., W. G. Read, A. Anderson, I. R. Dagg, and W. Smith, Temperature-dependent collision-induced absorption in nitrogen, *Can. J. Phys.*, *62*, 338–347, 1984.

Stratton, A. J., Optical and radio refraction on Venus, *Journal of the Atmospheric Sciences*, *25*, 666–667, 1968.

Thayer, G. D., An improved equation for the radio refractive index of air, *Radio Science*, *9*, 803–807, 1974.

Thomas, G., and K. Stamnes, *Radiative Transfer in the Atmosphere and Ocean*, Cambridge Atmospheric and Space Science Series, Cambridge University Press, 2002.

Thorne, A., U. Litzen, and S. Johansson, *Spectrophysics : principles and applications*, Springer, 1999, 1999, ISBN 3-540-65117-9.

Townes, C. H., and A. L. Schawlow, *Microwave Spectroscopy*, Mc Graw-Hill, 1955.

Ulaby, F., R. Moore, and A. Fung, *Microwave remote sensing: Active and passive, Volume I: Microwave remote sensing fundamentals and radiometry*, Addison-Wesley Publishing Company, 1981, ISBN 0-201-10759-7 (v. 1).

van de Hulst, H., *Light Scattering by Small particles*, Dover Publications, New York, 1957, corrected republication 1981.

Van Vleck, J. H., The relation between absorption and dispersion, in *Propagation of Short Radio Waves*, edited by D. E. Kerr, pp. 641–664, Peter Peregrinus Ltd, 1987, first published in 1951 by McGraw-Hill Book Comp. Inc.

Van Vleck, J. H., and D. L. Huber, Absoption, emission, and linebreadths: a semihistorical perspective, *Reviews of Modern Physics*, *49*, 939–959, 1977.

Van Vleck, J. H., and V. F. Weisskopf, On the shape of collision–broadening lines, *Reviews of Modern Physics*, *17*, 227—236, 1945.

Verdes, C., A. von Engeln, and S. A. Buehler, Partition function data and impact on retrieval quality for a mm/sub-mm limb sounder, *Journal of Quantitative Spectroscopy and Radiative Transfer*, *90*, 217–238, 2005.

Westwater, E. R., J. B. Snider, and M. J. Falls, Ground-based microwave radiometric retrieval of precipitable water vapor in the presence of clouds with high liquid content, *Radio Science*, *15*, 947–957, 1980.

# Part II

# Index

# Index